

Volume 1, Issue 1

2011

PLASMA MEDICINE

EDITORS IN-CHIEF

ALEXANDER A. FRIDMAN, GARY FRIEDMAN,
KLAUS-DIETER WELTMANN & AXEL KRAMER



begell house, inc.
publishers

Plasma Medicine™ (ISSN 1947-5764) is published quarterly and owned by Begell House, Inc., 50 Cross Highway, Redding, Connecticut, 06896.

Copyright© 2010 by Begell House, Inc. All rights reserved. Printed in the United States of America. Authorization to photocopy items for internal or personal use, or the internal or personal use of specific clients, is granted by Begell House, Inc. for libraries and other users registered with the Copyright Clearance Center (CCC). Transactional Reporting Service, provided that the base fee of \$35.00 per copy, plus .00 per page is paid directly to CCC, 222 Rosewood Drive, Danvers, MA 01923, USA. For those organizations that have been granted a photocopy license by CCC, a separate payment system has been arranged. The fee code for users of the Transactional Reporting Service is: [ISSN 1947-5764/11\$35.00 + \$0.00]. The fee is subject to change without notice. Begell House, Inc.'s consent does not extend to copying for general distribution, for promotion, for creating new works, or for resale. Specific permission must be obtained from Begell House, Inc., for such copying.

Subscriptions: United States rate for 2011 is \$708.00. For orders outside the United State and Canada please add an additional \$10.00 per issue for foreign airmail shipping and handling fees. Personal (individual) subscriptions must be paid for by personal check or credit card. All subscriptions are payable in advance. Subscriptions are entered on an annual basis, i.e., January to December. For immediate service and charge card sales, call Begell House at (203) 938-1300 Monday through Friday, 9 A.M.-5 P.M. EST. To order by fax: (203) 938-1304. Send written orders to Begell House, Inc., Subscriptions Department, 50 Cross Highway, Redding, Connecticut, 06896. This journal contains information from authentic and highly regarded sources. Reprinted material is quoted with permission, and sources are indicated. A wide variety of references are listed. Reasonable efforts have been made to publish reliable data and information, but the editor and the publisher assume no responsibility for any statements of fact or opinion expressed in the published papers or in the advertisements.

Printed September 10, 2010

Plasma Medicine

EDITORS-IN-CHIEF

ALEXANDER A. FRIDMAN

Director of A. J. Drexel Plasma Institute
Nyheim Chair Professor, Department of Mechanical
Engineering, Drexel University, 3141 Chestnut Street
Philadelphia, PA 19104-2884

fridman@drexel.edu

KLAUS-DIETER WELTMANN

INP Greifswald
Greifswald, Germany

weltmann@inp-greifswald.de

GARY FRIEDMAN

Professor, Dept. of Electrical and Computer
Engineering, Drexel University
3141 Chestnut Street
Philadelphia, PA 19104-2875

gary@ece.drexel.edu

AXEL KRAMER

Inst. for Hygiene and Environmental Medicine
Greifswald, Germany

kramer@uni-greifswald.de

EDITORIAL BOARD MEMBERS

PIETRO FAVIA

University of Bari, Italy
favia@chimica.uniba.it

MOUNIR LAROUSI

Old Dominion University, USA
mlarouss@odu.edu

MICHAEL WERTHEIMER

Montreal University, Canada
Michel.Wertheimer@courriel.polymtl.ca

ANDREAS OHL

I'NP-Greifswald, Germany
ohl@inp-greifswald.de

VICTOR VASILETS

Institute for Energy Problems of Chemical Physics
Russia
vvasilets@gmail.com

JEAN-MICHEL POUVESLE

University of Orleans, France
jean-michel.pouvesle@univ-orleans.fr

RICHARD SATAVA

University of Washington, TATRC, USA
rsatava@u.washington.edu

DAVID GRAVES

University of California, Berkley, USA
graves@berkeley.edu

GREGOR MORFILL

Max-Planck Institute for Extraterrestrial Physics
D-85748 Garching, Germany
gem@mpe.mpg.de

GREGORY FRIDMAN

Drexel University, USA
gregfridman@gmail.com

MICHAEL KONG

Loughborough University, UK
m.g.kong@lboro.ac.uk

SATOSHI HAMAGUCHI

Center for Atomic and Molecular Technologies
Graduate School of Engineering
Osaka University, Japan
hamaguch@ppl.eng.osaka-u.ac.jp

JAE KOO (J.K.) LEE

Pohang University of Science and Technology
Pohang 790-784, Republic of Korea
jkl@postech.ac.kr

MICHEL MOISAN

Université de Montréal
Montréal H3C 3J7, Québec, Canada
michel.moisan@umontreal.ca

SYLVAIN COULOMBE

Department of Chemical Engineering, McGill
University, Montréal (QC), Canada
coulombe.sylvain@gmail.com

FARZANEH AREFI-KHONSARI

Laboratoire de Génie des Procédés Plasmas et
Traitement de Surface, ENSCP, Université Pierre et
Marie Curie, 75231 Paris cedex 05, France
farzi-arefi@enscp.fr

VALERIJA A. GOSTEV

Petrozavodsk State University
Petrozavodsk, Russia
vgostev@psu.karelia.ru

RICHARD HAMILTON

Drexel College of Medicine, USA
Richard.Hamilton@DrexelMed.edu

GREGORY GINSBERG

University of Pennsylvania, USA
gregory.ginsberg@uphs.upenn.edu

ARI D. BROOKS

Drexel College of Medicine, USA
ari.brooks@drexelmed.edu

2010 Editorial Board

AIMS & SCOPE

Technology has always played an important role in medicine and there are many journals today devoted to medical applications of ionizing radiation, lasers, ultrasound, magnetic resonance, and others. Plasma technology is relatively new to the field of medicine. Experimental work conducted at several major universities, research centers and companies around the world over the recent decade demonstrates that plasma can be used in a variety of medical applications. It is already widely used in surgeries and endoscopic procedures and has been shown to control properties of cellular and tissue matrices, including biocompatibility of various substrates. Non-thermal plasma has been demonstrated to deactivate dangerous pathogens and to stop bleeding without damaging healthy tissue. Plasma can also be used to promote wound healing and to treat cancer. Recently the understanding of various mechanisms by which plasma can interact with living systems, including effects of reactive oxygen species, reactive nitrogen species and charges, has begun to emerge. The aim of the Plasma Medicine journal is to provide a forum where the above topics as well as topics closely related to them can be presented and discussed. Existing journals on plasma science and technology are aimed for audiences with primarily engineering and science backgrounds, whereas the field of Plasma Medicine is highly interdisciplinary. We would expect that some of the prospective readers and contributors to the journal of Plasma Medicine will have backgrounds in medicine and biology while others might be more familiar with plasma science. The goal of Plasma Medicine journal is to bridge the gap between audiences with such different backgrounds, without sacrificing the quality of the papers by their emphasis on medicine, biology or plasma science and technology.

Plasma Medicine

Volume 1 / Issue 1

2011

TABLE OF CONTENTS

| | |
|--|-----------|
| Cold Spark Discharge Plasma Treatment of Inflammatory Bowel Disease in an Animal Model of Ulcerative Colitis | 3 |
| <i>Kalyan Chakravarthy, Danil Dobrynin, Gregory Fridman, Gary Friedman, Sreekant Murthy & Alexander Fridman</i> | |
| Comparison of Point-to-Plane and Point-to-Point Corona Discharge for the Decontamination or Sterilization of Surfaces and Liquids | 21 |
| <i>V. Scholtz, J. Julák & B. Štěpánková</i> | |
| Response of Human Glioma U87 Xenografted on Mice to Non Thermal Plasma Treatment | 27 |
| <i>Marc Vandamme, Eric Robert, Sébastien Dozias, Julien Sobilo, Stéphanie Lerondel, Alain Le Pape & Jean-Michel Pouvesle</i> | |
| Targeted Cancer Treatment Using Anti-EGFR and -TFR Antibody-Conjugated Gold Nanoparticles Stimulated by Nonthermal Air Plasma | 45 |
| <i>G. J. Kim, S. R. Park, G. C. Kim & J. K. Lee</i> | |
| Use of Proteomics to Investigate Plasma-Cell Interactions | 55 |
| <i>K. Landsberg, Ch. Scharf, K. Darm, K. Wende, G. Daeschlein, E. Kindel, K.-D. Weltmann & Th. von Woedthe</i> | |
| Analysis of Streamer Propagation for Electric Breakdown in Liquid/Bioliquid | 65 |
| <i>Yong Yang, Andrey Starikovskiy, Alexander Fridman & Young I. Cho</i> | |
| Plasma-Controlled Cell Migration: Localization of Cold Plasma-Cell Interaction Region | 85 |
| <i>O. Volotskova, A. Shashurin, M. A. Stepp, S. Pal-Ghosh & M. Keidar</i> | |
| Live Pig Skin Tissue and Wound Toxicity of Cold Plasma Treatment | 93 |
| <i>Danil Dobrynin, Andrew Wu, Sameer Kalghatgi, Sin Park, Natalie Shainsky, Kimberly Wasko, Essel Dumani, Robert Ownbey, Suresh Joshi, Rachel Sensenig & Ari D. Brooks</i> | |

Cold Spark Discharge Plasma Treatment of Inflammatory Bowel Disease in an Animal Model of Ulcerative Colitis

Kalyan Chakravarthy^{1,†}, Danil Dobrynin^{2,*†}, Gregory Fridman¹, Gary Friedman², Sreekant Murthy³ & Alexander Fridman⁴

¹School of Biomedical Engineering, Science and Health Systems, Drexel University, ²Electrical and Computer Engineering Department, College of Engineering, Drexel University, ³College of Medicine, Drexel University, ⁴Department of Mechanical Engineering and Mechanics, College of Engineering, Drexel University

*Address all correspondence to Danil Dobrynin, 3400 Lancaster Avenue, HESS #117, Philadelphia, PA 19104; Tel.: 215-895-6254; Fax: 215-895-1633; dvdobrynin34@gmail.com

†These authors contributed equally.

ABSTRACT: Cold plasma discharges have been shown to have medically-relevant therapeutic effects when applied to living tissues, including blood coagulation and wound healing; thus, plasma treatment of inflamed tissues in ulcerative colitis disease may be an effective approach to reduce adverse consequences if not cure the disease. Here we discuss results of the first experimental study of cold plasma treatment of ulcerative colitis in a mouse model. As a plasma source, a cold spark discharge has been used. The results show that plasma treatment of experimental model of ulcerative colitis in mice has some beneficial effects by suppressing the progression of the disease while no damage to colon tissues is observed; and these effects are comparable to standard therapy.

KEY WORDS: non-equilibrium plasma, cold spark discharge, animal model, plasma therapy, plasma medicine

I. INTRODUCTION

Recently, non-thermal atmospheric pressure plasmas have emerged as a promising new tool in medicine. Compared to conventional thermal plasma¹⁻⁵, cold plasma is selective in its treatment while no macroscopic tissue damage is observed. Non-thermal plasmas generate free radicals, charged species, and ultraviolet radiation, which may be used for targeted chemical modification and catalysis^{6,7} unlike thermal plasmas which employ high temperature that causes significant thermal tissue desiccation, burning, and scar formation. An example of thermal plasma is the Argon Beam or Argon Plasma Coagulator (APC) developed mainly to cauterize wounds⁸. On the other hand, cold plasma discharges have many potential medical applications that include sterilization of living tissue without macroscopic damage⁹, blood coagulation¹⁰, induction of apoptosis in cancer and other cells^{11,12}, and control of cell attachment¹³. Another promising field of cold plasma applications in medicine is gastroenterology, where strong antibacterial effect can be successfully combined with healing and anti-inflammatory effects. Thus, the focus of this study is to evaluate whether cold plasma in vivo is detrimental to gastro-

intestinal tissue in health and disease conditions and whether cold plasma provides any therapeutic benefit in an animal model of murine experimental colitis. The disease in this model produces experimental colitis reminiscent of human ulcerative colitis, which is a form of inflammatory bowel diseases. Inflammatory bowel diseases (IBD) consist of two major chronic, relapsing and debilitating forms of diseases known as ulcerative colitis and Crohn's disease that affect the gastrointestinal tract. The etiology of these diseases remains a mystery though genetic, environmental and immunological factors are found to play a major role in the induction, chronicity and relapses of these diseases. Crohn's disease may appear in any part of the gastrointestinal tract from the mouth to anus and affects the entire thickness of the bowel wall. On the contrary, ulcerative colitis is an inflammatory disorder affecting colonic mucosa and sub-mucosa¹⁴. There are no known curative therapies for these diseases; however, recent advances in IBD therapeutics have shown that certain biological therapies have been successful in maintaining remission particularly in Crohn's disease^{15,16}.

This study was designed to evaluate the effects of cold plasma treatment of both healthy colon tissue and experimentally-induced ulcerative colitis disease in a live animal model. The goals of the study were to examine whether cold plasma treatment adversely affects the mucosa in normal condition, and to evaluate if cold plasma treatment results in acceleration or worsening of the disease during its induction phase. Additional pilot experiments were conducted to study whether cold plasma discharges provide therapeutic effects, and whether these effects are comparable to a standard therapy, or cold plasma treatment enhances the beneficial effect of a standard therapy.

II. MATERIALS AND METHODS

A. Cold Pin-to-Hole Spark Discharge (PHD) Plasma

Currently, the primary reason of gastroenterological inflammatory diseases, and particularly ulcerative colitis, is still unknown; however, two major candidates are bacterial infections and autoimmune disorders. In order to be able to address these problems using plasma, the treatment should meet several conditions, namely:

- Average plasma temperature should be low, i.e. close to room temperature, when there is no or minimal thermal damage due to contact of plasma with tissues;
- Have strong bactericidal effect;
- Be able to provide anti-inflammatory effect.

Another set of criteria which are important in the present mouse model experiments refer to plasma system engineering problems:

- Electrode system ("plasma probe") should be small (maximum outer diameter is approximately 2 mm) in order to cause minimal mechanical damage to colon tissue of a mouse;

- Plasma should be easily ignited inside of a colon, and should not be sensitive to the distance between electrode and inner colon wall.

All these conditions may be satisfied if one is using cold spark discharge plasma. Dr. Gostev and colleagues reported that this cold discharge^{17,18} (authors used similar system as in the current study, but of about 10 times greater in size) is extremely effective in sterilization of bacteria both in liquid¹⁹ and on tissue surface²⁰, and due to production of significant amount of nitric oxide (NO) has pronounced “healing” effect through faster tissue regeneration, and other beneficial effects^{17,18,21,22}. The pin-to-hole electrode configuration makes the discharge ignition process not sensitive to the presence of surrounding tissues and natural liquids, in contrast to direct methods of creating arc, dielectric barrier, or corona discharges where treated surface is used as a second electrode. Also, PHD treatment allows operator to provide relatively high energy input resulting in shorter treatment time and less discomfort to an animal.

In our study we have used modified PHD system which consists of central copper needle covered by dielectric material which is inserted into a grounded stainless steel cylindrical electrode (Figure 1). In order to cause minimal mechanical damage to colon tissues external electrode is covered by polyethylene sleeve. The discharge was ignited by applying high positive potential to the central electrode. In order to provide high discharge energy while keeping average gas temperature low, the electrode system was powered through a capacitor. This resulted in a formation of dense energetic spark which exists for about 3.5 μ s. Due to low repetition frequency of about 7 Hz and short pulse duration, the average gas temperature did not exceed room temperature.

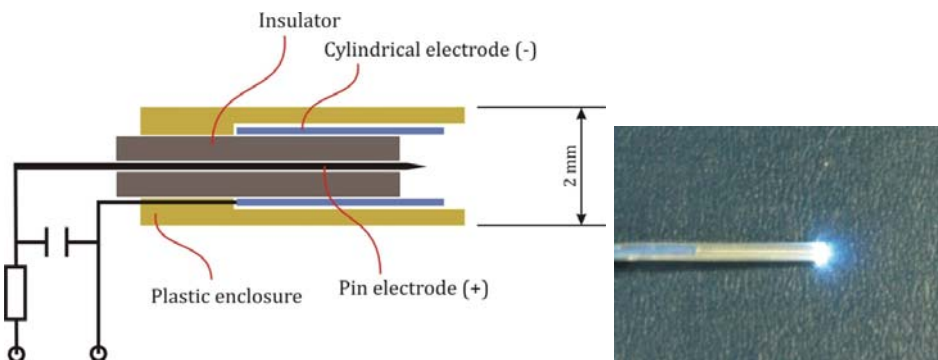


FIGURE 1 General schematic of the Pin-to-Hole spark Discharge (PHD) plasma system, and photograph of the discharge in operation.

The main average PHD plasma characteristics are the following:

- Peak voltage: 3.2 kV;
- Pulse duration: 3.5 μ s;
- Frequency: 7 Hz;
- Energy per pulse: 0.1 J;
- Plasma diameter: \sim 2 mm;
- Typical waveforms are shown in Figure 2.

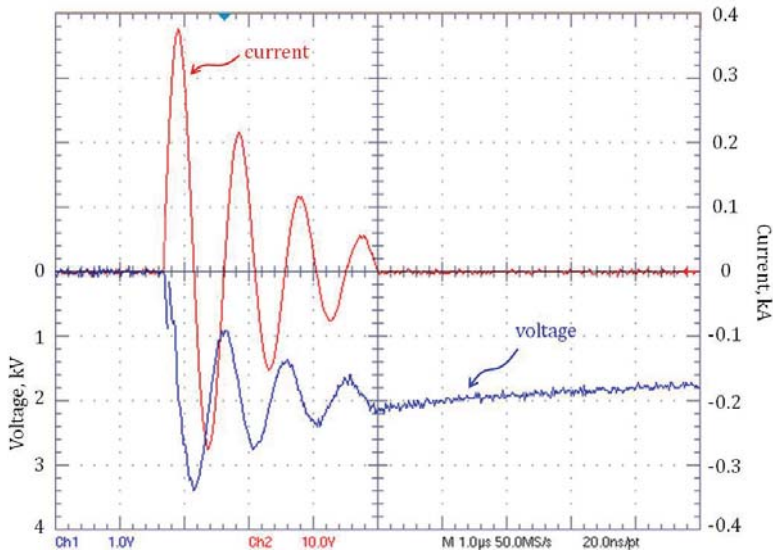


FIGURE 2 Typical voltage and current waveforms of cold Pin-to-Hole spark Discharge (PHD) plasma.

Although the average gas temperature is low, plasma temperature itself in order to cause production of significant amount of NO is expected to be relatively high. We have estimated plasma temperature using Boltzmann plot method^{23,24} which may be applied for estimation of gas temperature of sparks²⁵. This method uses the relative ratio of emission intensities on multiple spectra lines. Under plasma conditions at local thermal equilibrium, the plasma temperature is derived from the following equation:

$$\ln \frac{I\lambda}{Ag_u} = -\frac{1}{T}E_u + \ln C,$$

where I is the relative ratio of the emission intensity, λ - the wavelength, A - the transition probability, g_u - the statistical weight of the upper level, E_u - the energy of the upper level, C - a constant for various atoms. We used spectral lines of copper (material of central electrode) to estimate the temperature in the center of the discharge. The transition probabilities, the statistical weights of the upper level and the energy of the upper

levels of the copper lines are shown in Table 1²⁶. The copper emission lines from the spark discharge were measured using Acton SpectraPro 500i spectrophotometer; Figure 3 shows the result obtained which indicates that plasma temperature of about 7200 K, which is sufficient to generate significant amount of NO.

TABLE 1. Parameters of copper spectral lines³⁹

| Wavelength λ , nm | Transition probability $A \times 10^8 \text{ s}^{-1}$ | Statistical weight, g_u | Upper energy level E_u , eV |
|------------------------------|--|------------------------------|----------------------------------|
| 510.55 | 0.02 | 4 | 3.822 |
| 515.32 | 0.60 | 4 | 6.195 |
| 521.82 | 0.75 | 6 | 6.196 |

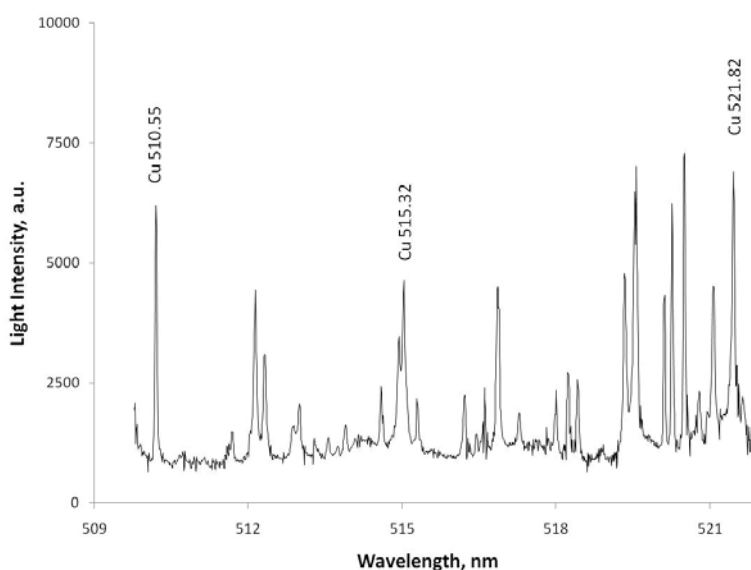


FIGURE 3 Spectrum obtained from spark discharge plasma in room air with the copper spectral lines used for plasma temperature estimation identified.

As can be seen from spectrum of radiation (Figure 4), PHD plasma radiates intensely in the UV range. In order to be sure that plasma will cause minimal DNA damage to cells due to direct exposure to UV, the outer tubing was made of about the size of plasma diameter, i.e. about 1.5 mm, longer than electrode system, covering the discharge from the sides. In addition to that we have measured total amount of UV irradiated by plasma using IL1700 photometer (International Light Technologies) to be about $5 \pm 1 \mu\text{W}/\text{cm}^2$. Recent studies show that DNA damage induced by UV-C and UV-B radiation occurs after about $0.4 \text{ mJ}/\text{cm}^2$ and $10 \text{ mJ}/\text{cm}^2$ respectively²⁷. Considering the fact that most of

UV radiation of PHD plasma comes from UV-C band, minimum 60 seconds of plasma treatment should be safe, causing none or minimal and reversible DNA damage to colon tissue.

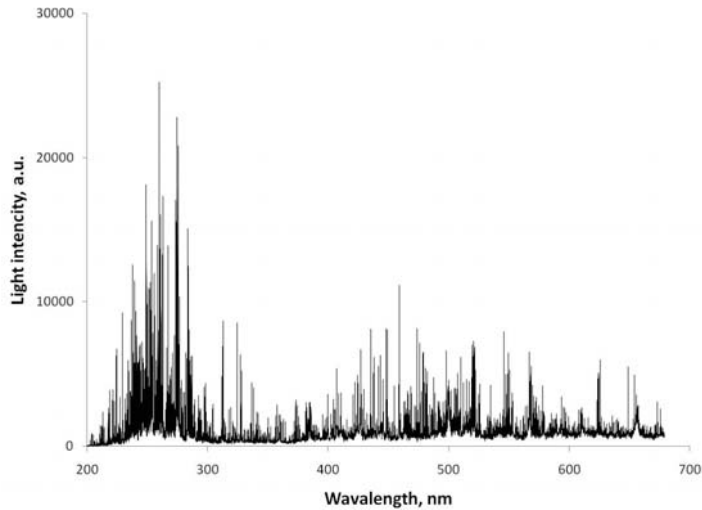


FIGURE 4 PHD plasma spectrum in room air

Lastly, it was necessary to check if miniaturized PHD plasma system indeed produces significant amount of NO, thus delivering the therapeutic effect (so-called, “NO-therapy”²⁸⁻³¹). The NO production was measured using gas chromatograph Agilent 3000 MicroGC, calibrated with 700 ppm NO balanced with nitrogen. The discharge cell was inserted inside of a syringe tip, and plasma treated room air was collected with slow plunger pulling during plasma treatment. Then, collected air was analyzed chromatographically. The results of our measurements (see Figure 5) show that NO concentration is varied from 900 to 1200 ppm depending on plasma treatment dose, which allow us to expect that plasma treatment of colon ulcer may cause “healing” effect.

Although one can argue that plasma characterizations mentioned above were made in different atmosphere (room air), and therefore the results could differ from real experimental situation when plasma is ignited inside of intestine, we do not expect qualitative difference between these two conditions. This assumption is based on data on gas composition inside of a colon, which is mostly consists of air-like mixture (up to 80% of N₂ and 2.3% of O₂) with small additives of hydrogen, methane, and carbon dioxide³². Moreover, before the treatment procedure, the colon was cleansed with saline, and also room air was introduced into the colon during probe insertion. Therefore, air is expected to be a dominant plasma-forming gas.

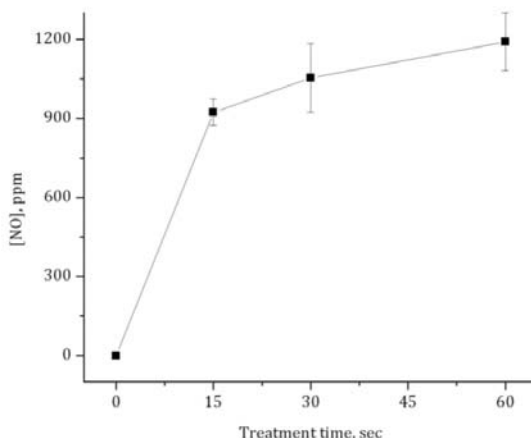


FIGURE 5 Nitric oxide production by PHD plasma

B. Dextran Sodium Sulphate (DSS) Induced Experimental Colitis in Mice

The DSS model was used in the current study to produce ulcerative colitis in mice which is representative of human ulcerative colitis^{33,34}. The disease is induced in an animal through a daily oral administration of 2.5% DSS dissolved in drinking water at concentration of 2.5%. Animal develops an acute form of inflammation beginning on the third day and they have a full blown colitis on the day of DSS feeding cycle. The primary characteristics of acute inflammation are the increased number of neutrophils in the mucosal layer, shortening of the epithelial crypts, hyalination in the lamina propria, accompanied by severe weight loss, diarrhea, and blood in the stool. This form of the disease gives an opportunity to use it as a model in efficacy studies of drugs and compounds³⁴. The most striking feature of this model is that it works using a very simple pathway to produce the disease as DSS overcomes the barrier of the epithelium to expose the mucosa to the flora present in the intestine resulting in an inflammatory response; this in turn leads to activation of macrophages and monocytes. The model also shows close links to the disease in human beings and it is simple to induce and reproduce³³⁻³⁵.

To quantify the disease induced by the DSS model a Disease Activity Index (DAI) have been used³³. A scale of 0 to 4 is used to quantify the disease with 4 being the lethal stage of the disease. DAI is scored on the parameters of weight loss, consistency of the stool and presence of blood in the stool. This index has been shown to be in a linear correlation with the histology score based on changes in the architecture of the crypt³³.

C. Animal Study Design

All experiments were done on live animals. The study consisted of 3 stages:

1. Toxicity study of plasma treatment of a colon.

2. Study DSS model disease progression after plasma treatment.
3. Comparison of effectiveness of plasma treatment with conservative therapy

In all the experiments Female Swiss Webster mice approximately aged six to eight weeks of 25 to 30 grams in weight were used. Prior to plasma treatment animals were anesthetized with 0.4 ml Nembutal®. The effect of the anesthetic was checked using the toe relax by pinching. The colon was cleansed with saline before inserting the probe.

III. RESULTS AND DISCUSSION

A. Toxicity of Plasma Treatment of Colon Tissue

The primary objective of the study was to ascertain if cold plasma treatment would cause any damage, to colon tissue or to the animal itself. To ascertain this effect, 12 mice were divided into 4 groups of three animals in each group. The first group was a control group which did not receive any treatment and the other three groups remained as experimental groups. In experimental groups a laparotomy was performed and the colon was exposed and kept moist covered with a saline gauze. The plasma probe was introduced through the anal verge up to 4 cm into the colon (Figure 6). Plasma treatment was administered for 0, 4, 30 and 60 seconds in the respective group (for “0” time point, the probe was inserted into the colon with no plasma ignited). To check colon tissue damage, mice were intravenously injected with 30 mg/kg of Evans Blue (EB), ten minutes after the administration colon was washed with 1 ml physiological saline and EB presence was analyzed spectrophotometrically. Animals were euthanized with an over dose of Nembutal® and colon tissue samples were surgically removed and were preserved in formalin for further histopathological analysis.

Spectrophotometrical analysis of the saline fluid collected from the colon showed no traces of EB, indicating that plasma did not affect the tissue integrity. Histology analysis also showed that no macroscopic damage was induced to the colon tissues by plasma treatment or probe manipulation (Figure 7).



FIGURE 6 Photograph of cold spark plasma inside of the mouse colon: the colon here is not punctured and the light generated by plasma is seen through the thin tissue.

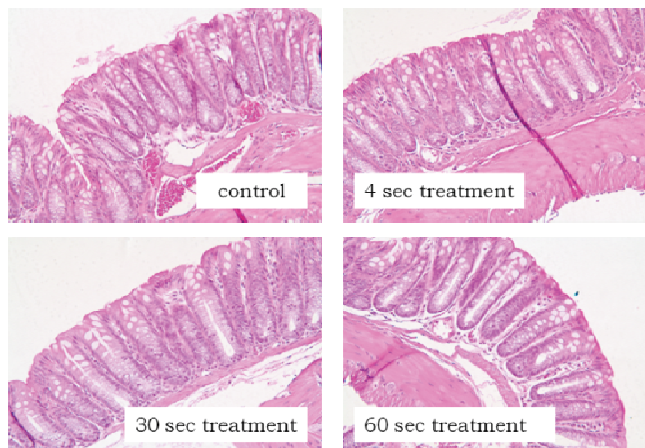


FIGURE 7 Colon tissue histology shows no detectable damage

B. DSS model Disease Progression After Plasma Treatment

The next step was to check the response of the disease progression to plasma treatment; hence 24 animals were divided into 4 groups each receiving 0, 4, 30 or 60 seconds of plasma treatment every alternate day for 7 days. All animals were fed 2.5% DSS for 7 days in parallel with plasma treatment. DAI was scored everyday to see which dosage of plasma was most effective in controlling the progression of the disease. For the plasma probe to be inserted and to go through the colon, the colon has to be cleansed of stool specks. To do so, the animals were fed a polyethylene glycol based laxative along with DSS one day before plasma treatment. However, the stool consistency on the next day was compromised as the laxative made the stool consistently loose. Hence, data extracted from the study were bifurcated and were analyzed using a three pronged approach considering:

- a. Weight, stool consistency, and presence of blood in the stool.
- b. Weight, and presence of blood in the stool (without stool data)
- c. Mean hemocult (visible blood in the stool)

Results of the experiment (Figure 8) show that, in the control group the DAI scored using weight, stool consistency, and blood visibility in the stool reaches a value of 2.3 by the end of 7 days. The group which received 60 seconds of plasma treatment reached a DAI of 1.6 on day 7. Hence, the disease is not controlled very well in the 60 second plasma group; on days 3, 4 and 5 one minute of plasma treatment stabilized the disease and prevented it from progression. However, as the severity of the disease increased the plasma treatment effectiveness ceased. 4 seconds of treatment resulted in disease reduction during the end stage of the study and it is comparatively better than the 60 second

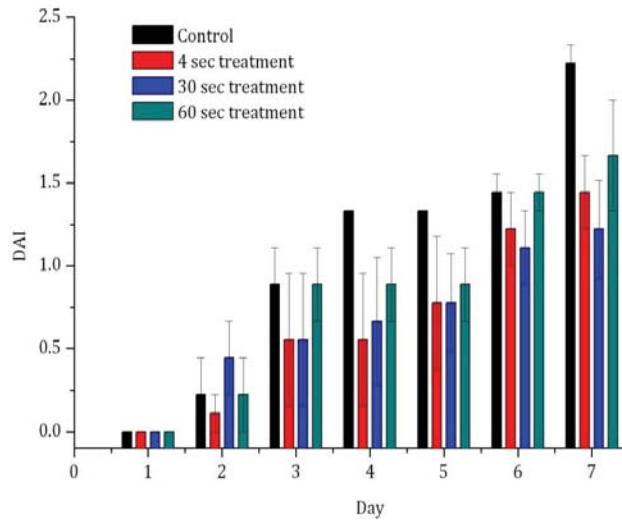


FIGURE 8 Progress of colitis, mean DAI: results of the second stage of the study (considering weight, stool consistency and hemmocult)

treatment. Here the disease was well controlled through the course of the study. The most efficient dosage of plasma as shown by the study is 30 seconds exposure. This group showed high resilience against the progression of the disease, and as compared to the control, showed great ability in stopping the progression of the disease even when DSS is being fed in parallel. The maximum DAI in this group was 1.2 as observed on day 7, the day of maximum disease prevalence.

The laxative that was administered to the animals on days prior to plasma treatment might have compromised the score based on stool consistency as this makes the stool comparatively loose, and therefore on Figure 9 only hemocult data have been considered as one of expected effects of plasma treatment is blood coagulation inside the inflamed colon. As the prime facet of tissue degradation of colitis is through bleeding out of the tissue which can be observed on the stool study. Hence this data is critical to check if plasma can actually clot and coagulate the blood inside the colon. Data shows that a statistically significant difference was obtained between untreated animals in control group and animals treated with plasma for 30 seconds. On the final days of study hemocult reached DAI of 4 in the control group while the “30 seconds” group had a DAI of just over 0.5. It can be inferred from the data that the “30 seconds” and “4 seconds” groups are showing blood coagulation inside the colon.

C. Comparison of Effectiveness of Plasma Treatment With Conservative Therapy of Ulcerative Colitis

The goal of the last stage of the study was to investigate the effectiveness of plasma treatment as an adjuvant to conventional antioxidant drug (5-amino salicylic acid (5-

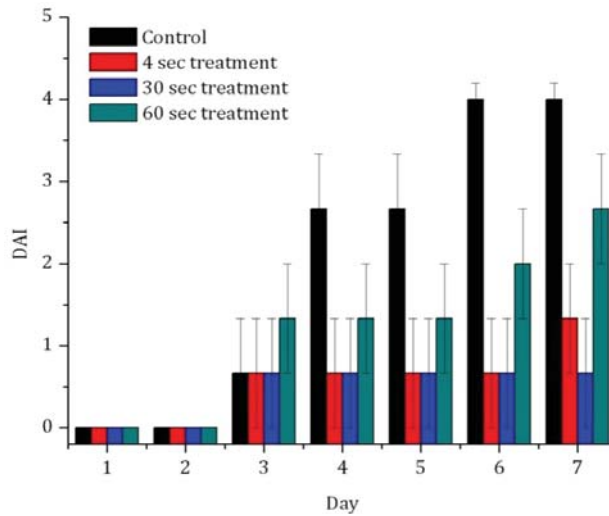


FIGURE 9 Progress of colitis, mean DAI: results of the second stage of the study (considering hemocult only)

ASA)) treatment. Based on previous results, where it was shown that 30 seconds of plasma treatment gives the best results in controlling and reducing the disease progression compared to all other groups, this treatment dose was selected for the next step. In this set of experiments 24 animals were divided into 4 groups: control group 1, where no plasma or drug treatment was performed, and groups where mice were treated either with plasma alone (group 2), 5-ASA alone (group 3), or drug and plasma together (group 4). All four groups of animals were fed with DSS for six days. On days 2, 4, and 6 they received 2.5 % DSS dissolved in water and for days 1, 3, and 5 (one day before plasma treatment) they received 2.5% DSS dissolved in 15% poly ethylene glycol based laxative to clean the colon. Plasma probe was introduced into the colon 4 cm from anal verge in groups 2 and 4, where group 2 received 30 second dose of plasma treatment only, while group 4 received same dose of plasma treatment in together with 0.1 ml of 5-ASA treatment. Animals in groups 3 and 4 were treated with 0.1 ml of 5-ASA. The DAI was scored everyday during the tenure of the study. On the seventh day of DSS treatment and final plasma treatment DAI was measured and animals were euthanized with an over dose of Nembutal®.

The disease progression for all four experimental groups is shown on Figure 10. The control group showed a steady increase through the course of seven days with the DAI reaching 2.7 on day 7. The plasma treatment group was administered 30-second plasma treatment and obtained data are in direct correlation with the data acquired in the previous study and also show a constant increase of disease progression. However, the disease curtailed to near 1.8 on the DAI scale. The group 4 showed very positive results as both in combination proved to be effective in controlling the disease and keeping the DAI on a level of 1.2 on the DAI scale.

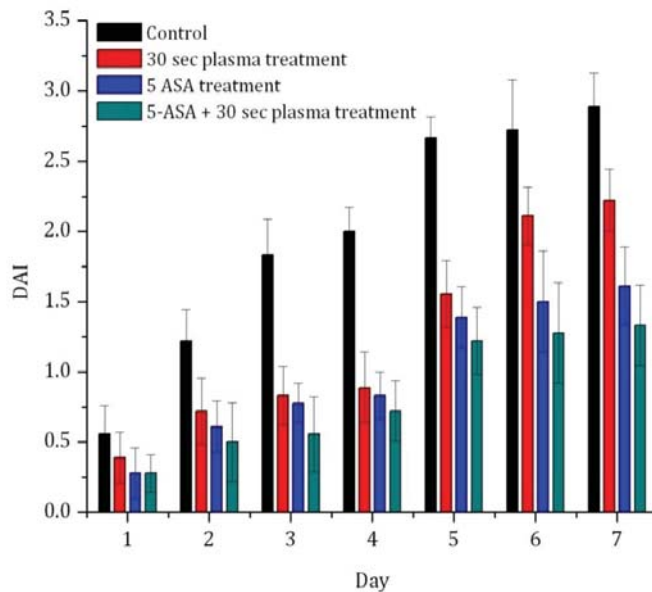


FIGURE 10 Progress of colitis, mean DAI: results of the third stage of the study (considering weight, stool consistency and hemmocult)

Figure 11 is designed to express the mean hemocult charted on a scale of 0 to 4 with 4 being the advanced stage of the disease. The plasma treatment resulted in a significant drop on the hemocult scale as compared to the control. This shows that plasma actually was working in clotting the blood that was being pumped out of the inflamed region in the colon. The combination treatment further reduced the hemocult score as a two pronged approach is taken against the disease.

The most important aspect of the study is to verify the hypothesis that plasma can be used as an add-on to the conventional drug treatment to cure the disease faster and with renewed vigor. Experimental results show that in the group which received combination treatment, disease progression was further decreased as compared to the groups which received the drug or plasma alone (Figure 10). The bars show a statistical significance in the two groups as plasma and 5-ASA reduce the disease as compared to the control group on days 5 and 7.

The results of our first invasive in-vivo experiments of cold plasma treatment of colon tissue in case of ulcerative colitis mouse model show that plasma can significantly reduce severity of the disease progression. In fact, while untreated (control) animals undergo weight loss, loss of stool consistency, and excessive bleeding, showing disease progression up to DAI number 3.1 (when 4 corresponds to lethal stage of the disease), plasma treated ones appeared to have significantly lower disease progression rate with reduced reaction to inflammation.

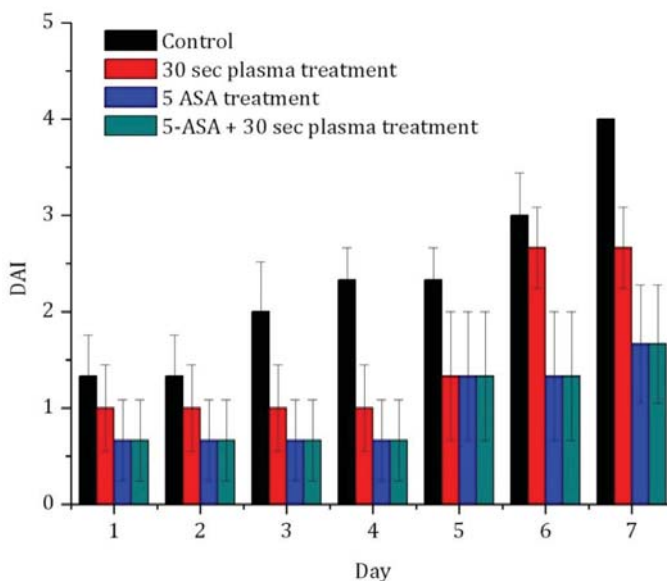


FIGURE 11 Progress of colitis, mean DAI: results of the third stage of the study (considering hemocult only)

Cold plasma treatment apparently has positive effect on inflamed colon tissue when applied for ulcerative colitis treatment. First, analyzing contribution of hemocult level to the DAI, it is shown that plasma may cause effective blood coagulation in colon ulcers. Indeed, Fridman et al. have experimentally shown that treatment of normal whole blood both in in-vitro and in-vivo cases with floating electrode dielectric barrier discharge (FE-DBD) plasma leads to initiation of natural coagulation cascade followed by fast, on the order of seconds, formation of blood clot^{10,28}. However, contribution of various plasma species and detailed mechanism of this effect remain unclear.

Another possible effect of cold spark plasma is related to nitric oxide production. It is well known today, that NO plays an important role in wound healing and tissue regeneration by regulation of blood vessel tone and blood coagulation, immune system and early apoptosis, etc.²⁸ Exogenic delivery of NO-donors (compounds that contain and release or synthesize nitric oxide upon contact with tissue) to the wound promotes and speeds up healing processes²⁸. At the same time, overdosage of NO is known to have cytotoxic effect, however exact concentrations of exogenic NO that provide either healing of “killing” effects are not yet established²⁸⁻³¹, especially, for gaseous NO.

Additionally, the role of NO may be related to “deactivation” of oxidants with formation of acidic environment. One possible explanation of pathogenesis of ulcerative colitis is given by so-called “Radical Induction Theory”, which suggests that the main cause of inflammation is excess un-neutralized H_2O_2 ³⁶. Hydrogen peroxide is produced within colonic epithelial cells, and then easily diffuses through cell membranes, and

through formation of highly reactive hydroxyl radical extensively causes oxidative damage to the cells. In this situation, increased acidity may play an important role in process of inhibition of inflammation: currently used drugs, for example, 5-ASA, which is acid, probably acts as an “antioxidant”. To check this hypothesis, we have treated 100 μl of H_2O_2 water solution with initial concentration of about 30 mg/l with spark discharge plasma (Figure 12). In order to simulate closed environment of the treated colon, discharge cell and solution holder were incased using tygon tube.

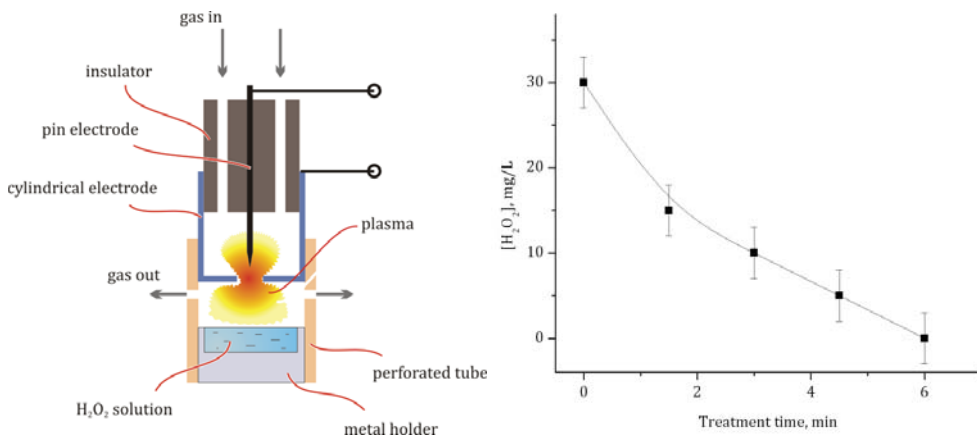
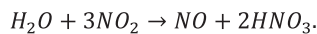
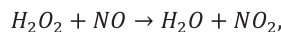


FIGURE 12 Scheme of the experimental setup and the results of hydrogen peroxide PHD plasma treatment

The result of the experiment shows that hydrogen peroxide was decomposed completely within 6 minutes of treatment. Similar effect may appear significantly faster in the colon tissues, since amount of treated liquid in this case is much lower. Possible mechanism of the destruction may be related to chemical reaction of H_2O_2 with NO with formation of nitric acid:



IV. CONCLUSIONS

Experimental study presented in this paper points to a possibility of internal cold plasma treatment of inflammatory disease model — a DSS mouse model of ulcerative colitis. Major results presented may be summarized as follows:

1. In the first stage of the plasma study, the primary goal was to understand the interaction of cold plasma with a living animal. The study showed that the cold plasma alone in graded doses did not cause any damage to

the colonic tissue or the animal based on Evan's Blue extravasation and histological analysis.

2. The second stage of the plasma study posed the challenge of ascertaining the graded dose at which the progress of the disease (ulcerative colitis) can be controlled. It is concluded that plasma did not adversely affect the animals and did not increase the progress of the disease. Surprisingly, it reduced the disease from progressing rapidly as compared to the control. The exact mechanism by which cold plasma induced its beneficial effect remains unknown.
3. The final stage of the plasma study was designed to evaluate and check the activity of plasma as an adjuvant to the industry standard drug 5-ASA in controlling the disease. Combination therapy of 5-ASA and cold plasma showed that there is a significant therapeutic relevance when it comes to adding plasma to the drug in controlling colitis in the DSS model during the induction phase.
4. Possible explanations of observed positive effects of plasma treatment were proposed. First, it was noticed, that plasma treatment caused significant decrease of blood oozing from ulcerated colon tissues. Also, reduced progression rate of the disease may be related to "antioxidant" and "healing" effects of plasma produced nitric oxide.

Although presented results are very promising, many questions remain unanswered and further development of the model and accurate extensive study are both needed. First, possible adverse long-term effects of plasma treatment should be carefully investigated. Another set of questions is related to mechanisms of plasma interaction with tissues, including effects of NO, UV, temperature, acidity, other active neutral and charged plasma components. However, this study clearly demonstrates feasibility that the cold plasma treatment may be safely applied not only for sterilization of living tissues, but also to achieve a medically relevant therapeutic effect(s), which opens new possibilities of cold plasma applications in the field of medicine.

REFERENCES

1. Watson JP, Jowett S, Oppong K, Record CO, Matthewson K. Colonoscopic Argon Plasma Coagulation for Benign and Malignant Rectal Tumours Gut, 1997;40: Th156–Th156.
2. Vargo JJ. Clinical Applications of the Argon Plasma Coagulator Gastrointestinal Endoscopy 2004;59(1):81–88
3. Raiser J, Zenker M. Argon plasma coagulation for open surgical and endoscopic applications: state of the art. J Phys D: Appl Phys, 2006;39(16):3520.
4. Watson JP, Bennett MK, Griffin SM, Matthewson K. The tissue effect of argon plasma coagulation on esophageal and gastric mucosa. Gastrointestinal endoscopy, 2000;52(3):342–5.
5. Colt HG, Crawford SW. In Vitro Study of the Safety Limits of Bronchoscopic Argon Plasma

- Coagulation in the Presence of Airway Stents *Respirology*, 2006;11(5):643–647
6. Stoffels E, Flikweert AJ, Stoffels WW, Kroesen GMW. Plasma Needle: A Non-Destructive Atmospheric Plasma Source for Fine Surface Treatment of (Bio)Materials. *Plasma Sources Science and Technology* 2002;11(4):383–388
 7. Anderson KM, Seed T, Ou D, Harris JE. Free Radicals and Reactive Oxygen Species in Programmed Cell Death *Medical Hypotheses* 1999;52(5):451–463
 8. Ginsberg GG, Barkun AN, Bosco JJ, Burdick JS, Isenberg GA, Nakao NL, Petersen BT, Silverman WB, Slivka A, Kelsey PB. The Argon Plasma Coagulator *Gastrointestinal Endoscopy* 2002;55(7):807–810
 9. Kalghatgi S, Dobrynin D, Fridman G, Cooper M, Nagaraj G, Peddinghaus L, Balasubramanian M, Barbee K, Brooks A, Vasilets V, Gutsol A, Fridman A, Friedman G. Applications of Non Thermal Atmospheric Pressure Plasma in Medicine. in NATO Advanced Study Institute on Plasma Assisted Decontamination of Biological and Chemical Agents. 2007. Cesme-Izmir, Turkey.
 10. Kalghatgi SU, Fridman G, Cooper M, Nagaraj G, Peddinghaus M, Balasubramanian M, Vasilets VN, Gutsol A, Fridman A, Friedman G. Mechanism of Blood Coagulation by Non-thermal Atmospheric Pressure Dielectric Barrier Discharge Plasma. *IEEE Transactions on Plasma Science*, 2007;35(5, Part 2):1559–1566.
 11. Kieft IE, Broers JL, Caubet-Hilloutou V, Slaaf DW, Ramaekers FC, Stoffels E. Electric Discharge Plasmas Influence Attachment of Cultured Cho K1 Cells *Bioelectromagnetics*, 2004;25(5):362–368
 12. Fridman G, Shereshevsky A, Jost M, Brooks A, Fridman A, Gutsol A, Vasilets V, Friedman G. Floating Electrode Dielectric Barrier Discharge Plasma in Air Promoting Apoptotic Behavior in Melanoma Skin Cancer Cell Lines. *Plasma Chemistry and Plasma Processing*, 2007;27(2):163–176.
 13. Kieft I, Kurdi M, Stoffels E. Reattachment and Apoptosis after Plasma-Needle Treatment of Cultured Cells *Plasma Science, IEEE Transactions on* 2006;34(4):1331–1336
 14. Sonnenberg A, McCarty DJ, Jacobsen SJ. Geographic variation of inflammatory bowel disease within the United States. *Gastroenterology* 1991;100(1):143–9.
 15. Wakefield AJ, Ekbom A, Dhillon AP, Pittilo RM, Pounder RE. Crohn's disease: pathogenesis and persistent measles virus infection. *Gastroenterology* 1995;108(3):911–6.
 16. Sartor RB. Pathogenesis and immune mechanisms of chronic inflammatory bowel diseases. *Gastroenterology* 1997;92(12 Suppl):5S–11S.
 17. Gostev V. Cold Plasma in Biological Investigations. in NATO Advanced Study Institute (ASI): Plasma Assisted Decontamination of Biological and Chemical Agents. 2007. Cesme, Turkey.
 18. Gostev V, Dobrynin D. Medical microplasmatron in 3rd International Workshop on Microplasmas 2006. Greifswald, Germany.
 19. Misyn F, Besedin E, Gostev V, Komkova O. Experimental Studying of Bactericidal Action of Cold Plasma, in *Diagnostics and Treatment of Infectious Diseases 2000*: Petrozavodsk University, Petrozavodski Russia.
 20. Misyn FA, Besedin EV, Komkova OP, Gostev VA. Experimental Investigation of Bactericidal Influence of “Cold” Plasma and Its Interaction with Cornea, in *Diagnostics and Treatment of Infectious Diseases 2000*: Petrozavodsk University, Petrozavodski Russia.
 21. Misyn FA, Besedin EV, Obraztsova AM, Gostev VA. Experimental curing of bacterial ulcer-

- ous keratitis with “cold” plasma Diagnostics and treatment of infectious diseases, Petrozavodsk University, Petrozavodsk Russia, 2000.
22. Misyn FA, Gostev VA. “Cold” plasma application for curing of eyelid phlegmon Diagnostics and treatment of infectious diseases, Petrozavodsk, Russia, 2000.
 23. Hu H, Liang H, Li J, Zhao Q, He J. Study on Production of Inhaled Nitric Oxide for Medical Applications by Pulsed Discharge. *IEEE TPS*, June 2007;35(3):619–625.
 24. Sueda T, Katsuki S, Akiyama H. Early phenomena of capillary discharges in different ambient pressures. *IEEE Trans. Magn.*, Jan. 1997. 33(1):334–339.
 25. Lochte-Holtgreven W. Production and measurement of high temperatures. *Repts. Progr. Phys*, 1958;21(312).
 26. Wavelength and transition probabilities for atoms and atomic ions: Part II-Transition probabilities. 1990.
 27. Landsberg K, Wende K, Blackert S, Kindel E, Lindequist U, Weltmann KD, von Woedke T. Cold atmospheric plasma generated UV light - friend or foe? , in *Second International Conference on Plasma Medicine*. March 16–20, 2009: San Antonio, Texas, USA.
 28. Fridman G, Shekhter AB, Vasilets VN, Friedman G, Gutsol A, Fridman A. *Applied Plasma Medicine. Plasma Processes and Polymers*, 2008;5(6):503–533.
 29. Reshetov IV, Kabisov RK, Shekhter AB, Pekshev AV, Maneilova MV. The use of a “Plason” air-plasma apparatus for coagulation and NO-therapy in plastic reconstructive surgery for oncologic patients. *Annals of Plastic, Reconstructive and Aesthetic Surgery*, 2000;4:24–38.
 30. Shekhter AB, Kabisov RK, Pekshev AV, Kozlov NP, Perov YL. Experimental and clinical validation of plasmadynamic therapy of wounds with nitric oxide. *Bulletin of Experimental Biology and Medicine*, 1998;126(2):829–834.
 31. Shekhter AB, Serezhenkov VA, Rudenko TG, Pekshev AV, Vanin AF. Beneficial effect of gaseous nitric oxide on the healing of skin wounds. *Nitric Oxide-Biology and Chemistry*, 2005;12(4):210–219.
 32. Babb R. Intestinal gas (Medical Information). *West J Med*, Oct. 1977. 127:362–363.
 33. Cooper HS, Murthy SN, Shah RS, Sedergran D J. Clinicopathologic study of dextran sulfate sodium experimental murine colitis. *Lab Invest* 1993;69(2):238–49.
 34. Flangian SM. Animal models of Inflammatory bowel disease. *In vivo model of Inflammation*. Birkhause Publication 1999, Switzerland.
 35. Kitajima S, Takuma S, Morimoto M. Changes in colonic mucosal permeability in mouse colitis induced with dextran sulfate sodium. *Exp Anim* 1999. 48(3): p. 137–43.
 36. Pravda J. Radical induction theory of ulcerative colitis. *World J Gastroenterology*, 2005;11(16):2371–84.

Comparison of Point-to-Plane and Point-to-Point Corona Discharge for the Decontamination or Sterilization of Surfaces and Liquids

V. Scholtz,^{1,*} J. Julák,² & B. Štěpánková¹

¹Department of Physics and Measurements, Faculty of Chemical Engineering, Institute of Chemical Technology, ²Institute of Immunology and Microbiology, 1st Faculty of Medicine, Charles University

*Address all correspondence to: V. Scholtz, Department of Physics and Measurements, Faculty of Chemical Engineering, Institute of Chemical Technology, Technická 5, 166 28, Praha, Czech Republic; scholtzv@vscht.cz

ABSTRACT: We studied the decontamination of surfaces and inactivation of bacteria and yeast in liquids by low-temperature plasma generated in the DC corona discharge of an open-air type in the point-to-plane or point-to-point arrangement. We found that the inactivation in liquid suspensions is slightly more efficient with the point-to-plane discharge in comparison with the point-to-point one. In the case of agar surface decontamination, two types of inhibition zones were observed, which indicates the different mechanism of action for the point-to-point and point-to-plane discharges. This knowledge may be important in the future selection of microbicidal agents and in the development of efficient methods for low-temperature plasma decontamination or sterilization.

KEY WORDS: decontamination, inactivation, corona discharge, bacteria, yeast

I. INTRODUCTION

The action of the plasma generated by electric discharges is one of the possible methods of inactivation of bacteria and other microbes, mediated by the bactericidal action of UV light and reactive particles. The method is not yet frequently used in practice, but it is potentially important, especially for the decontamination or even sterilization of heat-labile or otherwise sensitive materials. The various experimental arrangements, advantages, and status of research in this field were reviewed in detail in many works, e.g.,^{1–5} This contribution is a part of our systematic study of properties and differences of various types and arrangements of DC discharges and their microbial effects.

II. APPARATUS, METHODS, AND THE MICROORGANISMS UNDER STUDY

We studied the inactivation of microbial suspensions on wet surfaces and in liquids by low-temperature plasma generated in the DC corona discharge. The used simple apparatus of an open-air type enabling the point-to-plane or point-to-point arrangement was previously described in Ref. 6 and is schematically shown in the Figure 1.

The negative point-to-plane corona discharge was generated on the point electrode

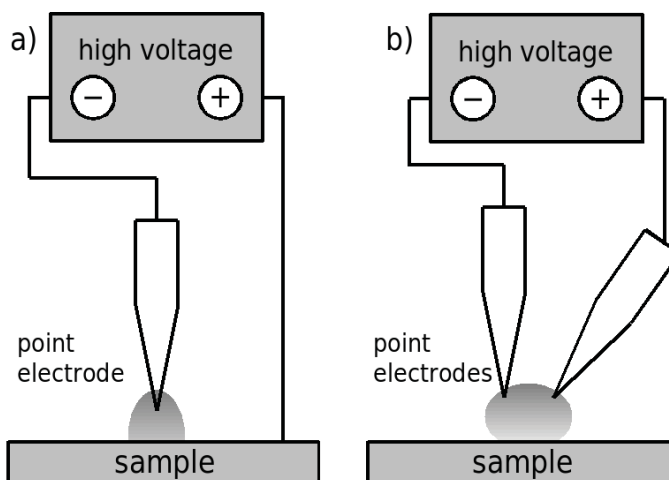


FIGURE 1. Schematic arrangement of used apparatus and the negative point-to-plane (a) and point-to-point (b) corona discharge.

represented by the tip of a hypodermic needle and situated 4 mm over the sample. The plane anode was the conducting surface of an agar cultivation medium. The bipolar point-to-point corona discharge was generated on a pair of hypodermic needles arranged at an angle of 30 deg with tips approximately 4–6 mm apart and situated 4 mm over the sample.

For the surface decontamination, 1 ml of the microbial suspensions were inoculated onto the surface of Sabouraud or Mueller-Hinton agar (Lab M, Ltd.), diluted to obtain a microbial concentration of 10^6 cfu/cm². After the suspension soaked, the samples were exposed to the corona discharge and incubated at 37 °C for 24 h, and the inhibition zones were measured. In the case of liquid samples, a 0.25 µl drop of an appropriate microbial suspension in physiological saline, adjusted to the concentration of ca. 10^6 cfu/ml, was placed on the hydrophobic surface of a sterile silicone disk and exposed to the discharge. The disk was then washed in 1 ml of physiological saline; this saline was inoculated onto Sabouraud or Mueller-Hinton agar, incubated as above, and the number of colonies was counted.

The microorganisms under study were “wild” strains of the following species isolated at the Institute of Immunology and Microbiology: a yeast, *Candida albicans*, a gram-negative bacterium, *Escherichia coli*, and a gram-positive bacterium, *Staphylococcus epidermidis*.

III. EXPERIMENTS

The experiments were performed under the following parameters. The point-to-plane discharge was adjusted to the current $I = 0.05$ mA and its voltage was $U = 4.6$ kV or

$U = 9$ kV for the surface or liquid sterilization, respectively. The point-to-point corona discharge was adjusted to the current $I = 0.2$ mA and voltage $U = 10$ kV. The different parameters for particular discharge types were determined by the different character and geometry of discharges. The values represent a compromise between discharge stability (transition into spark) and its energy, and enable the qualitative comparison of both discharge types.

The samples on the surface of agar were exposed for 8 min. The samples of liquid suspension were exposed for different times from 0.5 min up to 8 min, with the step of 30 s.

IV. RESULTS

For liquid samples exposed to the point-to-plane discharge, we found that all bacterial and yeast suspensions yielded no growth on Mueller-Hinton or Sabouraud agar after 2 min of exposure. In the case of point-to-point discharge, the complete inactivation was observed after 2 min for *S. epidermidis*, 2.5 min for *E. coli*, and 4 min for *C. albicans*. Although the parameters and power of both discharge types were different, for the liquid decontamination, a comparable inactivation effect may be concluded.

More interesting results were obtained after exposure of inoculated agar surfaces. In the case of point-to-plane discharge, we obtained circular and sharply bordered inhibition zones with diameters of 5–6 mm, which were completely clear and contained no growing microbes. However, after exposure to point-to-point discharge, we obtained two types of asymmetric fan-shaped zones of incomplete inhibition. In the case of *C. albicans* yeast and gram-positive bacterium *S. epidermidis*, the inhibition zones were well bordered and almost clear of any surviving colonies, whereas for the gram-negative bacterium *E. coli*, we obtained larger fan-shaped zones containing a reduced number of surviving colonies and very small, if any, zone of total inhibition only. The areas of total inhibition were approximately of 3 cm² for *C. albicans* and 1 cm² for *S. epidermidis*. The zone of incomplete *E. coli* inhibition was of 10 cm². The representative photographs of the zones obtained for point-to-plane and point-to-point discharges are shown in Figures 2 and 3, respectively. As contrasted to the inactivation in suspension, the inhibition effect of the point-to-point discharge differs from the effect of the point-to plane arrangement. This is probably caused by the different plasma-chemical processes in the discharge.

V. CONCLUSIONS

We found that the microbial inactivation in liquid suspensions is slightly more efficient using the point-to-plane discharge geometry than in the point-to-point arrangement. In the case of surface decontamination, it can be concluded that the mechanisms of microbial inactivation are different in these two discharge types. While in the case of point-to-plane discharge the inhibition zones are similar, in the case of point-to-point discharge, the appearance of two different inhibition zones occurs. This fact supports the conclusion that the sterilization agents are of a different nature in the point-to-point and

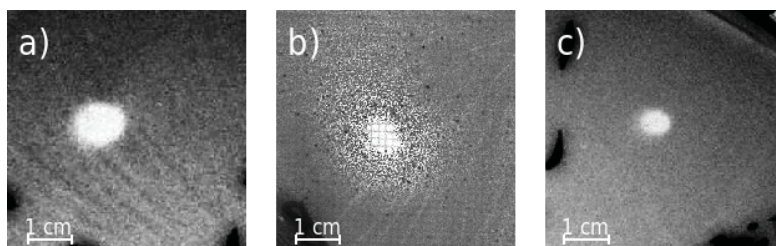


FIGURE 2. Representative photographs of the inhibition zones after 8 min of exposure to the negative point-to-plane corona discharge at $I = 0.05$ mA and $U = 4.6$ kV. Tested microorganisms were *C. albicans* (a), *S. epidermidis* (b), and *E. coli* (c)

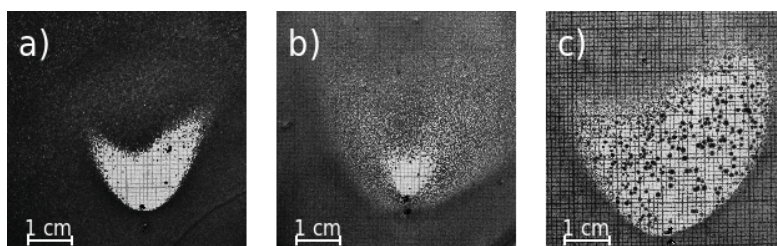


FIGURE 3. Representative photographs of the inhibition zones obtained after 8 min of exposure to the point-to-point bipolar corona discharge at $I = 0.2$ mA and $U = 10$ kV. Tested microorganisms are *C. albicans* (a), *S. epidermidis* (b), and *E. coli* (c)

point-to-plane discharges, displaying different efficiency and probably different mechanisms of action on microorganism's structures. We still have no explanation of this difference, which should be the subject of the future study, because it may be important for the selection of adequate microbicidal agents and for the development of efficient low-temperature plasma decontamination methods.

ACKNOWLEDGMENTS

This study has been supported by Grants No. MSM ČR 6046137306 and No. MSM ČR 0021620806 and No. SVV-2010-260506.

REFERENCES

1. Birmingham JG. Mechanisms of bacterial spore deactivation using ambient pressure non-thermal discharges. *IEEE Trans Plasma Sci.* 2004;32:1526–31.
2. Fridman Gregory, Brooks AD, Balasubramanian M, Fridman A, Gutsol A, Vasilets VN, Ayan H, Fridman Gary. Comparison of direct and indirect effects of non-thermal atmospheric pressure plasma on bacteria. *Plasma Process Polym.* 2007;4:370–5.
3. Laroussi M. Nonthermal decontamination of biological media by atmospheric-pressure plasma: review, analysis and prospects. *IEEE Trans Plasma Sci.* 2002;28:1409–15.

4. Laroussi M. Low temperature plasma-based sterilization: overview and state-of-the-art. *Plasma Process. Polym.* 2005;2:391–400.
5. Scholtz V, Julák J, Kříha V. The microbicidal effect of low temperature plasma generated by corona discharge: comparison of various microorganisms on an agar surface or in aqueous suspension. *Plasma Process Polym.* 2010;7:237-43.
6. Julák J, Kříha V, Scholtz V. Corona discharge: a simple method of its generation and study of its bactericidal properties. *Cz J Phys.* 2006;56:B1333–8.

Response of Human Glioma U87 Xenografted on Mice to Non Thermal Plasma Treatment

Marc Vandamme,^{1,2,*} Eric Robert,¹ Sébastien Dozias,¹ Julien Sobilo,² Stéphanie Lerondel,² Alain Le Pape,² & Jean-Michel Pouvesle¹

¹GREMI UMR-6606 CNRS, France, Université d'Orléans, ²TAAM-CIPA, UPS44 CNRS, France

*Address all correspondence to: Marc Vandamme, GREMI UMR-6606 CNRS, Université d'Orléans, 14 rue d'Issoudun, BP 6744, 45067 Orleans cedex 2, France; Fax: 33 (0) 2 38.41.71.54; marc.vandamme@cns-orleans.fr

ABSTRACT: Non thermal atmospheric plasma is a new promising candidate in anticancer therapy. We have already reported the absence of skin damage induced by our plasma treatment. Preliminary results suggested that this treatment could also induce an antitumor effect on U87 malignant glioma xenografts, and we conducted this work to evaluate the antitumor efficacy of plasma in this model. Antitumor effects were assessed by tumor volume measurement and bioluminescence imaging (BLI). Plasma treatment was applied during five consecutive days in open air with a μ s-duration pulsed floating electrode dielectric barrier discharge (FE-DBD), which delivered about 0.75 W at 200 Hz on the mouse skin. Our results showed a significant tumor volume decrease of 56% for treated mice at the end of the treatment, with a concomitant decrease of BLI intensity. Moreover, this tumor volume reduction translated into an increase of mouse life span of 60%, median survival being 9.5 and 15.0 days for control and plasma-treated mice, respectively. In conclusion, our study demonstrates a marked antitumor effect of plasma treatment in U87 glioma xenografts. These results, obtained in both a radio and chemoresistant model, are very promising and highlight the potential of plasma treatment as an anticancer treatment with little or no toxic side effects.

KEY WORDS: cancer therapy, dielectric barrier discharge (DBD), non thermal plasma, glioma, xenograft model antitumor assay

I. INTRODUCTION

In Europe, estimated new cancer cases in 2006 were about 3.2 million and represented 1.7 millions of deaths.¹ In many tumor types, survival has not significantly increased in the past decades, despite the emergence of new targeted chemotherapy. New treatment concepts or cytotoxic drugs are urgently needed to improve cancer patient outcome. In this context, we evaluated the interest of a local treatment with non thermal atmospheric pressure plasma as a new antitumor treatment. We choose to perform this evaluation on U87-MG, a high-grade glioma model, which is a representative model of brain tumor typically used for treatment efficacy screening. Malignant gliomas are the most common primitive human brain tumors and represent one of the most aggressive tumor types.^{2,3} Indeed, despite aggressive treatment including chemo- and radiotherapy, the median survival for patients of newly diagnosed malignant glioma is restricted to 8–15 months.^{2,3}

Over the past few years, non thermal atmospheric pressure plasma has emerged as a novel promising tool in medicine.⁴ Non thermal plasma is a partially ionized gas, containing electrons, positive/negative ions, radicals, various excited molecules, energetic photons (UV), and generating transient electric field. Electrons present in non thermal plasma are highly energetic, with a typical temperature above 10,000 K, while ions and neutral species remain at room temperature.

Numerous applications of plasma have been investigated, including sterilization and bacterial decontamination.^{5,6} Chemically reactive species and especially short-lived radicals such reactive oxygen species (ROS) are of major importance for bacterial decontamination.⁷ Atmospheric plasmas have also proved their efficacy in blood coagulation by catalyzing the natural blood coagulation processes.⁸ Moreover, treatment of biological tissue and cells has been investigated. Pioneer studies exploring plasma effects on cells have shown an instantaneous detachment of Chinese hamster ovarian (CHO-K1) cultured cells from the surface for low doses of plasma (<0.2 W), while higher doses induce severe damage and necrosis.⁹⁻¹¹ Cell detachment after plasma treatment was also observed in other models.^{12,13}

An induction of apoptosis on 3T3 mouse fibroblast was observed 24 hr after plasma needle treatment,¹⁰ and induction of in vitro tumor cells death was reported by several authors.^{14,15} For example, Fridman et al. have shown an apoptosis induction of the melanoma cancer cell line with the use of an FE-DBD plasma.¹⁴ Kim et al. have also reported that plasma treatments induce cell death in a melanoma cell line, and that this effect was potentiated by association of plasma with antibody-conjugated nanoparticles.¹⁵ DNA damages, cytoskeletal damages, membrane cell charging, and permeation have been proposed to participate in apoptosis induction.^{14,16} However, apoptotic processes involved remain rather unclear and need further investigations.

These encouraging results dealing with in vitro induction of apoptosis on different cell lines led us to explore effects of plasma treatment on xenograft tumor, the first in vivo approach on potential antitumor effect of non thermal treatment. Results of this treatment were unpredictable due to the fact that interaction between plasma and tumor cell might be quite different in in vitro and in vivo experiments. In particular, the presence of the skin and the use of a 3D tumor model might introduce crucial changes and modify the in vivo antitumor effects of plasma.

To develop plasma for in fine clinical applications, plasma tolerance and effects on organisms have to be determined. Fridman et al. have shown that plasma can be applied directly to a living tissue, and have determined the maximum tolerated dose of plasma DBD on mouse skin by histology analysis.⁸ We have previously shown the safety of our plasma treatment protocol for the whole mouse organism and the absence of skin damages of the treated zone.¹⁷ Moreover, an in vivo antitumor effect of plasma treatment was also observed in a small cohort of mice.¹⁷

The U87-MG glioma cell line was chosen to perform this in vivo antitumor efficacy study. This cell line is characterized by a high radio and chemoresistance, and is an adequate model to explore a significant antitumor effect. Moreover, heterotopically

grafted, this cancer cell line presents a hemispherical growth that is a well-suited configuration for treatment with plasma and allows an accurate following of tumor growth by caliper measurement. This plasma treatment was performed in open air with a μ -duration pulsed FE-DBD that delivered less than 0.75 W on the mouse skin at 200 Hz. In this configuration, discharge ignites when the powered electrode approaches the tumor surface at a distance of less than ~ 3 mm.

In this work, we first characterized the plasma generated by the developed FE-DBD system through electrical measurements. Plasma homogeneity during tumor treatment was analyzed with an ICCD camera. Then, we investigate whether five consecutive days of plasma treatment during 6 min per day induced an antitumor effect on U87 glioma-bearing mice by tumor volume measurement and bioluminescence imaging.

II. MATERIAL AND METHODS

A. Experimental Setup

For all experiments, we used a dielectric barrier discharge (DBD) plasma. Figure 1 presents the whole experimental equipment, and Figure 2 represents the DBD power supply schematic.

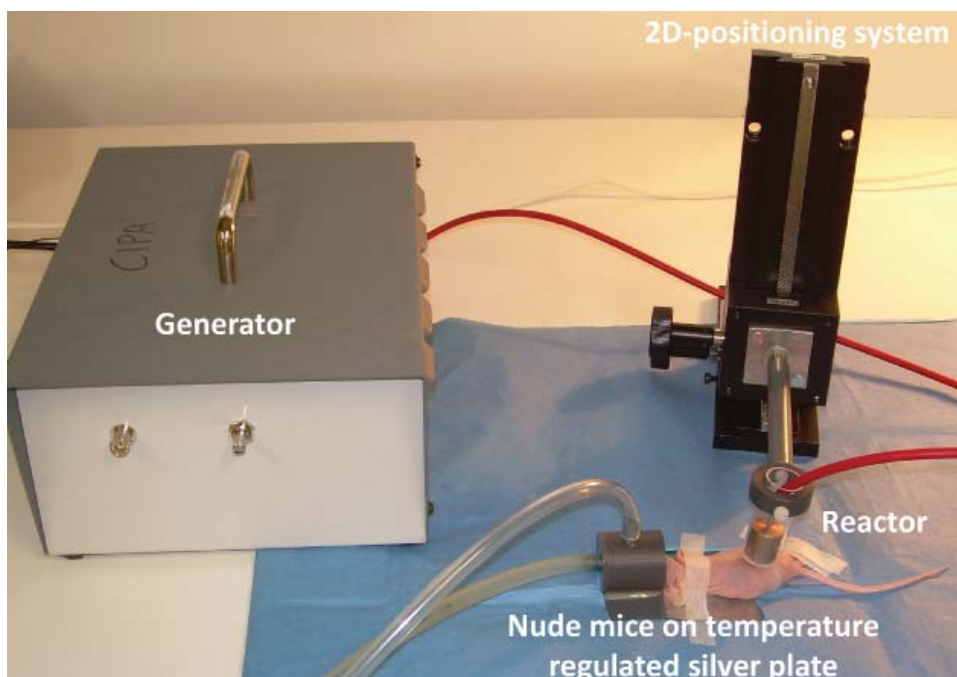


FIGURE 1. Picture representing the whole experimental equipment used to produce DBD plasma. To perform plasma treatment, mice were placed on a temperature-regulated silver plate.

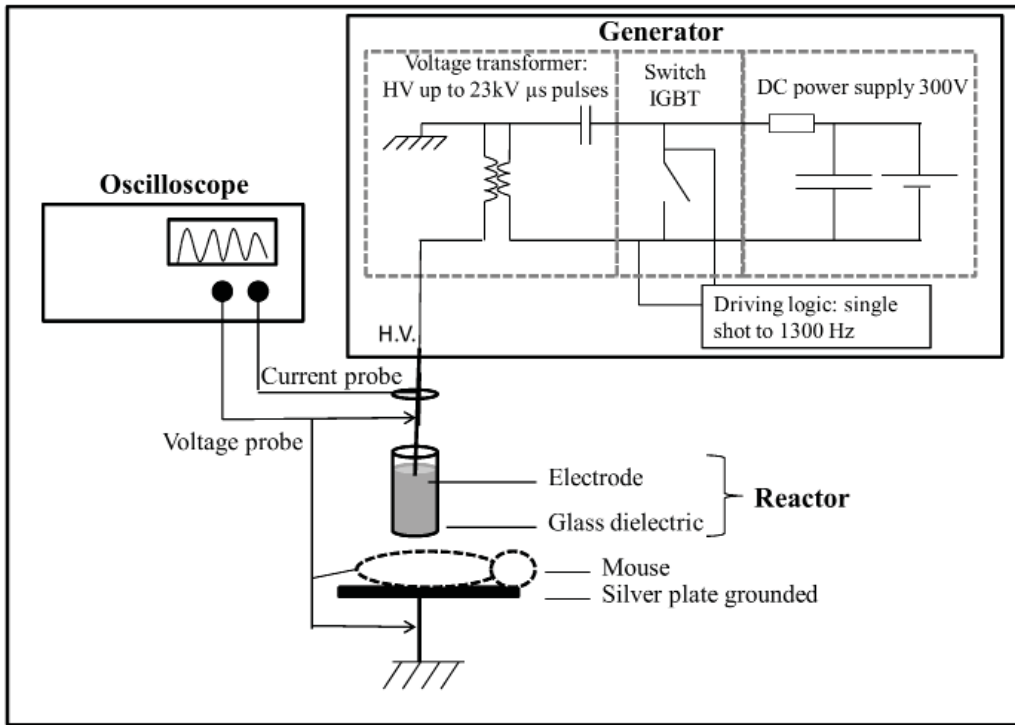


FIGURE 2. Schematics of the DBD setup and of the pulsed power supply.

The electrical driver articulates around three main subassemblies, namely, a DC power supply, a solid state switch, and a voltage pulse transformer. The 300 V amplitude DC power supply is used to store energy in a 700 nF capacitor. The fast discharge of this capacitor is triggered at a variable repetition rate through an IGBT switch in the primary coil of a transformer that allows to produce a voltage pulse amplitude reaching up to 23 kV in the present setup. The high-voltage (HV) pulse is applied on an HV voltage electrode consisting of a 10 mm high, 17 mm diameter aluminium cylinder. This HV electrode is inserted inside a 1 mm thick, 60 mm high, and 19 mm outer diameter borosilicate glass tube. The bottom base of this glass tube is glued with a 1 mm thick borosilicate disk, 19 mm in diameter, which acts as the dielectric wall of the DBD reactor. This system generates air plasma from the external surface of the dielectric barrier disk and a living organism that is placed on a ground plate electrode. This DBD system can produce discharges with frequency that can vary from a single shot to 1300 Hz. The energy stored in the DC powered capacitor multiplied by the generator repetition rate provides the maximum available power.

For a pulse repetition rate of 200 Hz, the maximum power available is ~ 6.3 W, leading to a maximum power density of 2.7 W/cm², when considering a uniform distribution of the discharge over the 2.3 cm² surface of the glass disk. This rough estimate indicates

the maximum mean power density, since it neither accounts for the random filamentary nature of the DBD discharge nor for the power losses associated with the impedance mismatching between the driver output and the DBD reactor. For all tests discussed in this paper, non thermal plasmas were generated in ambient air at atmospheric pressure.

B. Diagnostics

A HV probe (Tektronix P6015A, 75 MHz bandwidth) and a current probe (Tektronix TCP202, 50 MHz bandwidth) were used to characterize the voltage and current waveforms delivered across the DBD reactor. Both probes were connected to an oscilloscope (Tektronix TDS510A).

Discharge homogeneity was analyzed with the use of an ICCD camera (PI-Max, Princeton Instruments) equipped with a 60 mm lens. Experiments were performed both in single-shot or multishot acquisition mode on few discharges, and by image accumulation over a few thousands of discharges, this latter measurement being much more representative of the mouse plasma treatment.

C. Animals and Tumors

Female athymic NCr/Sed nude (nu/nu) mice, five to six weeks of age, were purchased from Charles River (St. Germain sur l'Arbresle, France) and housed for one week before experimentation. For all experiments, animals were housed in plastic cages inside a controlled ventilated rack and had access to food and water ad libitum. Animal procedures were performed according to institutional and national guidelines (EC directive 86/609/CEE, French decree No. 87-848). Tumor grafts, plasma irradiation, and bioluminescence imaging were carried out under general gaseous anesthesia obtained with 3% isoflurane (Aerrane, Baxter, Deerfield, Connecticut) in air.

Tumor xenografts were originally obtained by subcutaneous injection of a suspension of U87-Luc human malignant glioma cells (10^6 cells in 0.1 mL 0.9% NaCl) into the hind legs of mice. This cell line purchased from Caliper is stably transfected with firefly luciferase gene. U87 xenografts were then maintained in vivo by sequential passages of tumor fragments in nude mice grafted in the inguinal pit.

D. Treatment Procedures

Treatment started when tumors reached a volume of $150 \pm 50 \text{ mm}^3$ (D_0). Mice were randomly assigned into two groups. In the control group, mice were not treated. In the plasma group, mice received plasma treatment for five consecutive days. Tumor treatments on mice were performed at 200 Hz in open air each day during 6 min (three periods of 2 min separated by 1 min). To perform plasma treatment, anesthetized mice were placed on a humidified, temperature-regulated silver plate, and the plasma reactor was positioned at a distance of 2 mm from the tumor (Fig. 1). These treatment parameters and procedure ensure reproducibility of plasma treatment and limit side effects on mice.

E. Antitumor Effect of Plasma Treatment

To follow tumor growth, tumor volume was determined every day with the international current standard technique for tumor volume measurement.^{18,19} Two perpendicular diameters were measured with a caliper. Tumor volume (V in cubic millimeters) was calculated as $V = (\text{length} \times \text{width}^2)/2$.^{18,19} Mice were anesthetized and killed by cervical dislocation when a tumor reached 1000 mm³, thus defining the “survival times.” The percentage of increase in the life span was calculated as $(T-C)/C \times 100$, where T and C are the survival times of the treated and control animals.

Tumor response to plasma treatment was also assessed by BLI before D_0 and 48 hr after treatment completion (D_6). Bioluminescence allows the evaluation of very early stages of antitumor effect prior to physical reduction of tumor volume since bioluminescence intensity is closely dependant on tumor activity.²⁰ Mice were intraperitoneally injected with 2 mg beetle luciferin (potassium salt, Promega) and were then anesthetized. Ten minutes later, bioluminescence imagings were carried out using an ORCA II BT C4742-98-26 LW (Hamamatsu Photonics, Massy, France). Data acquisition was achieved using HiPic software (Hamamatsu Photonics). Merging of bioluminescence images and regions of interest quantification were obtained using ImageJ software (<http://rsb.info.nih.gov/ij/index.html>).

F. Statistical Analysis

Unless otherwise noted, data were reported as mean \pm SEM (standard error of the mean). Statistical analysis was performed using GraphPad 5.0 software (GraphPad Prism 5.0 Software MacKiev GraphPad Software, Inc. 1994–2005). For each parameter analyzed, treated and nontreated tumors were compared using the nonparametric Mann-Whitney U test. Kaplan-Meier curve analysis was performed using the log-rank test. Differences were considered significant at p values <0.05 .

III. RESULTS

A. Plasma Characterization

Figure 3 presents the voltage and discharge current signals measured for a 200 Hz repetition rate operation. The voltage waveform exhibits a 4.5 μs rising front up to a 23 kV amplitude, and a damped oscillation vanishing over about 25 μs . This voltage waveform was measured to be constant whatever the pulse repetition rate is up to 1300 Hz, and also for gap thicknesses ranging from 0.5 mm to a few millimeters; this latter condition corresponding to the absence of the DBD plasma associated with streamer formation across the air gap. The current probe, surrounding the cable connected to the HV electrode, measures the total current, which is the sum of the displacement current across the dielectric barrier and the actual discharge current flowing across the air plasma. The discharge current presented in Figure 3 is thus inferred from the probe measurement

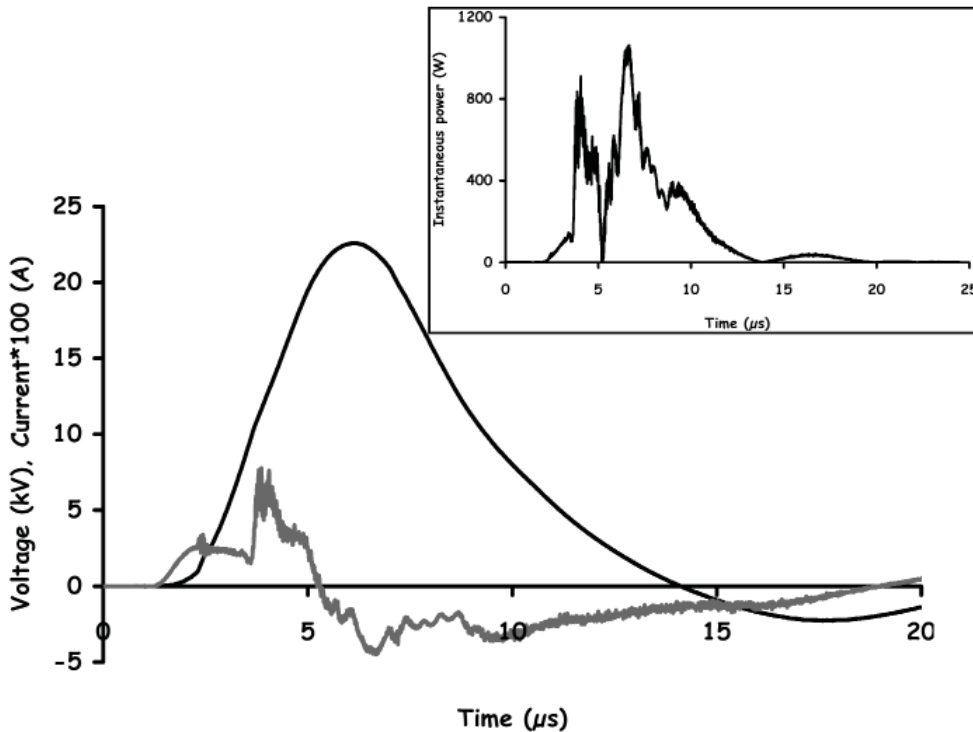


FIGURE 3. Voltage (dark line) and current (gray line) measured during a treatment with the discharge repetition rate at 200 Hz.

by subtracting to the total current waveform, the displacement current signal measured when no plasma is produced, which is for an air gap larger than 5 mm in our experimental conditions. This method for actual plasma discharge current measurement was inspired by the results published by Lu and Laroussi.²¹ With the relatively slow rise time of the voltage pulse delivered by our electronic driver, the discharge current consists of a superposition of current spikes having duration of a few nanoseconds; the limited bandwidth of the probe used in this work results in the temporal integration of these spikes, which are measured as 20 ns long current pulses. Time-resolved ICCD imaging experiments, not presented in this paper, have shown that streamer production in the air gap is observed during about 20 μs after the current signal onset. The insert in Figure 3 presents the evolution of the instantaneous power delivered across the plasma during the whole voltage pulse application. Peak power reaches about 1 kW while the whole temporal integration of the power signal indicates that, for a 200 Hz repetition rate, 0.75 W are coupled to the DBD plasma. This corresponds to a maximum power density applied on the mouse skin of 0.33 W/cm². This value is below that required for a safe treatment without any significant damage on the skin for a three times 2 min exposure.¹⁷

Figure 4 presents two ICCD images recorded during application of the air plasma on the mouse skin at a 200 Hz repetition rate and for a gap of about 2 mm. Figure 4A and the corresponding radial profile Figure 4C are obtained for a 10-discharge averaging, while Figures 4B and 4D correspond to an average over 5000 discharge events. The radial profiles, extracted from the ICCD images, are averaged along the vertical axis over a distance of 0.5 mm above the mouse skin, and correspond to the same space location. Each profile was then normalized to allow for a more straightforward comparison of their radial shape along the 14 mm wide zone, corresponding to the visible light air plasma emission region observed by the ICCD camera, in the horizontal axis direction. Both for 10 and 5000 discharge accumulations, the images and the corresponding profiles exhibit some rather flat background intensity level over which narrow and intense channels superimpose. Nevertheless, the calculations performed from the image profiles indicate that a significant reduction of about 40% of the standard deviation of the mean intensity value, from pixel position 50 to pixel position 200 in Figures 4C and 4D, is achieved for the 5000-accumulation recording in comparison with the 10-discharge averaging measurement. It must be remembered that plasma treatment of tumor is performed during 6 min at 200 Hz, thus involving the accumulation of 72000 discharges. The mouse's breathing and the accumulation of such a large number of discharge result in the averaging of the gap thickness and the homogenization of the plasma action over the mouse skin.

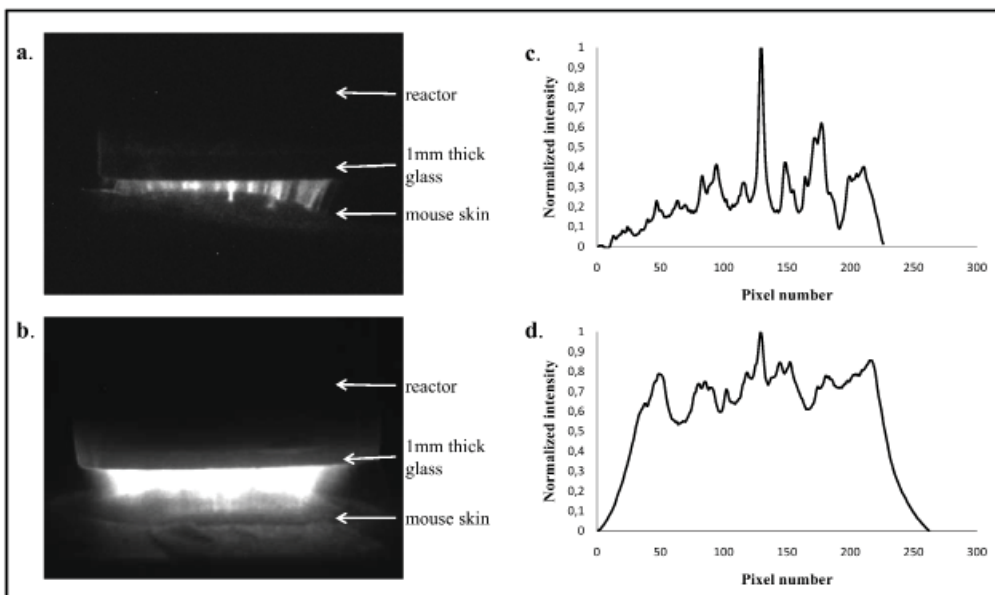


FIGURE 4. ICCD images recorded during application of the air plasma on the mouse skin at a 200 Hz repetition rate and for a gap of about 2 mm. Image in (A) and the corresponding radial profile (C) are obtained for a 10-discharge averaging, while (B) and (D) correspond to an average over 5000 discharge events.

B. Plasma Induces Short-Term Antitumor Effects

To explore the antitumor effect of plasma, treatment was applied every day for five consecutive days. We explored plasma treatment efficacy by tumor volume determination and by bioluminescence assay.

We first evaluated plasma antitumor activity after plasma treatment completion. To this end, treatment started when tumors reached a volume of $150 \pm 50 \text{ mm}^3$, corresponding to D_0 . Mice were randomly assigned into two groups, namely, the control (CTRL) and plasma (PLASMA) groups. Tumor volume was measured at day six (D_6), corresponding to 48 hr after the last plasma treatment. As shown in Figure 5, at the beginning of treatment, mean tumor volumes of CTRL and PLASMA groups were similar ($p = 1.0$). At D_6 , mean tumor volume was $585 \pm 101 \text{ mm}^3$ in CTRL group, whereas the mean volume of plasma-treated tumors only reached $259 \pm 45 \text{ mm}^3$. This significant reduction of tumor growth ($\sim 56\%$, $p = 0.03$) showed a marked plasma antitumor effect as early as the end of our treatment protocol (Fig. 6). However, tumor volume determination by caliper reflects total tumor tissue mass including areas of necrosis and edema, and so does not necessarily assess the effect of a treatment on the number of viable tumor cells.

Therefore, bioluminescence imagings were performed at D_0 and D_6 . Figure 7 represents the ratio D_6/D_0 of BLI intensity, corresponding to the evolution of tumor activity between the beginning and the end of the treatment. As expected, plasma treatment induced a lower increase of BLI ratio than the increase obtained in the CTRL group. Indeed, in the CTRL group, we observed a 24-fold BLI intensity increase during the

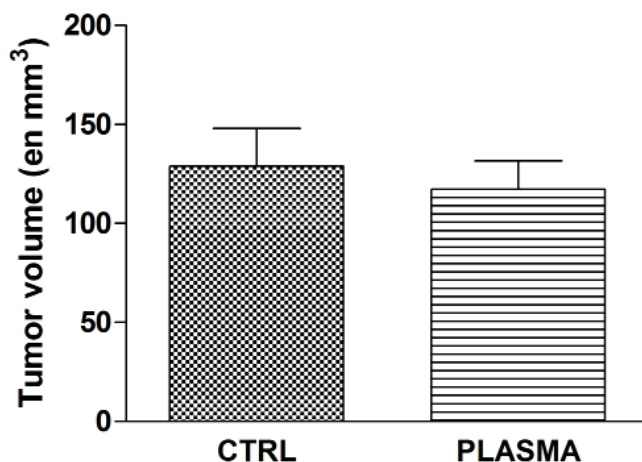


FIGURE 5. Tumor volume at the beginning of plasma treatment. Tumor volumes were measured with a caliper at the beginning of plasma treatment (D_0). The column represents the mean (\pm SEM) of tumor volume. $*p < 0.05$, $n = 8$ for each group.

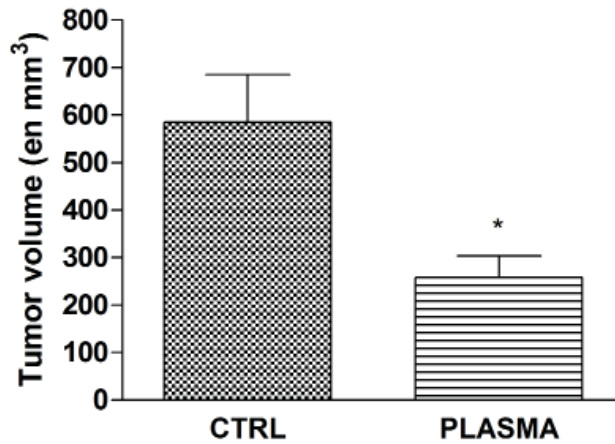


FIGURE 6. Effect of five consecutive plasma treatments on tumor volume. Plasma was administered when tumor reached $150 \pm 50 \text{ mm}^3$ and consisted of five daily fractions (6 min, 200 Hz). Tumor volumes were measured with a caliper on the sixth day. The column represents the mean (\pm SEM) of tumor volume. * $p < 0.05$, $n = 8$ for each group.

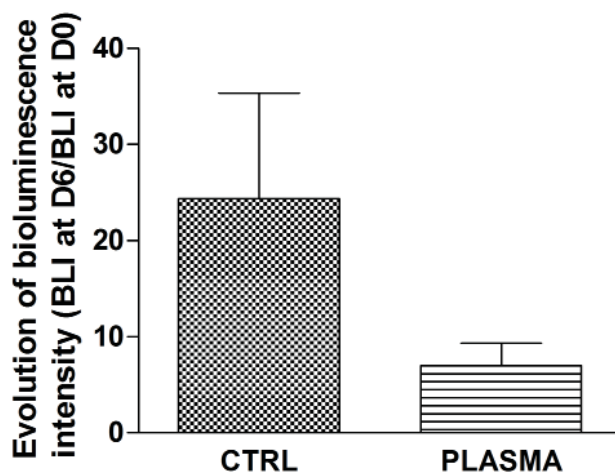


FIGURE 7. Tumor bioluminescence intensity at the end of plasma treatment. Plasma was administered when tumor reached $150 \pm 50 \text{ mm}^3$ and consisted of five daily fractions (6 min, 200 Hz). In vivo bioluminescence imaging were performed before and then 24h after five consecutive days of treatments. Columns represent the mean (\pm SEM) of tumor bioluminescence intensity at day six normalized to tumor bioluminescence intensity before treatment. $n = 8$ for each group.

treatment period, while in the PLASMA group, BLI intensity only increased sevenfold during the same treatment course. This reduction of BLI ratio ($\sim 70\%$) is consistent with the effect of plasma treatment on tumor volume at D_6 described above.

C. Plasma Induces Long-Term Antitumor Effects

To evaluate long-term treatment effects, tumor growth was followed every day until the tumors reached 1000 mm^3 (Fig. 8). In the CTRL group, tumors grew exponentially and the mean time to reach 1000 mm^3 was 9.6 ± 0.9 days. Plasma treatment was administered for five consecutive days from D_0 to D_4 . During the treatment course, tumors did not significantly grow, mean tumor volume remaining stable between D_0 and D_4 (Fig. 8). After treatment completion, we observed a raise of tumor growth in plasma-treated mice, but tumor growth seemed less rapid than in the CTRL group. The mean time to reach 1000 mm^3 was 15.0 ± 0.8 days. Tumor growth delay, corresponding to the difference of times needed to reach 1000 mm^3 between CTRL and PLASMA groups, was 5.4 days for plasma-treated tumors, illustrating a significant antitumor effect of plasma. Moreover, we have included in our study a few mice bearing two xenografts (in each inguinal pit), the first one receiving plasma treatment, and the second one being used as a control, to determine whether plasma effects are localized. We have observed that kinetic growths of CTRL and plasma-treated tumors were similar to those of mice bearing only one tumor, highlighting a plasma effect limited to the treated zone.

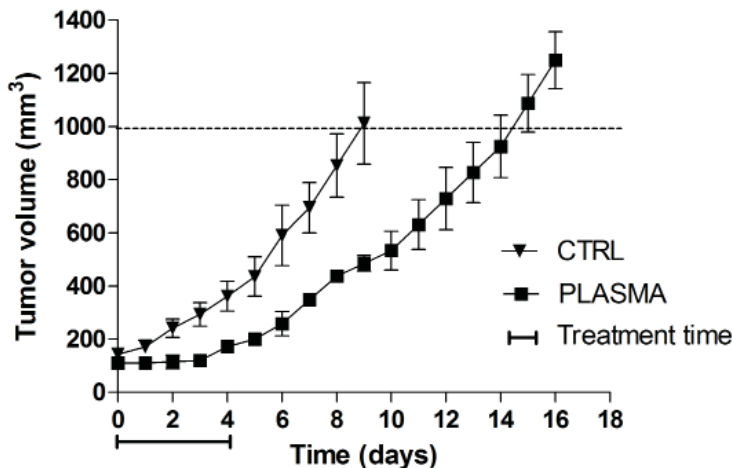


FIGURE 8. In vivo antitumor efficacy of plasma treatment. Plasma was administered when tumor reached $150 \pm 50 \text{ mm}^3$ and consisted of five daily fractions (6 min, 200 Hz). Tumor volumes were measured every day with a caliper until tumor reached a volume of 1000 mm^3 . Each point represents the mean (\pm SEM) of tumor volume. $n = 8$ for each group.

The plasma effect was also evaluated using Kaplan-Meier curve analysis (Fig. 9), considering the percentage of tumor not having reached 1000 mm³ as the survival endpoint. Median survival was 9.5 days in the CTRL group. When mice received plasma treatment, the survival curve clearly shifted to the right, and the median survival was 15.0 days in the PLASMA group (versus CTRL $p = 0.002$). This translates into an increase of life span of mice of ~58%.

IV. DISCUSSION

Non thermal atmospheric plasma has emerged as a novel, promising tool in medicine. Indeed, the existence of various components in plasma such as electric field, UV radiation, uncharged species, electrons, and ions, which could interact with the treated tissue, makes plasma a good candidate for cancer treatment. Our preliminary data showed the safety of plasma treatment for the whole mouse organism and the absence of skin damages with our treatment parameters.¹⁷ An antitumor effect of plasma treatment was also observed using a small cohort of mice.¹⁷ To confirm these promising results, we performed this study on a larger number of U87-bearing mice.

In our experiments, we treated mice during five consecutive days for 6 min each day at 200 Hz. This treatment protocol did not show any life-threatening effects on mice. We

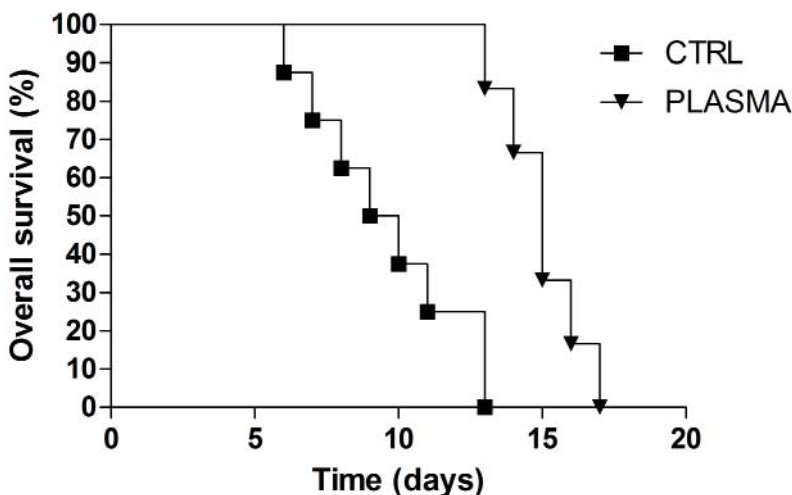


FIGURE 9. Response of subcutaneous glioma xenografts to plasma antitumoral treatments. When tumor reached 150 ± 50 mm³, mice were randomly assigned into two groups, namely, CTRL and PLASMA, eight mice per group. Plasma treatments were delivered for five consecutive days (6 min, 200 Hz). Results are expressed as Kaplan-Meier plots, considering the percentage of tumor not having reached 1000 mm³ as the survival endpoint.

evaluated plasma discharge homogeneity during mice treatment with an ICCD camera. It has been shown that the accumulation of a few thousands of discharges result in a significant homogenization of the plasma treatment over the mouse skin, while single-shot or a reduced number of discharge event operations would result in a very inhomogeneous skin surface treatment, inherent with the microsecond-duration DBD plasma including very narrow streamer channels. One promising issue to achieve a much higher spatial homogeneity, which may be required if the plasma treatment is fractioned in a great number of short duration exposures, each involving a reduced number of discharge accumulation, being to develop nanosecond DBD plasmas.²²

In this study, we chose to evaluate the potential antitumor effect of plasma on U87 high-grade glioma. Malignant brain tumors remain a therapeutic challenge, i.e., despite aggressive surgery, radiotherapy, and chemotherapy, prognosis of patients with high-grade glioma remains poor and their life expectancy is reduced to few months.^{2,3} In the U87 model, our plasma treatment showed a significant reduction of tumor volume (~56%) at the end of the treatment period, as compared to nontreated mice. This result was confirmed by BLI imaging, which exhibited a lower increase of BLI intensity for treated tumor as compared to CTRL, with a reduction of BLI ratio of ~70%. This demonstrates an important effect of plasma on tumor activity, since BLI represents a gene expression closely dependent on proliferation and metabolism of all tumor cells. This result also showed that plasma treatment on a tumor of 200–300 mm³ (corresponding to a tumor length of ~10–11 mm and thickness of ~7–8 mm) induces an effect on the majority of tumor cells, reflecting a high penetration depth of plasma effect. All of these illustrate a marked plasma antitumor effect as early as five days after treatment onset. To the best of our knowledge, plasma has already shown an antitumor activity, but only in *in vitro* experiments. Here, we described an *in vivo* antitumor activity of plasma, which is in accordance with previously published data reporting an apoptosis induction on the CHO cell line and the melanoma cancer cell line.^{10,14,15}

Several reports have demonstrated the high resistance of U87-bearing mice to the cytotoxic effect of radiation therapy. The tumor control dose 50% or TCD₅₀ (the radiation dose necessary to locally control 50% of the tumor) of U87 malignant glioma *in vivo* was as high as 75.2 Gy for single-dose radiotherapy treatment,^{23,24} and this TCD₅₀ was even higher when radiation treatment was daily fractionated and applied at low dose (2 Gy per day).²⁵ This treatment schedule of 2 Gy per day during two weeks has been reported to produce an increase in life span of about 200% in U87-bearing mice.²⁶ In our study, plasma showed an increase of 60% of mice life span, which reflects a high cytotoxic effect of plasma treatment. Even if this increase in life span was smaller for plasma treatment than for radiotherapy, our treatment was applied during only five consecutive days at three times 2 min at 200 Hz. Given the very good tolerability of plasma, frequencies and treatment protocol duration could be increased to improve plasma efficacy. Indeed, we observed a stabilization of tumor volumes during treatment course, suggesting that a more prolonged treatment should be of valuable interest.

The high cytotoxic effect observed in this study could be mediated by several com-

ponents of plasma and involved different mechanisms. We have previously shown an increase of BLI intensity after the first day of plasma treatment,¹⁷ reflecting a possible tumor reoxygenation. This increase of oxygen supply and tumor reoxygenation could be linked to tumor temperature increase²⁷ and the diffusion through the skin of NO, a potent vasodilator.^{28,29} This tumor reoxygenation generally observed after radiotherapy induced a tumor cell sensitization to chemo-/radiotherapy, and such an effect could be transposed in our case.³⁰ Moreover, the authors have demonstrated a cytotoxic effect of UV-C radiation on *in vitro* U87 cell lines.³¹ However, UV-C penetration through the skin was limited (2 μm),³² and cannot reach the subcutaneous tumor in our model considering mouse skin thickness. Furthermore, electric fields are an important component of plasma and have also shown to induce an antitumor effect on U87 *in vivo* xenografts. This new antitumor strategy is currently evaluated in clinical trial for patients with recurrent glioblastoma.^{33,34} The presence of nanosecond electric pulse in plasma could induce an arrest of cell proliferation and contribute to the observed antitumor effect.

All these parameters (i.e., species, temperature, electric fields, etc.) could be toxic to cells, inducing membrane damages and changes in intracellular signaling pathways, finally leading to cell death. It is rather probable that, as observed for radiotherapy, efficacy of plasma treatment was tumor cell type dependent, and different parameters could be implicated in this effect as tumor hypoxia, cell cycle phase, and DNA repair capacities.^{35,36} Specific plasma can be created to produce either neutrals or charged particles: in particular, with the adjunction of gas mixtures such air/argon to raise up long-lived (O_3 , NO) and short-lived (OH, O) particles. This will help us to elucidate the critical mechanism(s) involved in plasma cytotoxic effects and thereafter to increase plasma treatment efficacy.

In the future, to improve plasma antitumor efficacy, it should be kept in mind that plasma treatment presents a broad range of effects. In particular, it has been shown that cells become transiently permeable during plasma exposure.^{37,38} This property could be of valuable interest to increase intracellular chemotherapy penetration and/or transfect therapeutic DNA into cancer cells. A concomitant administration of targeted chemotherapy with plasma treatment could improve efficacy of chemotherapy and plasma alone.

V. CONCLUSIONS

In conclusion, our study demonstrates a marked antitumor effect of plasma treatment in U87 glioma xenografts with a significant decrease of tumor volume at the end of treatment and an increase of mouse life span of 60%, thus confirming our previous data. These results, obtained in a radio and chemoresistant model, are very promising and highlight the potential of plasma treatment as an anticancer treatment with little or no toxic side effects. However, many questions remain unanswered, and further studies are required to elucidate mechanisms involved in this decrease of tumor volume; in particular, by apoptosis and cell cycle analysis. Moreover, studies to identify the main components of plasma implicated in the cytotoxic effect will allow us to develop plasma types with a greater efficacy. Indeed, our lab developed a pulsed plasma gun delivering

a very fast moving plasma bullet in a 200 μm inner diameter flexible dielectric capillary a few tens of centimeters long.³⁹ In the future, this plasma gun could be used for in situ cancer treatment by endoscopic application.

ACKNOWLEDGMENTS

This work was supported by Region Centre through the APR program "PlasMed." The authors thank the PlasMed medical advisory board of University Hospital in Tours and Regional Hospital in Orleans. M.V. is supported by a Germitec doctoral fellowship.

REFERENCES

1. Ferlay J, Autier P, Boniol M, Heanue M, Colombet M, Boyle P. Estimates of the cancer incidence and mortality in Europe in 2006. *Ann Oncol.* 2007;18:581–92.
2. Furnari FB, Fenton T, Bachoo RM, Mukasa A, Stommel JM, Stegh A, Hahn WC, Ligon KL, Louis DN, Brennan C, Chin L, DePinho RA, Cavenee WK. Malignant astrocytic glioma: genetics, biology, and paths to treatment. *Genes Dev.* 2007;21:2683–710.
3. Ohgaki H, Kleihues P. Epidemiology and etiology of gliomas. *Acta Neuropathol.* 2005;109:93–108.
4. Favia P. Special Issue: Biomedical Applications of Plasma Processes. *Plasma Process Polym.* 2006;3:383–561.
5. Laroussi M. Non thermal decontamination of biological media by atmospheric-pressure plasmas: review, analysis, and prospects. *IEEE Trans Plasma Sci.* 2002;30:1409–15.
6. Weltmann KD, Brandenburg R, von Woedtke T, Ehlbeck J, Foest R, Stieber M, Kindel E. Antimicrobial treatment of heat sensitive products by miniaturized atmospheric pressure plasma jets (APPJs). *J Phys D.* 2008;41:194008-194014.
7. Moisan M, Barbeau J, Moreau S, Pelletier J, Tabrizian M, Yahia LH. Low-temperature sterilization using gas plasmas: a review of the experiments and an analysis of the inactivation mechanisms. *Int J Pharm.* 2001;226:1–21.
8. Fridman G, Peddinghaus M, Ayan H, Fridman A, Balasubramanian M, Gutsol A, Brooks A, Friedman G. Blood coagulation and living tissue sterilization by floating-electrode dielectric barrier discharge in air. *Plasma Chem Plasma Process.* 2006;26:425–42.
9. Kieft IE, Broers JLV, Caubet-Hilloutou V, Slaaf DW, Ramaekers FCS, Stoffels E. Electric discharge plasmas influence attachment of cultured CHO k1 cells. *Bioelectromagnetics.* 2004;25:362–8.
10. Kieft IE, Kurdi M, Stoffels E, editors. Reattachment and apoptosis after plasma-needle treatment of cultured cells. 4th International Symposium on Non thermal Medical/Biological Treatments Using Electromagnetic Fields and Ionized Gases; 2005 May; Portland, OR: IEEE-Inst Electrical Electronics Engineers Inc.; 2005.
11. Stoffels E, Kieft IE, Sladek REJ, van den Bedem LJM, van der Laan EP, Steinbuch M, editors. Plasma needle for in vivo medical treatment: recent developments and perspectives. European Summer School on Low Temperature Plasma Physics; 2004 Sep 26–Oct 8; Bad Honnef, Germany: IOP Publishing Ltd.; 2006;15:169-180.

12. Yonson S, Coulombe S, Leveille V, Leask RL. Cell treatment and surface functionalization using a miniature atmospheric pressure glow discharge plasma torch. *J Phys D*. 2006;39:3508–13.
13. Shashurin A, Keidar M, Bronnikov S, Jurjus RA, Stepp MA. Living tissue under treatment of cold plasma atmospheric jet. *Appl Phys Lett*. 2008;93:181501-181503.
14. Fridman G, Shereshevsky A, Jost MM, Brooks AD, Fridman A, Gutsol A, Vasilets V, Friedman G. Floating electrode dielectric barrier discharge plasma in air promoting apoptotic behavior in melanoma skin cancer cell lines. *Plasma Chem Plasma Process*. 2007;27:163–76.
15. Kim GC, Kim GJ, Park SR, Jeon SM, Seo HJ, Iza F, Lee JK. Air plasma coupled with antibody-conjugated nanoparticles: a new weapon against cancer. *J Phys D*. 2009;42:032005-032010.
16. Stoffels E, Sakiyama Y, Graves DB. Cold atmospheric plasma: charged species and their interactions with cells and tissues. *IEEE Trans Plasma Sci*. 2008;36:1441–57.
17. Vandamme M, Robert E, Pesnel S, Barbosa E, Dozias S, Sobilo J, Lerondel S, Le Pape A, Pouvesle J-M. Antitumor effect of plasma treatment on U87 glioma xenografts: preliminary results. *Plasma Process Polym*. 2010;7 :264-273.
18. Euhus DM, Hudd C, Laregina M, Johnson FE. Tumor measurement in the nude-mouse. *J Surg Oncol*. 1986;31:229–34.
19. Tomayko MM, Reynolds CP. Determination of subcutaneous tumor size in athymic (nude) mice. *Cancer Chemother Pharmacol*. 1989;24:148–54.
20. Jenkins DE, Oei Y, Hornig YS, Yu SF, Dusich J, Purchio T, Contag PR. Bioluminescent imaging (BLI) to improve and refine traditional murine models of tumor growth and metastasis. *Clin Exp Metastasis*. 2003;20:733–44.
21. Lu X, Laroussi M. Dynamics of an atmospheric pressure plasma plume generated by submicrosecond voltage pulses. *J Appl Phys*. 2006;100:063302-063308.
22. Ayan H, Staack D, Fridman G, Gutsol A, Mukhin Y, Starikovskii A, Fridman A, Friedman G. Application of nanosecond-pulsed dielectric barrier discharge for biomedical treatment of topographically non-uniform surfaces. *J Phys D: Appl Phys*. 2009;42:125002-125007.
23. Suit HD, Zietman A, Tomkinson K, Ramsay J, Gerweck L, Sedlacek R. Radiation response of xenografts of a human squamous cell carcinoma and a glioblastoma multiforme: a progress report. *Int J Radiat Oncol Biol Phys*. 1990;18:365–73.
24. Taghian A, DuBois W, Budach W, Baumann M, Freeman J, Suit H. In vivo radiation sensitivity of glioblastoma multiforme. *Int J Radiat Oncol Biol Phys*. 1995;32:99–104.
25. Baumann M, DuBois W, Pu A, Freeman J, Suit HD. Response of xenografts of human malignant gliomas and squamous cell carcinomas to fractionated irradiation. *Int J Radiat Oncol Biol Phys*. 1992;23:803–9.
26. Labussiere M, Aarnink A, Pinel S, Taillandier L, Escanye JM, Barberi-Heyob M, Bernier-Chastagner V, Plenat F, Chastagner P. Interest of liposomal doxorubicin as a radiosensitizer in malignant glioma xenografts. *Anticancer Drugs*. 2008;19:991–8.
27. Hildebrandt B, Wust P, Ahlers O, Dieing A, Sreenivasa G, Kerner T, Felix R, Riess H. The cellular and molecular basis of hyperthermia. *Crit Rev Oncol/Hematol*. 2002;43:33–56.
28. Palmer RMJ, Ferrige AG, Moncada S. Nitric-oxide release accounts for the biological-activity of endothelium-derived relaxing factor. *Nature*. 1987;327:524–6.

29. Tucker AT, Pearson RM, Cooke ED, Benjamin N. Effect of nitric-oxide-generating system on microcirculatory blood flow in skin of patients with severe Raynaud's syndrome: a randomised trial. *Lancet*. 1999;354:1670–5.
30. Song CW, Shakil A, Griffin RJ, Okajima K. Improvement of tumor oxygenation status by mild temperature hyperthermia alone or in combination with carbogen. *Semin Oncol*. 1997;24:626–32.
31. Batista LFZ, Roos WP, Kaina B, Menck CFM. p53 mutant human glioma cells are sensitive to UV-C-induced apoptosis due to impaired cyclobutane pyrimidine dimer removal. *Mol Cancer Res*. 2009;7:237–46.
32. Anderson RR, Parrish JA. The optics of human-skin. *J Invest Dermatol*. 1981;77:13–9.
33. Kirson ED, Dbaly V, Tovarys F, Vymazal J, Soustiel JF, Itzhaki A, Mordechovich D, Steinberg-Shapira S, Gurvich Z, Schneiderman R, Wasserman Y, Salzberg M, Ryffel B, Goldsher D, Dekel E, Palti Y. Alternating electric fields arrest cell proliferation in animal tumor models and human brain tumors. *Proc Natl Acad Sci U S A*. 2007;104:10152–7.
34. Kirson ED, Gurvich Z, Schneiderman R, Dekel E, Itzhaki A, Wasserman Y, Schatzberger R, Palti Y. Disruption of cancer cell replication by alternating electric fields. *Cancer Res*. 2004;64:3288–95.
35. Moeller BJ, Richardson RA, Dewhirst MW. Hypoxia and radiotherapy: opportunities for improved outcomes in cancer treatment. *Cancer Metastasis Rev*. 2007;26:241–8.
36. Seiwert TY, Salama JK, Vokes EE. The concurrent chemoradiation paradigm—general principles. *Nat Clin Pract Oncol*. 2007;4:86–100.
37. Ogawa Y, Morikawa N, Ohkubo-Suzuki A, Miyoshi S, Arakawa H, Kita Y, Nishimura S. An epoch-making application of discharge plasma phenomenon to gene-transfer. *Biotechnol Bioeng*. 2005;92:865–70.
38. Sakai Y, Khajooe V, Ogawa Y, Kusuhara K, Katayama Y, Hara T. A novel transfection method for mammalian cells using gas plasma. *J Biotechnol*. 2006;121:299–308.
39. Robert E, Barbosa E, Dozias S, Vandamme M, Cachoncinlle C, Viladrosa R, Pouvesle J-M. Experimental study of a nanosecond plasma gun. *Plasma Process Polym*. 2009;6:795-802.

Targeted Cancer Treatment Using Anti-EGFR and -TFR Antibody-Conjugated Gold Nanoparticles Stimulated by Nonthermal Air Plasma

G. J. Kim,¹ S. R. Park,² G. C. Kim,^{2*} & J. K. Lee¹

¹Department of Electronic and Electrical Engineering, Pohang University of Science and Technology. ²Department of Oral Anatomy, School of Dentistry, Pusan National University

*Address all correspondence to: G. C. Kim, Department of Oral Anatomy, School of Dentistry, Pusan National University, Busan 602-739, Republic of Korea; ki91000m@pusan.ac.kr

ABSTRACT: Nonthermal air plasma killed G361 melanoma and SCC25 oral cancer cells targeted by antibody-conjugated gold nanoparticles. Although plasma alone is effective in killing cancerous cells, it also affects normal cells during the treatment process. For enhanced effects, gold nanoparticles and cancer-specific antibodies were pretreated before plasma treatment. Gold nanoparticles taken up by the cancerous cells are stimulated by the plasma treatment. Stimulation of gold nanoparticles results in an increase in death rate of cancerous cells. The selectivity of the killing process is achieved by conjugating gold nanoparticles with anti-epidermal growth factor receptor and transferrin receptor antibodies. These conjugates can bind specifically to cancer cells. Gold nanoparticles stimulated by plasma kill these cancerous cells effectively. In this way, the killing efficiency of the plasma treatment process in the presence of conjugates is amplified about 18 times compared to the plasma treatment in the absence of conjugates. This technique shows the possibility of using plasma therapy for killing cancer cells selectively and effectively.

I. INTRODUCTION

Human oral squamous carcinoma (OSC) and melanoma are oral cavity cancers. Especially, OSC is responsible for the majority of malignancies in the oral cavity. The conventional methods for the treatment of oral cavity cancers are based on surgical extirpation, radiation, chemotherapy, or a combination of these treatments. These methods have some limitations. For example, surgical removal of oral cancer can result in facial distortion with physical and psychological consequences. Use of chemotherapy is limited due to its side effects (toxicity) and the development of high resistance to chemotherapeutic agents at later stages of malignancy.¹ Therefore, the treatment of OSC oral cancer cells favors the use of new methodologies that are not only effective in killing cancerous cells, but also must be selective so that normal cells remain undisturbed during the treatment.

Recently, it has been shown that well-designed nonthermal plasmas are effective in killing cancer cells.² Plasma alone, however, is unable to achieve selectivity because it kills both normal and cancerous cells. Recent advances in nanotechnology have resulted in the use of gold nanoparticles as diagnostic and drug delivery tools.^{3,4} More applica-

tions of gold nanoparticles are found in cancer therapy when the plasma interacts with gold nanoparticles. Gold nanoparticles can be used by conjugating with a cancer-specific antibody to achieve the selectivity in plasma treatment. Conjugated nanoparticles can bind selectively to target cells, which are then affected by the plasma. In this regard, we have previously demonstrated the enhanced effects of antifocal adhesion kinase (FAK) conjugates and plasma.⁵

In this study, we have further investigated the synergistic effect of gold conjugates and plasma for the selective treatment of oral squamous carcinoma cells. In many oral cancer cells, the epidermal growth receptor (EGFR) and transferrin receptor (TFR) have been known to be overexpressed. These receptors are regarded as an attractive target for cancer therapy.^{6–8} Therefore, anti-EGFR antibody and anti-TFR antibodies were conjugated to gold nanoparticles for targeting oral cancer.

II. MATERIALS AND METHODS

A. Nonthermal Air Plasma Source

Figure 1A shows the schematic diagram of the experimental setup. The plasma source was designed to operate in ambient air with 22 kHz, with a few kilovolt sinusoidal voltage source. The plasma source consists of a polytetrafluoroethylene (PTFE) dielectric and Cu electrodes on both sides of the PTFE. The plasma source was a Cu-PTFE-Cu stacked structure of circuit board. The electrode structure was formed by a conventional chemical etching process. The plasma was generated by the fringing field near the front-face electrode.⁹ Figure 1B shows voltage and current waveforms of the plasma device. A high-voltage probe (Tektronix P6015A) and a current probe (Pearson current monitor Model 4100) were used. The capacitive load of the plasma source made the voltage lead the current waveform 90 deg in phase. An applied voltage of 4.2 kV (rms) induced the typical DBD type current waveform, showing several current peaks in positive rising and negative falling times of the voltage waveform due to the accumulation of charges on the dielectric surface. These random current peaks result from movement of charged particles in a very short time (~nanoseconds), which is a characteristic of filamentary discharges. Making plasma consumed 4.26 W, as calculated from the measured voltage and current waveforms. For the 40 s treatment, an energy density of about 27 J/cm² was estimated within the area of the plasma.

Optical emission spectroscopy was used to find the rotational temperature of the discharge. An optical emission spectrometer, consisting of a 750 mm focal length monochromator (Dong Woo Optron Co. Ltd. 750, Monora 750i) with a built-in high-sensitivity photomultiplier tube (PMT, R928 Hamamatsu) and a grating 2400 gr/mm blazed at 240 nm was utilized. The second positive system of nitrogen dominated in the 300–400 nm range. The rotational temperature of the second positive nitrogen C-B transition bands was also analyzed (Fig. 2B). To find the optimum fit between measured and simulated spectrums, the technique described by Phillips¹⁰ was used. The inset of Figure 2B shows how the optimum fit was found by varying the estimated rotational

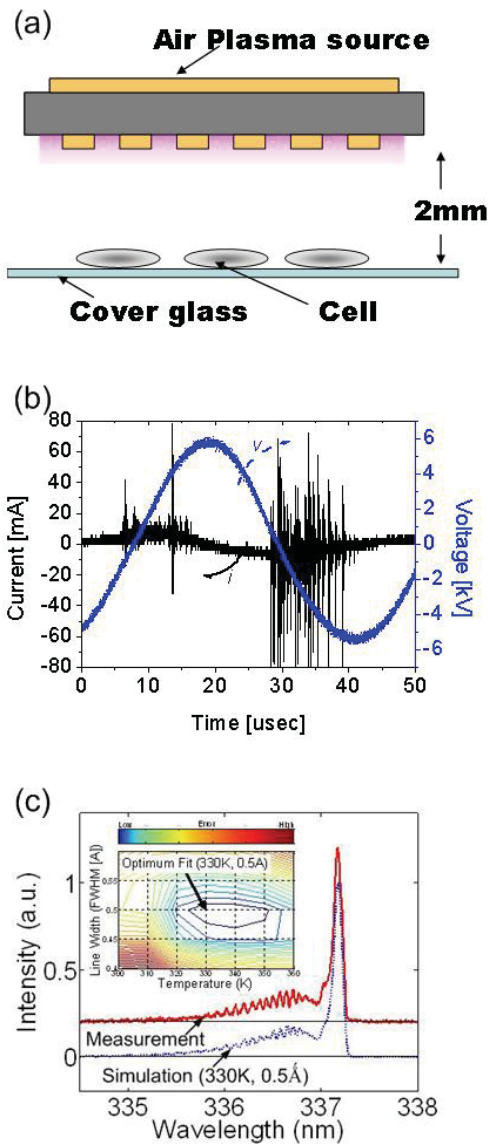


FIGURE 1. Plasma source. (A) Schematic diagram of experiment. (B) Current and voltage waveforms of plasma source. (C) Rotational temperature of plasma source.

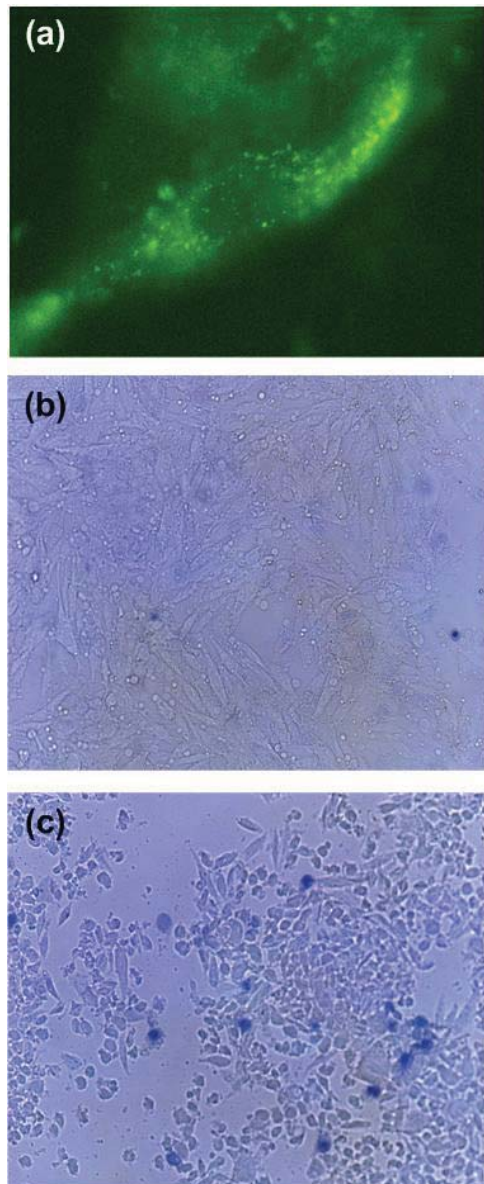


FIGURE 2. Plasma treatment on the G361 cells. (A) Uptake of gold nanoparticles. (B) Plasma treatment without gold nanoparticles. (C) Plasma treatment with gold nanoparticles

temperature and line width. Finally, the rotational temperature of the discharge was determined to be 330 K, and this value agrees with the temperature determined near the plasma source by the fiber optic temperature measurement technique.

B. Cell Culture

Human melanoma (G361), human tongue squamous carcinoma (SCC25), and mouse fibroblast (NIH3T3) cell lines were purchased from the ATCC (Rockville, Maryland). These cells were grown in Dulbecco's modified eagle's medium supplemented with 25 mM HEPES, 100 µg/ml penicillin/streptomycin, 4 mM L-glutamine, and 10% fetal bovine serum at 37°C in a 5% CO₂ humidified-air incubator.

C. Plasma Treatment and Cell Viability Assay

After 4×10^5 G361 and SCC25 cells were incubated on cover slips for 24 hr, cover slips without media were placed 2 mm from the plasma source and exposed to a 30 s plasma treatment. Cells treated with plasma were washed immediately with phosphate buffered saline (PBS), stained with trypan blue, and then counted using a hemocytometer.

D. Immunocytochemistry

Cells were treated with the mouse anti-TFR (anti-EGFR) antibody-conjugated gold nanoparticles (TFR-GNPs, EGFR-GNPs) and then fixed in 4% paraformaldehyde for 10 min. Cells were permeabilized with 0.2% Triton X-100 in PBS for 10 min and then incubated with goat FITC-antimouse secondary antibody for 1 hr. Samples were observed under a fluorescence microscope (Axioskop, Zeiss, Germany).

E. Conjugation

An aqueous solution of 11-mercaptoundecanoic acid (MUA) (0.1 mg/ml) was added to the colloidal gold suspension and incubated overnight. MUA-modified gold nanoparticles were reacted with a mixture of 1 mM N-hydroxysuccinimide (NHS) and 1 mM N-ethyl-N'- γ -(3-dimethylaminopropyl) carbodiimide (EDC) solution for 20 min. NHS-terminated gold nanoparticles were incubated with 250 µg/ml anti-EGFR anti-TFR antibodies in PBS buffer (1 mM, pH 7.0) for 6 hr.

F. Western Blot

Cells were lysed in ice-cold lysis buffer [300 mM NaCl, 50 mM Tris-Cl (pH 7.6), 0.5% TritonX-100, 2 mM PMSF, 2 µl /ml aprotinin, and 2 µl /ml leupeptin] and incubated at 4°C for 30 min. A quantity of 5c µg of proteins were loaded onto 7.5% SDS/PAGE. The gels were transferred to a nitrocellulose membrane and reacted with anti-EGFR and anti-TFR antibodies (Santa Cruz Biotechnology, Inc.). Immunostaining was performed using SuperSignal West Pico enhanced chemiluminescence substrate and detected with LAS-3000PLUS (Fuji Photo Film Company, Kanagawa, Japan).

III. RESULTS AND DISCUSSION

In order to see the synergistic effect of gold conjugates and plasma, it was required to verify the uptake of gold nanoparticles by cancer cells. Figure 2A shows an immunostaining image of the G361 human melanoma skin cancer cells after 24 hr incubation with 30 nm gold nanoparticles. Green fluorescence was taken under the fluorescent microscope due to a fluorescein conjugated, affinity-purified secondary antibody, which was made to bind with the gold nanoparticles. The figure shows spindle shape cell morphology and a nucleus surrounded by cytosol where a lot of gold nanoparticles reside. The colloidal gold nanoparticles can get into and out of the cell during the metabolism. A part of gold nanoparticles, which remained for 24 hr incubation, was observed. In this case, the gold nanoparticles can be placed within the cytosol. The position of gold nanoparticles can be controlled by binding the gold nanoparticles with the specific antibodies.

To show that plasma can stimulate the gold nanoparticles inside of the cell, G361 melanoma cancer cells were treated with the plasma for 30 s following 24 hr incubation together with colloidal gold nanoparticles. Figure 2 shows trypan blue-stained cells after the plasma treatment without (Fig. 2B) and with (Fig. 2C) gold nanoparticles. In the case of treatment with gold nanoparticles (Fig. 2C), the cell morphology was changed to a round shape and cells formed aggregates. On the other hand, when treatment was performed without gold nanoparticles, the cells retained their shape.

In order to obtain quantitative results after the plasma treatment, all treated cells were harvested, stained with trypan blue, and counted with a hemocytometer. Figure 3A shows the death rate and proliferation (growth) rate of G361 melanoma cells after plasma treatment with and without colloidal gold nanoparticles. In the case of low-dose plasma exposure (4.5 kV), the cell death rate for the two kinds of treatment (with and without gold nanoparticles) was not significantly different. However, when the applied voltage was increased, the death rate increased significantly in the cells treated with gold nanoparticles. When gold nanoparticles were used, the death rate increased more than twice (from 14% to 36%) immediately after the plasma stimulation. This shows that plasma stimulates gold nanoparticles to attack cancer cells. This also implies that addition of gold nanoparticles can reduce the required voltage for effective cell killing and improves the selectivity of plasma treatment. It must be noted that gold nanoparticles became effective after being exposed to plasma. If the cells in the presence of gold nanoparticles are not treated with plasma, gold nanoparticles have no effect on the cells.

We assumed that low-dosed plasma treatment would have no effect on the immediate death rate after plasma treatment. However, when the number of cells was checked 24 hr after the plasma treatment, the cell proliferation was significantly reduced. Figure 3B summarizes the proliferation rates of G361 cells with and without gold nanoparticles with 24 hr incubation after the plasma exposure. The plasma treatment of cells without gold nanoparticles decreased the proliferation rate to 54%. However, the proliferation rate of cells with gold nanoparticles was reduced to 15% after plasma treatment. This

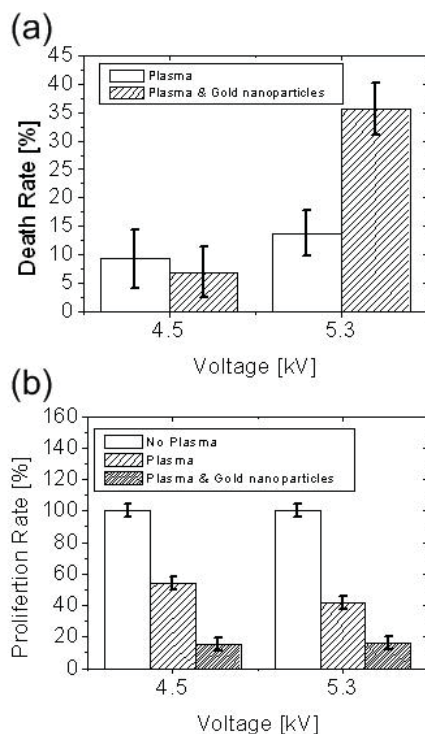


FIGURE 3. Effects of plasma exposure on G361 cells. (A) Cell death rate. (B) Proliferation rate.

indicates the therapeutic value of plasma alone and synergetic effect of plasma and gold nanoparticles for cancerous cell treatment.

To further investigate, gold nanoparticles were conjugated with EGFR and TFR. The EGFR is a transmembrane glycoprotein that constitutes one of four members of the erbB family of tyrosine kinase receptors (170 kDa). Binding of EGFR to its conjugate ligands leads to autophosphorylation of receptor tyrosine kinase and subsequent activation of signal transduction pathways that are involved in regulating cellular proliferation, differentiation, and survival. Although EGFR is present in normal cells, it is overexpressed in a variety of tumor cell lines, and has been associated with poor prognosis and decreased survival. EGFR activation also plays a role in resistance to chemotherapy and radiation treatment in tumor cells. Over the past two decades, much of chemotherapy research has focused on developing anticancer agents that can obstruct EGFR activity.^{11–13} The TFR is a cell membrane-associated glycoprotein involved in the cellular uptake of iron and in the regulation of cell growth. Iron uptake occurs via the internalization of iron-loaded transferrin mediated by the interaction with the TFR.¹ It is reported that the expression level of TFR in cancer cells may be up to 100-fold higher than average expression level

of TFR in normal cells. The high expression level of TFR in cancer cells and its central role in the cellular pathology of human cancer make this receptor an attractive target for cancer therapy.² Therefore, targeting the TFR is a promising strategy actively being explored as a drug alternative to offset dangerous side effects. Figure 4 shows the high expression of EGFR and TFR in SCC25 oral squamous carcinoma cells compared with NIH 3T3 normal cells. This suggests that both receptors could be suitable for target proteins.

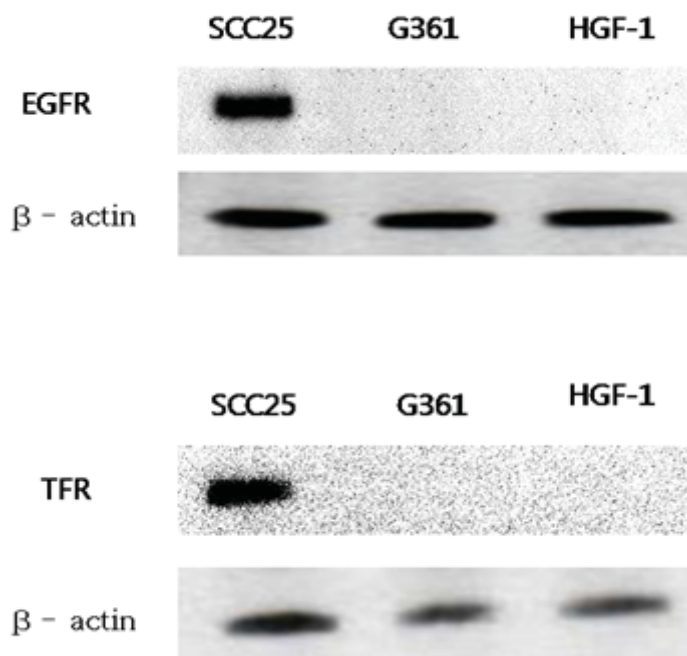


FIGURE 4. Western blotting analysis for EGFR and TFR in different cells. (A) Expression level of EGFR. (B) Expression level of TFR. β -actin was used for loading control.

The uptake of conjugates was observed before plasma treatment. Figure 5 shows the binding images of EGFR-GNP and TFR-GNP conjugates on the SCC25 cells. Figures 5A and 5B show EGFR-GNP conjugates, while Figures 5C and 5D show TFR-GNP conjugates. The green fluorescence of Figures 5A and 5C detected gold conjugates, while Figures 5B and 5D show corresponding phase contrast images. Because the EGFR and TFR are located on the cell membrane, the uptake images look like a shell covering cell membrane. It is important to mention that the attachment of gold nanoparticles on the cells can be controlled by selecting an appropriate antibody for conjugates. The colloidal

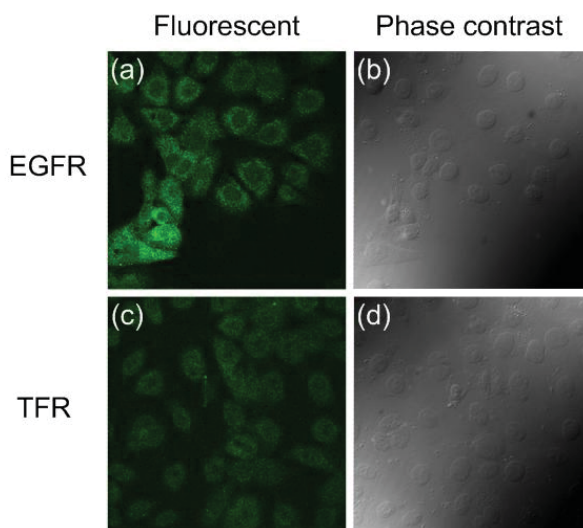


FIGURE 5. Immunocytochemistry. (A) Fluorescent image of SCC25 cells binding with EGFR conjugates. (B) Phase contrast image of (A). (C) Fluorescent image of SCC25 cells binding with TFR conjugates. (D) Phase contrast image of (C).

gold nanoparticles reside within the cytosol (Fig. 2A), while EGFR-GNP and TFR-GNP conjugates surround the cell membrane (Fig. 5).

In order to confirm the lethal effect of plasma plus EGFR-GNP or TFR-GNP, cells were divided into four groups: cells cultured in pure media (Fig. 6A); cells cultured in media containing gold nanoparticles (Fig. 6B); cells cultured in media containing TFR-GNP (Fig. 6C); and cells cultured in media containing EGFR-GNP (Fig. 6D). When these four groups of cells were treated by plasma for 30 s, the death rates were 5%, 21%, 66%, and 92%, respectively (Fig. 6E). In the case of cells treated with TFR-GNP, although the death rate right after plasma treatment was 66%, most alive cells were finally dead after 4 h incubation. Considering the instant death rate of 92% in the EGFR-GNP-treated group, the death mechanism might be necrosis, whereas in the TFR-GNP-treated group, apoptosis might be induced for 4 hr as well as necrosis. In our preliminary research, human normal gingival fibroblast showed a 5% death rate (data not shown) when they were treated with TFR-GNP and EGFR-GNP plus plasma, because they did not express TFR and EGFR on the cell surface (Fig. 4). While the death rate of the control group was 5%, those of TFR-GNP and EGFR-GNP were about 13-fold and 18-fold higher, suggesting that the combination treatment of plasma and TFR-GNP or EGFR-GNP has a strong selective treatment of SCC25 cells. Although the present results are promising, it is unclear how plasma stimulates GNP or what exact death mechanism was involved. Thus, those mechanisms are expected to be traced in the next research.

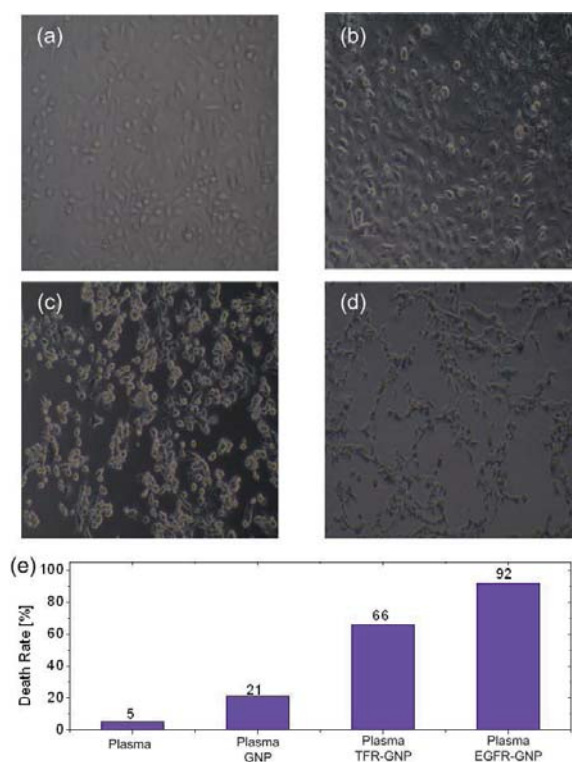


FIGURE 6. Enhancement of cell death by plasma treatment plus TFR-GNP and EGFR-GNP in SCC25 cells. (A) Control cells. (B) Cells treated with colloidal gold nanoparticles. (C) Cells treated with TFR-GNP. (D) Cells treated with EGFR-GNP. (E) Death rates.

IV. SUMMARY

In this work, we have proposed a nonthermal air plasma coupled with antibody conjugated gold nanoparticles for selective and effective melanoma and oral cancer therapy. In the absence of conjugated gold nanoparticles, nonthermal air plasma kills cancerous cells effectively, and its use results in reduction of proliferation rate, however, it also affects normal cells. This problem of killing normal cells by nonthermal air plasma can be taken care of by using gold nanoparticles. It shows that cells incubated with gold nanoparticles are vulnerable to plasma treatment. It is also shown that the efficiency of the treatment process can be enhanced when the gold nanoparticles are conjugated with anti-EGFR and anti-TFR antibodies. In the presence of EGFR-GNP conjugates, the treatment process became about 18 times more efficient as compared to the case when the plasma alone is used for treatment of cancerous cells. These results suggest that the attack against TFR and/or EGFR by means of plasma may be a prominent strategy for oral carcinoma cells.

ACKNOWLEDGMENTS

This work was supported by the Korea Science and Engineering Foundation (KOSEF) Grant No. R01-2007-000-10730-0 and the Brain Korea 21 program funded by the Korean Ministry of Education, Science, and Technology. This work was supported by the Institute for Research & Industry Cooperation of the Pusan National University (PNUIRIC, Research Development Promotion Fund) (Grant No. PNUIRIC-2009-201-○○○○○○○)

REFERENCES

1. D'Silva NJ, Ward BB. Tissue biomarkers for diagnosis & management of oral squamous cell carcinoma. *Alpha Omegan*. 2007;100(4):182–9.
2. Fridman G, Jost MM, Brooks AD, Fridman A, Gutsol A, Vasilets V, Friedman G. Floating electrode dielectric barrier discharge plasma in air promoting apoptotic behavior in melanoma skin cancer cell lines. *Plasma Chem Plasma Process*. 2007;27(2):163–76.
3. Service RF. Materials and biology. Nanotechnology takes aim at cancer. *Science*. 2005;310(5751):1132–4.
4. Rayavarapu RG, Petersen W, Ungureanu C, Post JN, van Leeuwen TG, Manohar S. Synthesis and bioconjugation of gold nanoparticles as potential molecular probes for light-based imaging techniques. *Int J Biomed Imaging* 2007;2007:29817.
5. Kim GC, Kim GJ, Park SR, Jeon SM, Seo HJ, Iza F, Lee JK. Air plasma coupled with antibody-conjugated nanoparticles: A new weapon against cancer. *J Phys D*. 2009;42(3):032005.
6. Daniels TR, Delgado T, Rodriguez JA, Helguera G, Penichet ML. The transferrin receptor part I: Biology and targeting with cytotoxic antibodies for the treatment of cancer. *Clin Immunol*. 2006;121(2):144–58.
7. Daniels TR, Delgado T, Helguera G, Penichet ML. The transferrin receptor part II: Targeted delivery of therapeutic agents into cancer cells. *Clin Immunol*. 2006;121(2):159–76.
8. Herbst RS. Review of epidermal growth factor receptor biology. *Int J Radiat Oncol Biol Phys*. 2004;59(2 suppl 1):S21–6.
9. Kim GJ, Kim W, Kim KT, Lee JK. DNA damage and mitochondria dysfunction in cell apoptosis induced by nonthermal air plasma. *Appl Phys Lett*. 2010;96:021502
10. Phillips DM. Determination of gas temperature from unresolved bands in the spectrum from a nitrogen discharge. *J Phys D*. 1976;9(3):507–21.
11. Ennis BW, Lippman ME, Dickson RB. The EGF receptor system as a target for antitumor therapy. *Cancer Invest*. 1991;9(5):553–62.
12. Herbst RS, Langer CJ. Epidermal growth factor receptors as a target for cancer treatment: the emerging role of IMC-C225 in the treatment of lung and head and neck cancers. *Semin Oncol*. 2002;(1 Suppl 4):27–36.
13. Kondapaka SB, Fridman R, Reddy KB. Epidermal growth factor and amphiregulin up-regulate matrix metalloproteinase-9 (MMP-9) in human breast cancer cells. *Int J Cancer*. 1997;70(6):722–6.

Use of Proteomics to Investigate Plasma-Cell Interactions

K. Landsberg,^{1,3} Ch. Scharf,² K. Darm,⁴ K. Wende,³ G. Daeschlein,⁴ E. Kindel,¹ K.-D. Weltmann,¹ & Th. von Woedtke^{1,*}

¹Leibniz Institute for Plasma Science and Technology (INP Greifswald), Greifswald, Germany,

²Department of Otorhinolaryngology and Head and Neck Surgery, Ernst Moritz Arndt University,

³Institute of Pharmacy, Department Pharmaceutical Biology, Ernst Moritz Arndt University,

⁴Department of Dermatology, Ernst Moritz Arndt University

*Address all correspondence to: Th. von Woedtke, Leibniz Institute for Plasma Science and Technology (INP Greifswald), Felix-Hausdorff-Str. 2, 17489 Greifswald, Germany; woedtke@inp-greifswald.de

ABSTRACT: The understanding of basic mechanisms of plasma effects on living cells is one of the main preconditions to develop systematically innovative therapy options in the new and emerging field of plasma medicine. In this study, proteomics have been used for the first time to analyze the influences of physical plasma on vital constituents of mammalian cells. Treatment of human keratinocytes (HaCaT cells) by an atmospheric pressure argon plasma jet resulted in changes of charges of several cell proteins, but not in mass changes. These first results indicate plasma-induced reactions of functional groups or ligands, but no fragmentation, degradation, or complexation of cell proteins. Hereby, the importance to examine internal cellular changes caused by plasma treatment to elucidate the influence of plasma on the metabolism of human cells next to morphological changes, cell performance, and cell viability could be demonstrated. Starting from now, proteomics will become a useful tool for basic research in the field of plasma medicine.

KEY WORDS: plasma medicine, proteomics, two-dimensional gel electrophoresis, cellular proteome, atmospheric pressure plasma

I. INTRODUCTION

During the last years, increasing research interest to use physical plasma for biological and medical applications has led to the development of the new research field of plasma medicine as an intersection of plasma physics and life sciences.^{1,2} However, to open up innovative options in medical therapies, basic understanding of the mechanisms of how physical plasma interacts with living system on the cellular level is essential.

Proteins are the main components of the physiological metabolic pathways of cells. The proteome is the entirety of proteins expressed by a living system, e.g., a cell, primarily dependent on the genome but influenced by several internal and external factors. Consequently, the cellular proteome is an indicator for the state of a particular cell type, at defined conditions at any given time. Proteomics is the use of techniques to define the protein pattern of a living system, e.g., a cell.³ Because the proteome is in a constant balance of new synthesis and degradation of proteins, it undergoes permanent alteration in its composition, depending on environmental and internal conditions of the cells. Proteomics is able to give us information regarding the proteins after all

posttranslational modifications, and determines the present interior situation of the cells. Current proteomic strategies offer qualitative and quantitative analysis of the protein entirety and allow assessment of protein modifications with high coverage.^{4,5} Therefore, the use of proteomics to investigate mechanisms of nonlethal plasma effects on living cells could open up a new dimension of basic understanding of plasma-cell interactions.

II. MATERIAL AND METHODS

A. Plasma Source

For plasma treatment, an atmospheric pressure plasma jet (INP Greifswald, Germany) was used (Fig. 1, left). Briefly, in the center of a quartz capillary (inner diameter 1.6 mm) a pin-type electrode (1 mm diameter) is mounted. Argon (technical, 5.0) as the feed gas flows through the capillary (gas flow up to 10 standard liters per minute). A high-frequency (HF) voltage (1.1 MHz, 2–6 kV) is coupled to the center electrode. The plasma is generated from the top of the center electrode and expands to the surrounding air outside the nozzle. The delivered power of the plasma was measured calorimetrically. The thermal output from the plasma jet is almost independent of the power at about 150 mW.⁶ For the experiments presented here, a gas flow of exactly 3.8 standard liters per minute was used, resulting in an apparent plasma jet of about 7 mm length and 1–2 mm width.⁶ Probe measurements have shown that electrical charges are present in a plasma tip. Axial temperature profiles of the plasma jet were obtained by fiber optic temperature measurement (Luxtron, model 755). A temperature-dependent fluorescent signal of luminescent magnesium fluorogermanate, which was excited with a Xe flash-lamp, was monitored (Fig. 2).⁷ Optical emission spectroscopy (OES) of the plasma was

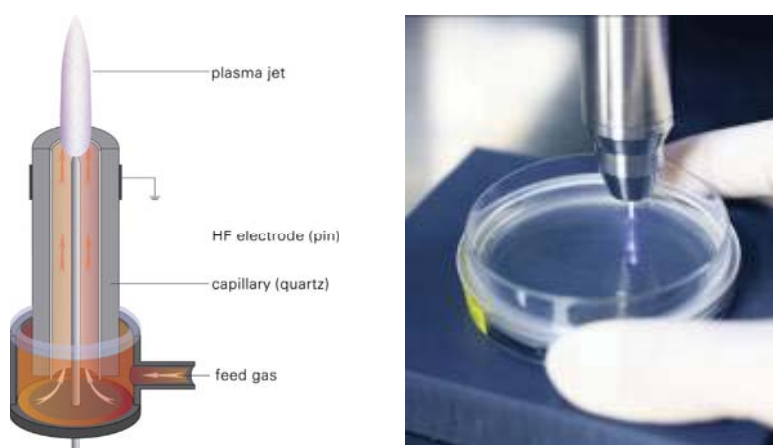


FIGURE 1. Schematic setup of the APPJ plasma source (left), and APPJ treatment of suspended cells in a Petri dish (right).

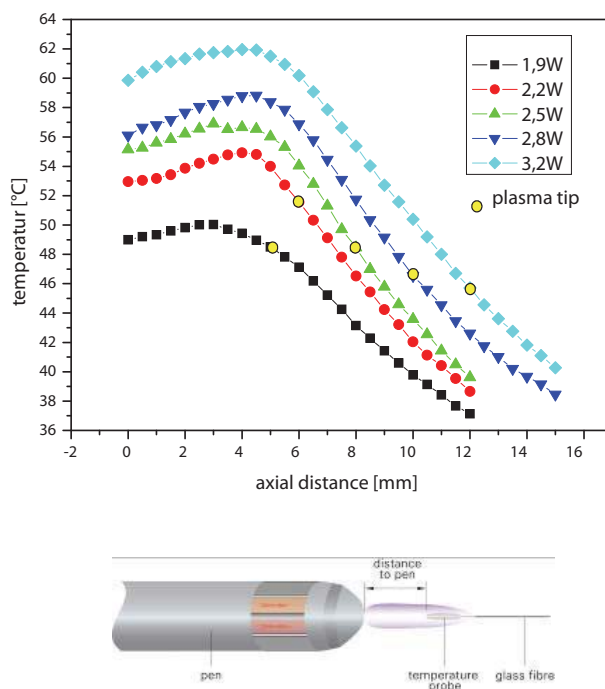


FIGURE 2. Gas temperature of the APPJ (continuous operating mode) and temperature measurement setup at an argon gas flow rate of 5 standard liters per minute dependent on the input power and the axial distance from the capillary nozzle of the plasma source (yellow points: tip of the visible range of the plasma jet).⁶

performed using a fiber spectrometer (StellarNet EPP2000-UVN). The plasma was imaged on the optical fiber of the spectrometer via two pinholes ($d = 1$ mm) and a quartz glass lens. By moving the optical setup along the plasma, spectra were taken at different but well defined axial positions with a spatial resolution of about 1 mm (Fig. 3).⁶ The spectral sensitivity of the detector was taken into account by calibrating it against a deuterium and a halogen lamp.

B. Cell Treatments

Immortalized human keratinocytes (HaCaT) were cultivated in cell culture medium RPMI 1640 (Roswell Park Memorial Institute, Lonza, Verviers, BE) supplemented with 1% penicilline/streptomycine (Biochrom, Berlin, Germany) and 8% fetal calf serum (Sigma-Aldrich, Deisenhofen, Germany) at 37°C and 5% CO₂ in a humidified atmosphere.⁸ RPMI is a culture medium for eukaryotic cells. It contains inorganic salts, glucose, amino acids, and vitamins. HaCaT cells were a gift of DKFZ Heidelberg, Germany.

1.8 Mio HaCaT cells in a 75 cm² tissue culture flask were grown for four days at 37°C and 5% CO₂ in a humidified atmosphere. On the fourth day, the cells were detached

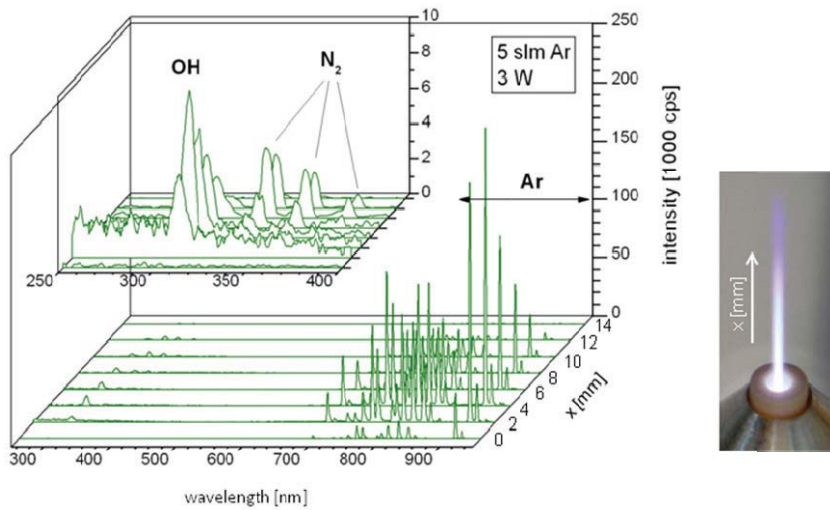


FIGURE 3. Optical emission spectra measured at different axial positions of the Ar-plasma jet.⁶

and suspended in a 5.5 cm diameter Petri dish containing 4 ml RPMI.

Two different experiments were performed related to a control: a 60 s plasma treatment and 60 s gas treatment. The entire Petri dish containing the cell suspension was plasma treated in a meandered track using an automatic program. The speed of the plasma jet over ground was 10 mm/s, resulting in a complete treatment time of 60 s. The plasma jet was adjusted in such a way that the visible plasma tip contacted the liquid surface (Fig. 1, right). The temperature was around 50°C in the visible plasma tip (Fig. 2, green line). For gas flow treatment, the same procedure was used, but without plasma ignition. The gas temperature was about 22°C. All cell treatments started after a 5 min warm-up period. During the treatment, there was no increase in temperature of the culture medium. Lethality of the cells was not observed under these conditions.

C. Proteomics

Immediately after plasma treatment, the cell suspension was centrifuged and the pelletized cells were suspended with urea buffer (8 M urea, 2 M thiourea) and frozen in liquid nitrogen. Protein extraction was performed by a thawing and freezing procedure. Briefly, frozen samples were processed by shaking the tubes in a thermomixer for 10 min at 30°C at 1400 rpm and frozen immediately again in liquid nitrogen. This procedure was carried out five times. Afterward, the cell debris was removed by centrifugation (20,000 \times g, 60 min, 4°C). The supernatants were transferred into new tubes, and the protein concentrations were determined with a Bradford assay (Bio-Rad, Munich, Germany).⁹ This sample preparation is a standard and well-proved method.¹⁰

Two-dimensional polyacrylamide gel electrophoresis (2D-PAGE) is the composition of two high-resolution electrophoresis procedures to provide much greater resolution than either procedure alone. In the first-dimension gel, solubilized proteins are separated along a pH gradient according to their isoelectric point (pI). The pI is equal to that pH where a given molecule has no net electrical charge. After this first separation, the proteins are separated in the second dimension dependent on their molecular weight. The result of the 2D-PAGE separation is a 2D gel presenting the pattern of the proteome of the cell type investigated.

For the 2D electrophoresis, the samples were rehydrated on IPG strips (24 cm; GE Healthcare, Munich, Germany) with a pH range from 4 to 7. Following a standard protocol previously described by Brigulla et al., the IPG strips were subjected to isoelectric focusing.¹¹ In the second dimension, proteins were separated on 12.5% SDS-polyacrylamide gels. The resulting gels were stained with colloidal Coomassie brilliant blue according to the manufacturer's instructions (GE Healthcare) and scanned with a light scanner (Epson Perfection V750 Pro).

Using Delta 2D software (Version 3.6, Decodon GmbH, Greifswald, Germany) allows to positionally correct gel images (image warping), spot detection, quantitation, and normalization of spot patterns of numerous gel images by overlay.¹² After defining a master gel, each gel can be compared with the mastergel while the non-master gels are warped automatically using the differences in spot positions between each gel and the master gel. The software calculates and adjusts the same protein spots on gels exactly. Manual corrections may be made. Identical spots are shown black, and spots that appear only in one gel are labeled with different stains.

III. RESULTS AND DISCUSSION

To analyze differences of the proteome of plasma-treated and untreated human keratinocytes (HaCaT cells), images of the 2D gels from the different preparations were overlaid (image warping) and variously colored using the software Delta-2D (Fig. 4: untreated, blue; plasma treated, orange).

Proteins that are not affected by plasma treatment appear black in this projection, which means that they are always in the same position in the different 2D gels. Furthermore, it is possible that constitutively expressed proteins change their position after treatment due to chemical modifications or changes in molecular mass. Plasma-affected proteins appear blue if they are only visible in the untreated control, implying that they are repressed after plasma treatment, or they appear orange if only visible in the plasma treated preparation, implying that they are induced by plasma treatment.

Comparing the proteome images of untreated and plasma treated keratinocytes (Fig. 4), there can be found mainly horizontal shifts of protein spots. These differences of proteins in the first separation dimension indicate changes of the charge state of those proteins resulting in a pI shift. Such changes of the protein charges could be caused by variations of functional groups or ligands by oxidation, methylation, phosphorylation, etc. However, because no mass-dependent vertical shifts of protein spots in the second

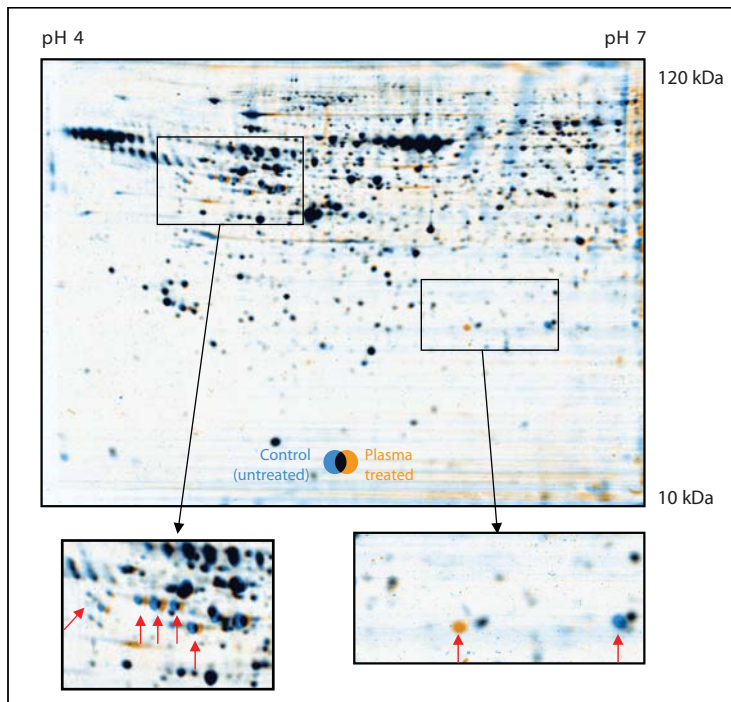


FIGURE 4. Dual-channel overlay image of 2D gels of the protein pattern of untreated (blue) and plasma-treated (orange) keratinocytes. Black spots indicate identical non-modified proteins from both preparations. Blue and orange spots indicate modified proteins being different in the different gels (labeled additionally by red arrows)

dimension of the 2D-PAGE separation are obvious, structural protein changes such as fragmentation, degradation, complexation, etc., caused by plasma treatment, at least under the conditions tested here, can be excluded.

To eliminate effects caused by carrier gas flow, HaCaT cells were exposed to argon gas flow without ignited plasma in an additional experiment. In Figure 5, the same control as in Figure 4 is compared with a cell suspension that was treated only with the gas flow. The spots changed by plasma treatment were unaffected by gas flow, i.e., all spots are black, so it can be concluded that the gas flow itself has no effect on the cells.

As was published elsewhere, radiation emitted from the APPJ plasma contains molecular bands of OH-radical and lines of excited argon atoms between 500 and 1000 nm. In the UV-A region between 350 and 400 nm, bands of nitrogen emission have been measured because of increasing mixing of the feed gas argon with the surrounding ambient air. There was no detectable emission in the UV-C range <250 nm (Fig. 3).⁶ Therefore, effects resulting from the well-known intensive biological activity, especially of UV-C around 254 nm, which is based on direct impact on DNA, can be largely precluded.

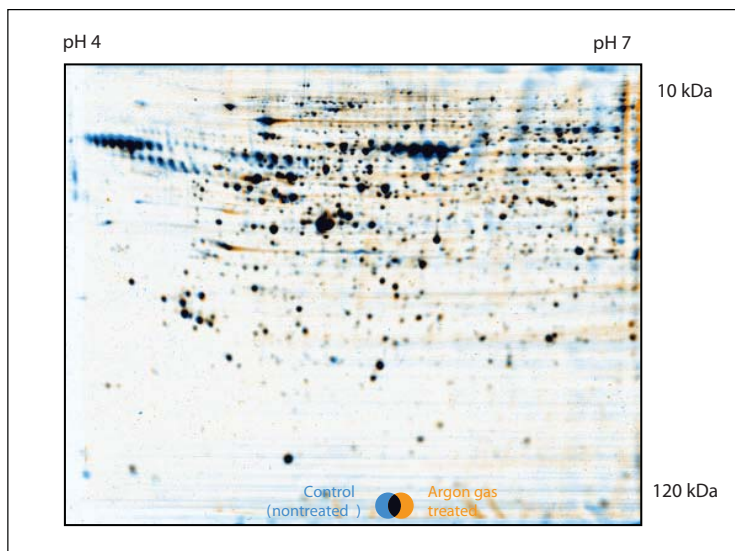


FIGURE 5. Dual-channel overlay image of 2D gels of the protein pattern of untreated (blue) and argon gas treated (orange) keratinocytes. Black spots indicate identical non-modified proteins from both preparations. Blue and orange spots indicate modified proteins being different in the different gels.

Moreover, APPJ emits a significant amount of VUV radiation, mainly the second continuum of the argon excimer Ar_2^* between 120 and 135 nm.¹³ The absolute VUV radiance of the APPJ reaches maximum values of $2.2 \text{ mW mm}^{-2} \text{ sr}^{-1}$.¹³ Because the plasma jet is operated in its own argon atmosphere, a considerable amount of VUV radiation can reach an object to be treated in principle. However, because of the fact the cells in the experiment presented here are suspended in a liquid environment, the biological effects of VUV irradiation seem to be unlikely because of its short effective reach and high absorption by air and liquids.¹⁴

Finally, temperature is one of the most critical factors in connection with plasma treatment of living systems. A slight heating from 37 to 38.5°C was shown to be a stimulus for keratinocyte proliferation.⁸ In principle, temperature should not exceed a threshold of 40°C if living systems are treated. In the experimental setup used in this study, the temperature at the tip of the plasma jet was around 50°C (Fig. 2).⁶ In principle, this is very close to biological intolerance. However, plasma-caused target heating is not only dependent on gas or plasma temperature, but is also a function of contact time. So, it could be demonstrated that fast-moving atmospheric microwave plasma with a temperature of about 3000°C can be used for decontamination of heat-sensitive hollow packaging materials that are melting above 70°C.¹⁵ Because the cell treatment was realized by moving the APPJ for 60 s along a meandered pattern across the complete surface

of the cell suspension in the Petri dish (area 23.8 cm²), inducing an additional stirring of the cell suspension, the contact time should be short enough and cooling effects should be sufficient to exclude temperature effects. A substantial warming of the Petri dish containing the cell suspension was not detectable after plasma treatment. However, further experiments should address this problem in a more detailed manner.

IV. CONCLUSION AND OUTLOOK

For the first time, proteomics have been used to investigate the influence of atmospheric pressure plasma on mammalian cells. With it, a very powerful bioanalytical technique has shown its usefulness for basic research in the field of plasma medicine. The pilot experiments presented here indicate the possibility to detect minute changes within vital cells after plasma treatment in a sophisticated manner. Moreover, based on the preparative electrophoretic separation realized by the 2D-PAGE technique, single proteins of interest can be identified by MALDI-TOF-MS (matrix-assisted laser desorption/ionization time-of-flight mass spectrometry). This was already performed with the gels presented here and is still part of an ongoing investigation.

With the experimental setup used in this study, only effects on cellular proteome immediately after plasma treatment have been demonstrated. To get more detailed insight into possible biochemical mechanisms influencing cell performance, cell reactions have to be investigated up to 72 h after plasma treatment. This will be the only way to get insight into the integral cellular answer and to seize hold on the wobbling expression patterns of proteins and the extent of cellular repair mechanisms in the course of time. Currently, we are preparing this type of experiment, and results will be presented in due time.

One intention of such an examination is the identification of reference proteins to assess a cell status after plasma treatment more easily and to verify the harmlessness of physical plasma to mammalian cells during medical approaches, e.g., in wound healing or dermatology. Hence, proteomics will be a valuable tool to screen effects of plasma treatment on cellular proteome under varying conditions. From its further use in plasma medicine research, detailed knowledge of interactions between physical plasma and cell structures or functions will be obtained. With the first results presented here, the importance to examine internal cellular changes caused by plasma treatment to elucidate the influence of plasma on the metabolism of human cells next to morphological changes, cell performance, and cell viability could be demonstrated.

ACKNOWLEDGMENTS

This work was realized within the framework of the multidisciplinary research cooperation "Campus PlasmaMed." The financial support of the German Ministry of Education and Research (BMBF, Grants No. 13N9774 and No. 13N9779) is gratefully acknowledged.

REFERENCES

1. Fridman G, Friedman G, Gutsol A, Shekhter AB, Vasilets V, Fridman A. Applied plasma medicine. *Plasma Process. Polym.* 2008;5:503-533
2. Laroussi M. Low-temperature plasmas for medicine? *IEEE Trans. Plasma Sci.* 2009; 37:714-725
3. Anderson NL, Anderson NG. Proteome and proteomics: New technologies, new concepts, and new words. *Electrophoresis.* 1998;19:1853-1861
4. Ferguson PL, Smith RD. Proteome analysis by mass spectrometry. *Annu. Rev. Biophys. Biomol. Struct.* 2003;32:399-424
5. Amoresano A, Carpentieri A, Giangrande C, Palmese A, Chiappetta G, Marino G, Pucci P. Technical advances in proteomics mass spectrometry: identification of post-translational modifications. *Clin. Chem. Lab. Med.* 2009;47:647-665
6. Weltmann K-D, Kindel E, Brandenburg R, Meyer Ch, Bussiahn R, Wilke Ch, von Woedtke Th. Atmospheric pressure plasma jet for medical therapy: Plasma parameters and risk estimation. *Contrib. Plasma Phys.* 2009;49:631-640
7. Foest R, Kindel E, Lange H, Ohl A, Stieber M, Weltmann K-D. Rf capillary jet – a tool for localized surface treatment. *Contrib. Plasma Phys.* 2007;47:119-128
8. Boukamp P, Petrussevska RT, Breitkreutz D, Hornung J, Markham A, Fusenig NE. Normal keratinization in a spontaneously immortalized aneuploid human keratinocyte cell line. *J. Cell Biol.* 1988;106:761-771
9. Deroee AF, Oweinah J, Naraghi M, Hosemann W, Athari B, Völker U, Scharf Ch. Regression of polypoid nasal mucosa after systemic corticosteroid therapy: A proteomics study. *Am. J. Rhinol.* 2009;23:480-485
10. Hammer E, Bien S, Gesell Salazar M, Steil L, Scharf C, Hildebrandt P, Schroeder HWS, Kroemer HK, Völker U, Ritter CA. Proteomic analysis of doxorubicin-induced changes in the proteome of HepG2 cells combining 2-D DIGE and LC-MS/MS approaches. *Proteomics.* 2010;10:99-114
11. Brigulla M, Thiele T, Scharf Ch, Breitner-Ruddock S, Venz S, Völker U, Greinacher A. Proteomics as a tool for assessment of therapeutics in transfusion medicine: evaluation of prothrombin complex concentrates. *Transfusion.* 2006;46:377-385
12. Berth M, Moser FM, Kolbe M, Bernhardt J. The state of the art in the analysis of two-dimensional gel electrophoresis images. *Appl. Microbiol. Biotechnol.* 2007;76:1223-1243
13. Lange H, Foest R, Schäfer J, Weltmann K-D. Vacuum UV radiation of a plasma jet operated with rare gases at atmospheric pressure. *IEEE Trans. Plasma Sci.* 2009;37:859-865
14. Brandenburg R, Lange H, Woedtke Th, Stieber M, Kindel E, Ehlbeck J, Weltmann K-D. Antimicrobial effects of UV and VUV radiation of nonthermal plasma jets. *IEEE Trans. Plasma Sci.* 2009;37:877-883
15. Ehlbeck J, Brandenburg R, von Woedtke Th, Krohmann U, Stieber M, Weltmann K-D. PLASMOSE – antimicrobial effects of modular atmospheric plasma sources. *GMS Krankenhaushygiene Interdisziplinär.* 2008;3:Doc14.

Analysis of Streamer Propagation for Electric Breakdown in Liquid/Bioliquid

Yong Yang, Andrey Starikovskiy, Alexander Fridman, & Young I. Cho*

Department of Mechanical Engineering and Mechanics, Drexel University, Philadelphia, PA

*Address all correspondence to: Young I. Cho, Department of Mechanical Engineering and Mechanics, Drexel University, Philadelphia, PA 19104; Tel.: +1-215-895-2425; Fax: +1-215-895-1478; choyi@drexel.edu

ABSTRACT: There is an increasing interest in the study of direct plasma generated in liquid/bioliquid as it finds more applications in both industry and academic research. For all the applications, it is important to get a better understanding of the key physical mechanisms of the breakdown process. In the present paper, streamer propagation during an electric breakdown process of dielectric liquid was analyzed quantitatively using two different mechanisms based on electrostatic expansion and local heating. It was proposed that at the early stage of the streamer propagation, the electrostatic force due to the charging of a liquid-gas interface under a high electric field might be the major driving force for filament growth. Over a submicro-second time scale, the local heating might dominate the streamer propagation process, and the growth of the filament could be caused by the continuous evaporation of liquid at the tip of the streamer. Analysis of linear instabilities that lead to the bushlike growth of the streamers was carried out. Both classic Rayleigh-Taylor instability and electric field-induced instability were identified. It was shown that with an increasing applied voltage, the electrostatic instability was enhanced, whereas the Rayleigh instability was suppressed.

KEY WORDS: electric breakdown, plasma, streamer propagation, stability analysis, Rayleigh instability

NOMENCLATURE

c_p specific heat, C speed of sound, e electron charge, E electric field, h peak-to-peak amplitude, H depth of wave influence, k wave number, k_1 ionization rate coefficient, L length, m mass, M Mach number, n number density, P pressure, R interelectrode distance, r radius, u velocity, V volume, t time, T temperature, Z internal energy, **Greek Symbols:** α specific heat ratio, γ surface tension, $\Delta_v H$ evaporation heat of water, ϵ permittivity, κ electric conductivity, λ thermal conductivity, ρ density, σ surface charge density, τ time, ν collision frequency, τ time constant, Φ voltage, ω oscillation frequency, χ curvature, **Subscripts:** b breakdown, c crest, e electron, E electrostatic, I ionization, HD hydrodynamic, n neutral, t trough, T tension.

I. INTRODUCTION

There is an increasing interest in the study of electric breakdown in water and other liquids as it finds more applications in both industry and academic research, ranging from dielectric insulation to water sterilization, organic contaminants destruction, and material synthesis.^{1–6} For all the applications, it is important to get a better understanding of the key physical mechanisms of the breakdown process. In most cases, the electric

breakdown of liquids is initiated by the application of a high electric field on the electrode, followed by rapid propagation and branching of streamers. The overall mechanism is complex since it involves different physical processes including field emission, bubble formation, ionization, heating, vaporization, etc. Thus, it is difficult to include all the effects in a single analytical model. A number of proposed theories for the initiation of the breakdown of dielectric liquids are available in the literature.^{7–12} The initial bubble formation could be attributed to pre-existing cavities in water, direct ionization, field-assisted emission, or joule heating induced by local field emission. However, the exact mechanism is still unclear.

Despite different mechanisms proposed, all the initiation theories lead to the formation of a low-density region so that self-sustained electron avalanche could be possible. Thus, the next question is what the driving force is to sustain and expand the cavity to form complex geometrical structures. Similar to the initiation process, the propagation is complicated because it involves interactions between plasma, gas, and liquid phases of the media. Recent experiments demonstrated the existence of different modes of propagation where both a primary streamer mode with a slow velocity and a secondary streamer mode with a high velocity were observed.¹³ Several models have been proposed to correlate the electric field to streamer velocity.^{14–16} Different effects, including liquid viscosity, trapping of positive and negative carriers in the conducting channel, and local electric charge at the streamer head, were taken into account. But again, there is not yet a commonly accepted model.

The objective of the present study was to develop a theoretical framework for understanding the propagation of streamers of electric discharge in water subjected to high voltage. The breakdown process is usually characterized by two typical features of breakdown, namely, the rapid propagation of discharge streamers and high tendency of branching and formation of random dendritic structures. Therefore, the present study consists of two components, i.e., a quantitative model for possible mechanisms to produce the driving force needed to sustain and promote the propagation, and a stability analysis of a single cylindrical filament with surface charges in an external electric field.

II. MODELS

Despite the fact that the mechanism is not fully understood, the propagation of streamers during electric breakdown of water clearly involves the displacement of adjacent liquid along their paths. The process requires a driving force, which is to be discussed in this section. Two quantitative models have been developed. One is based on the electrostatic effect on the streamer-water interface, and the other a more traditional local heating effect. Comparison was made to examine the validities of the two models.

A. Electrostatic Model

A schematic diagram of the present electrostatic model is shown in Figure 1A. A thin needle electrode with a rounded tip was aligned perpendicular to a ground plate elec-

trode. High voltage Φ_0 was applied to the needle electrode. According to Kupershtokh et al., liquids could become phase unstable under a high electric field so that gas channels could form along electric field lines.¹⁷ The time required for breakdown ignition in the channels can be estimated as $\tau_b = (k_1 n_0)^{-1}$, where k_1 is the direct ionization rate coefficient, and n_0 is the molecule density.¹⁸ Under atmospheric pressure, n_0 is on the order of 10^{19} cm^{-3} , while k_1 is on the order of 10^{-10} to $10^{-9} \text{ cm}^3/\text{s}$ in the reduced electric field E/n_0 of $10^3 \text{ V}\cdot\text{cm}^2$.¹⁸ Hence, τ_b is on the order of 0.1 to 1 ns. For negative discharges, due to the higher momentum transfer collision frequency and thus a low mobility in the liquid phase, electrons tend to deposit on the gas-liquid interface and charge it negatively. For positive discharges, the high mobility of electrons would leave the interface charged positively. Under both circumstances, it is possible that the charged interface would be pushed to displace the liquid under an external electric field by electrostatic force. A simplified calculation can be made to examine whether or not the electrostatic force would be sufficient to overcome the resistance of water at the interface. The pressure due to the surface tension γ on a water interface of a spherical bubble with a radius of curvature r can be approximated by the Young-Laplace equation $p = 2\gamma/r$. With $r \sim 1 \text{ }\mu\text{m}$, and $\gamma = 72.8 \times 10^{-4} \text{ N/m}$, the surface tension pressure is $\sim 15 \text{ kPa}$. The ultimate strength of water of approximately 30 MPa must be exceeded for rupturing the liquid.¹⁹ Considering forces due to charged particles only, and ignoring those due to field gradients and material property gradients, the electric force at the interface becomes simply the electrostatic force L , which is the product of charge density per unit area σ and the electric field E , i. e., $L = e\sigma E$, where e is the charge per electron. For $E = 10^8 \text{ V/cm}$, σ should have a value of $10^{12} \text{ charges/cm}^2$. For electrons with an average energy of 1 eV, the electron thermal velocity can be estimated as $6 \times 10^7 \text{ cm/s}$. So a modest electron density of 10^{13} cm^{-3} will provide the flux necessary to charge the surface to the breaking point within 1 ns. Although these estimations for water rupturing also neglect both loss mechanisms and the energy requirements to overcome the hydrodynamic resistance, the electrostatic mechanism still seems a likely candidate for streamer propagation, and such forces may dominate at a nanosecond time scale.

The growth of a plasma filament is determined by conservation equations of mass, momentum, and energy. To quantify the breakdown process described above, the equations for the formation and propagation of the plasma-filled filaments are defined as²⁰

$$\frac{\partial \rho}{\partial t} + \nabla \cdot (\rho u) = \frac{2\lambda(T)T}{\Delta_v H r_0^2} \quad (1)$$

$$\frac{\partial u}{\partial t} + u \cdot \nabla u + \frac{1}{\rho} \nabla P = 0 \quad (2)$$

$$\frac{\partial}{\partial t} [\rho(Z + u^2)] + \nabla \cdot \left[\rho u \left(\frac{P}{\rho} + \frac{u^2}{2} \right) \right] = \kappa(T)E^2 \quad (3)$$

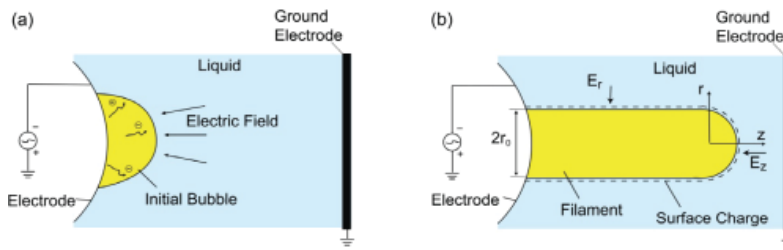


FIGURE 1. (A) Initiation of bubble formation; (B) schematic diagram of a cylindrical filament in water.

where t is time, ρ and P are the radial density and pressure inside streamer, respectively, u is the velocity of streamer, T is the temperature, λ is the thermal conductivity, $\Delta_v H$ is the evaporation heat of water, r_0 is the radius of streamer, Z is the internal energy of ionized gas, E is the electric field strength, and κ is the electric conductivity. It is usually difficult to directly solve Eqs. (1)–(3) because of the high nonlinearity of the equations.

For simplification, the streamer was assumed to be a cylinder with a hemispherical tip as shown in Figure 1B. The reference frame was fixed on the tip. The radius of the filament is r_0 . Although it appears from photographic evidences that the filament is usually of a conical shape, the cylindrical approach is still a good approximation when the length of the filament is much greater than the radius. The electric conductivity κ inside the filament could be described as

$$\kappa = \frac{n_e e^2}{m v_{en}} \quad (4)$$

where m is the mass of electron, and v_{en} is the frequency of electron-neutral collisions. Note that v_{en} is proportional to the gas number density and the value of v_{en}/p is usually on the order of $10^9 \text{ s}^{-1} \text{ Torr}^{-1}$.¹⁸ Sunka et al. measured the broadening of the $H\alpha$ line profile, which is commonly used to characterize the density of plasma, reporting the electron density inside streamers during the initial phase of water breakdown to be on the order of 10^{18} cm^{-3} .²¹ With the room temperature saturated water vapor pressure of 20 Torr, the electric conductivity inside the filament can be estimated to be on the order of 10^7 S/m , a value that is comparable to those for metals. Thus, the filament could be regarded as equipotential with the electrode, and thus could be treated as an extension of the electrode throughout the expansion. The external fluid provides drag force and constant external pressure for the development of the filament. Gravity is neglected here because the body force induced by gravity is much smaller than the electric forces.

The electric field outside a slender jet can be described as if it were due to an effective linear charge density (incorporating the effects of both free charge and polarization charge) of charge density σ on the surface. Since the charge density in liquid can be ignored compared to that on the filament surface, one can have the following equation for the space outside the filament by applying the Laplace equation in the radial direction:

$$\frac{1}{r} \frac{\partial}{\partial r} \left(r \frac{\partial \Phi}{\partial r} \right) = 0 \tag{5}$$

with boundary conditions $\Phi|_{r=r_0} = \Phi_0$ and $\Phi|_{r=R} = 0$. R is the distance between the anode and cathode. Because the filament could be regarded as an extension of the electrode, R decreases as the streamer propagates through the gap.

Solving the above equation with an assumption of negative discharge, the radial electric field E_r and local surface charge density σ_r can be written as

$$E_r = \frac{\partial \Phi}{\partial r} = - \frac{\Phi_0}{r_0 \ln(R / r_0)} \tag{6}$$

$$\sigma_r = \varepsilon E_r = - \varepsilon_r \varepsilon_0 \frac{\Phi_0}{r_0 \ln(R / r_0)} \tag{7}$$

There is no analytical solution for the electric field at the hemispherical tip of the filament. A frequently used approximation is $E_z \approx \Phi_0 / r_0$. Here, the equation for the electric field at the tip of a needle in a needle-to-plane geometry developed by Lama and Gallo was used,²²

$$E_z = - \frac{2\Phi_0}{r_0 \ln(4R / r_0)} \tag{8}$$

Similarly, the local charge density at the tip is:

$$\sigma_z = \varepsilon E_z = - \varepsilon_r \varepsilon_0 \frac{2\Phi_0}{r_0 \ln(4R / r_0)} \tag{9}$$

From Eqs. (6)–(9), one can conclude that the radial direction electrostatic pressure $E\sigma$ exerted on the sidewall of the streamer was weaker than the axial direction electrostatic pressure on the tip. Note that both electrostatic pressures were roughly inversely proportional to r_0^2 , meaning that at the initial stage of the filament growth when r_0 is small, the electrostatic forces on both directions were strong and the filament would grow both axially and radially. A direct consequence of both the axial and radial expansions of the streamer channel is the launching of compression waves into adjacent liquids.¹³ At some critical point, the electrostatic force would reach a balance with hydrodynamic resistance acting on the surface in the radial direction first, while the filament continued to grow in the axial direction.

Experimentally recorded propagation speeds of the filaments varied depending on the measurement techniques, ranging from a few kilometers to one hundred kilometers per second.^{13,23,24} In spite of the discrepancy observed by different groups, the propagation was clearly in the supersonic regime, and the formation of shockwaves had to be taken into consideration (see Fig. 2). The drag force on the tip of the streamer, which is a stagnation point, equals to the force produced by the total hydrodynamic pressure,

$$P_{hd} = P_1 \left(\frac{2\alpha}{\alpha + 1} M_1^2 - \frac{\alpha - 1}{\alpha + 1} \right) + \frac{1}{2} \rho (CM_2)^2 \tag{10}$$

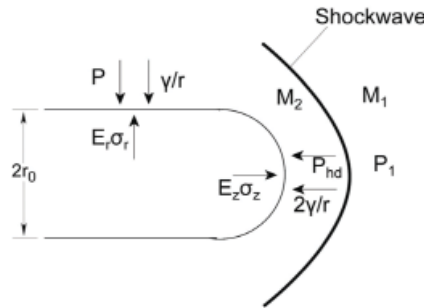


FIGURE 2. Force balance for the present electrostatic model.

where P_1 is ambient pressure, $P_1 \cdot \left(\frac{2\alpha}{\alpha+1} M_1^2 - \frac{\alpha-1}{\alpha+1} \right)$ is the pressure behind shock front, α is the specific heat ratio of water, M_1 is the Mach number of streamer, M_2 is the Mach number after the shock front, and C is the speed of sound in liquid. The relationship between M_1 and M_2 can be written as²⁵

$$M_2^2 = \frac{(\alpha-1)M_1^2 + 2}{2\alpha M_1^2 + 1 - \alpha} \quad (11)$$

Equating the hydrodynamic pressure to the sum of the electrostatic pressure and the pressure produced by surface tension at the tip can give the following equation for streamer propagation:

$$4\varepsilon_r \varepsilon_0 \frac{\Phi_0^2}{r_0^2 \ln^2(4R/r_0)} = P_1 \left(\frac{2\alpha}{\alpha+1} M_1^2 - \frac{\alpha-1}{\alpha+1} \right) + \frac{1}{2} \rho (CM_2)^2 + \frac{2\gamma}{r_0} \quad (12)$$

The balance between the electrostatic force and the force produced by the total hydrodynamic pressure in the radial direction can be given as

$$\varepsilon_r \varepsilon_0 \frac{\Phi_0^2}{r_0^2 \ln^2(R/r_0)} = P_1 + \frac{1}{2} \rho (CM_2)^2 + \frac{\gamma}{r_0} \quad (13)$$

Note that there are three unknowns, M_1 , M_2 , and r_0 , in the above equations. So it is possible to solve Eqs. (11)–(13) simultaneously when the applied voltage Φ_0 and the interelectrode distance R are specified.

To demonstrate the validity of the present model, the filament radius predicted by the model is shown in Figure 3. For a typical interelectrode distance of 1 cm, the filament radius increased from 3 μm to 50 μm as the applied voltage rose from 5 kV to 30 kV. The value was comparable to typical experimental values. For example, Baumung and Bluhm reported that the light emission from the discharge was restricted to a channel of 100 μm diameter, indicating the interaction of charged particles in the region.¹³

Figure 4 shows the filament propagation speed as a function of Φ_0 and R . The calculated propagation speed from the present model was around 15 km/s, which was higher

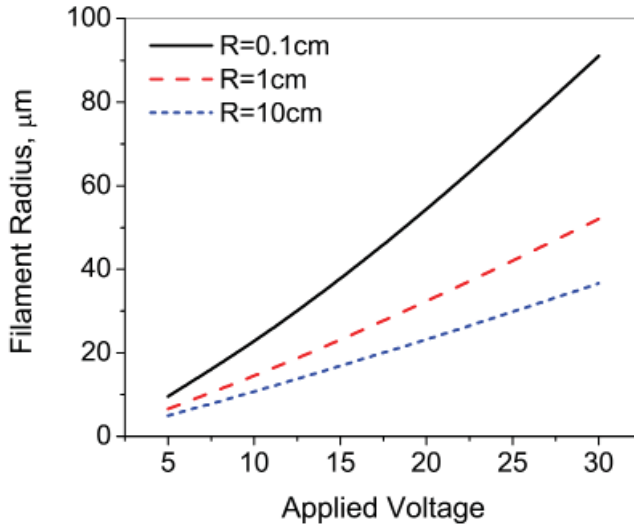


FIGURE 3. Variations of filament radius as a function of applied voltage and interelectrode distance.

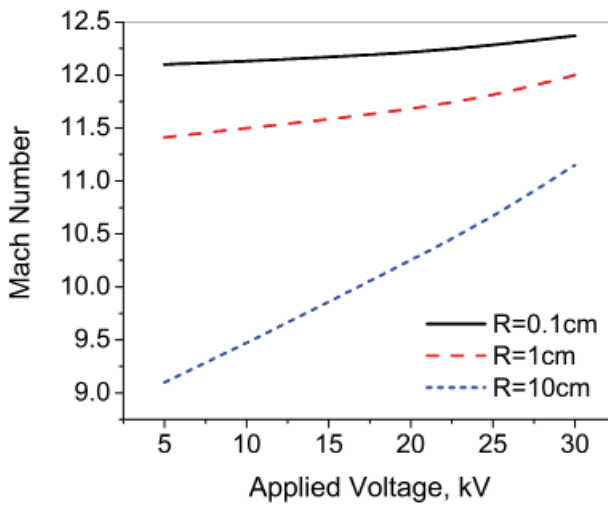


FIGURE 4. Variations of the Mach number of a streamer as a function of applied voltage and interelectrode distance.

than the primary streamer speed, but lower than the secondary streamer speed reported by Baumung and Bluhm.¹³ The Mach number increased moderately with the applied voltage, a phenomenon that is understandable from the point of view of energy conservation. The streamer propagation velocity was relatively independent of the interelectrode distance. For an applied voltage of 30 kV, the Mach number increased from 11.2 to 12.3 when the interelectrode distance decreased from 10 cm to 0.1 cm. This is consistent

with the known property of negative streamers since the previous experiment showed that for a given voltage the propagation, velocity was relatively constant as the streamer crossed the gap, and it increased as the streamer approached the plane electrode.¹⁴ This phenomenon could be understood by Eq. (6), i.e., the interelectrode distance R was decreased with the propagation of the streamers; as a result, the electric field at the tip of the streamer was increased, leading to a higher propagation speed. However, the amount of the increase in the electric field would not be significant because of the natural logarithm in the equation.

B. Thermal Mechanism

In the electrostatic model described above, it was assumed that the translational temperature inside the streamer was low, and the electrostatic force was the only driving force for the growth of the filament. The assumption was valid only at the initial stage of the filament development, since the temperature will keep rising as the molecules gain more energy through electron-neutral collisions. The heating time τ is approximately $\tau = \tau_{\text{en}} + \tau_{\text{vt}}$, where τ_{en} is the time for electron-neutral excitation, and τ_{vt} is the time for vibrational-translational (v-t) relaxation. For electron-neutral excitation, $\tau_{\text{en}} = 1/\nu_{\text{en}} = 1/(n_{\text{e}}k_{\text{en}})$, where ν_{en} is the electron-neutral nonelastic collision frequency, n_{e} is the electron density, and k_{en} is the rate constant for electron-neutral collisions; k_{en} can be expressed as $k_{\text{en}} = \sigma_{\text{en}} \nu_{\text{te}}$, where σ_{en} is the cross section for vibrational excitation of H_2O molecules by electron impact and ν_{te} is the electron thermal velocity.

For electrons with an average energy of 1 eV, the cross section for vibrational excitation is about $\sigma = 10^{-17} \text{ cm}^2$.²⁶ k_{en} is thus about $10^{-8} \text{ cm}^3/\text{s}$, as is typical ($\nu_{\text{te}} = 6 \times 10^7 \text{ cm/s}$). Spectroscopic measurements indicated that the stark broadening of the $H\alpha$ line corresponded to an electron density of about 10^{18} cm^{-3} at a quasi-equilibrium state.²¹ Thus, the typical electron-neutral excitation time can be estimated to be on the order of a few nanoseconds. For the v-t relaxation, $\tau_{\text{vt}} = 1/(n_{\text{v}}k_{\text{vt}})$, where n_{v} is the density of vibrational excited molecules, and k_{vt} is the v-t relaxation rate coefficient. For water molecules at room temperature, k_{vt} is about $3 \times 10^{-12} \text{ cm}^3/\text{s}$.¹⁸ Assuming that n_{v} is on the same order with the electron density, τ_{vt} could be estimated to be on the order of several hundred nanoseconds, suggesting that heating can take place inside the filaments under a submicrosecond time scale due to the energy transfer from the electrons to the translational energy of the water molecules; and furthermore, the propagation of the streamers could be caused by the continuous evaporation of water molecules at the tip. Here, the energy dissipation was not considered, and the actual heating time might be longer, but still the local heating mechanism under the submicrosecond time regime seems possible.

To quantify the process described above, it was assumed that a small cylindrical portion of water evaporated at the tip of the streamer during time Δt so that the length of the streamer grew from L to $L + \delta L$, as shown in Figure 5. The diameter of the evaporated water cylinder was assumed to be $2r_{\text{e}}$. There was no definitive value for pressure P_{e} inside the small vaporized portion given the extremely high temperature. However, P_{e} could be estimated to be on the order of 1000 atm because of the density difference

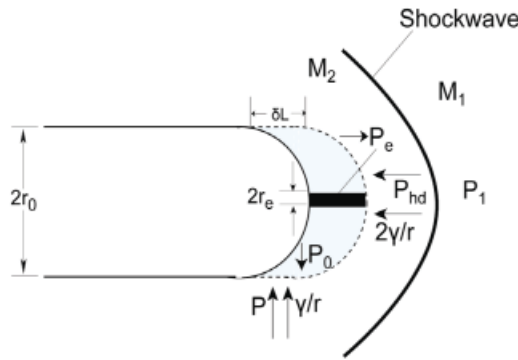


FIGURE 5. Force balance for the present thermal model.

between liquid water and vapor. Such a high pressure could provide the driving force needed for the growth of the filament. As in the previous section, one can get the force balance along the axial direction at the tip of the filament assuming a steady state condition as

$$P_1 \left(\frac{2k}{k+1} M_1^2 - \frac{k-1}{k+1} \right) + \frac{1}{2} \rho (CM_2)^2 + \frac{2\gamma}{r_e} = P_e \quad (14)$$

The energy required for the evaporation of water can be calculated as

$$E_e = \rho V_e (c_p \Delta T + \Delta_v H) \quad (15)$$

where ρ is the density of water, V_e is the volume of evaporated water, c_p is the specific heat of water. V_e can be written as

$$V_e = \pi r_e^2 \cdot \delta L \quad (16)$$

After evaporation, the overheated and overpressured water vapor will expand radially, while satisfying the force balance along the axial direction, until it reaches an equilibrium with the outside hydrodynamic pressure. The process could be regarded as adiabatic under a submicrosecond time scale, and thus one can have the following equations:

$$P_e V_e^{\alpha_s} = P_0 V_0^{\alpha_s} \quad (17)$$

$$\frac{P_0}{P_e} = \left[\frac{\epsilon_r \epsilon_0 \Phi_0^2}{\rho r_0 (c_p \Delta T + \Delta H_{1-g}) \ln(R/r_0)} \right]^{\alpha_s} \quad (18)$$

where P_0 and V_0 are the pressure and volume, respectively, of the water vapor after the expansion, r_0 is the radius of the filament after expansion, and α_s is the specific heat ratio of the water vapor. The force produced by P_0 should be in balance with the forces

created by both surface tension and total environmental hydrodynamic pressure as given below,

$$P_0 = P_1 + \frac{1}{2} \rho (CM_2)^2 + \frac{\lambda}{r_0} \quad (19)$$

Another set of equations can be obtained through the consideration of energy conservation. The energy required to vaporize water was the electric energy provided by the power supply. If the entire filament was viewed as a capacitor with capacitance C , the required energy could be calculated as

$$E = \frac{C\Phi_0^2}{2} \quad (20)$$

The capacitance of the cylindrical filament is

$$C = 2\pi\epsilon\epsilon_0 L / \ln(R / r_0) \quad (21)$$

So the energy change required to extend the length by δL becomes

$$\delta E = \pi\epsilon\epsilon_0 \delta L \Phi_0^2 / \ln(R / r_0) \quad (22)$$

By equating δE to E_e , one has

$$r_c = \sqrt{\frac{\epsilon\epsilon_0 \Phi_0^2}{\rho(c_p \Delta T + \Delta H_{1-g}) \ln(R / r_0)}} \quad (23)$$

Assuming $\alpha \approx 1$ due to the low compressibility of water, and rearranging Eqs. (11), (14), (18), (19), and (23) to eliminate M_2 , r_c , and P_g , one can get a set of equations about M_1 and r_0 as follows:

$$P_1 M_1^2 + \frac{\rho C^2}{2M_1^2} - P_e + 2\gamma \sqrt{\frac{\rho(c_p \Delta T + \Delta H_{1-g}) \ln(R / r_0)}{\epsilon_r \epsilon_0 r_0 \Phi_0^2}} = 0 \quad (24)$$

$$P_e \left[\frac{\epsilon_r \epsilon_0 \Phi_0^2}{\rho r_0 (c_p \Delta T + \Delta H_{1-g}) \ln(R / r_0)} \right]^{k_s} - P_1 - \frac{\rho C^2}{2M_1^2} - \gamma \sqrt{\frac{\rho(c_p \Delta T + \Delta H_{1-g}) \ln(R / r_0)}{\epsilon_r \epsilon_0 r_0 \Phi_0^2}} = 0 \quad (25)$$

For water vapor, α_s can be assumed to be 1.3.²⁷ For high-temperature underwater discharges, the translational plasma temperature was measured to be between approximately 4000 K and 6500 K.²⁸ An average value of 5000 K was used for ΔT in the present study. Figure 6 shows the Mach number of filament propagation, M_1 , as a function of Φ_0 and R . The propagation velocity was about 50 km/s, which was higher than the secondary streamer velocity of 25 km/s reported by Baumung and Bluhm¹³, but lower than the value of 200 km/s reported by Woodworth et al.²⁴ The discrepancy in the two

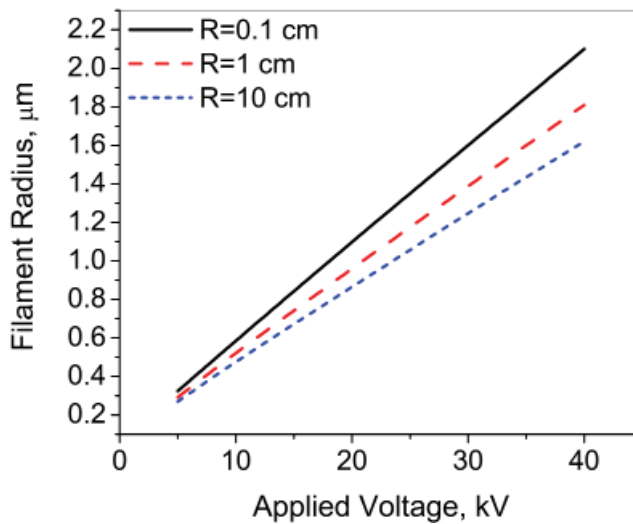


FIGURE 6. Variations of filament radius as a function of applied voltage and interelectrode distance.

measurements probably came from the different techniques used for the velocity measurements. The value of M_1 remained constant for various values of Φ_0 and R , indicating that the propagation velocity of the streamers was independent of either the applied voltage or interelectrode distance. A similar phenomenon was observed previously,^{13,24} where the propagation velocity of secondary streamers was constant over a wide voltage range. Figure 7 shows the filament radius as a function of Φ_0 and R . The radius increased slightly as the streamers approached the other electrode, while it decreased almost linearly as the applied voltage dropped. The absolute value of r_0 was about one order smaller than that obtained from the electrostatic model. This could be understood if one considers the energy requirements for the two mechanisms. For the evaporation of water, the energy needed to break the hydrogen bonds between water molecules should be much greater than that required to displace the same volume of water.

The different models based on the electrostatic force and evaporation gave different results of the streamer propagation speed and filament radius. The electrostatic model showed streamers with a larger radius and a lower Mach number, while the thermal model demonstrated that the streamers could move much faster, but were thinner than those determined from the electrostatic model. The different findings from the two models led us to postulate that different mechanisms might be associated with the different modes of the streamer propagation. At the initial primary streamer mode before any significant heat was generated, the electrostatic force might have played a major role. The appearance of the secondary streamer required more time, during which the electron energy could be transferred to the translational energy of water molecules, and subsequently evaporation could become the dominant force to drive the filament to move forward. The transition time between the primary and secondary streamers was on the order of 100 ns,¹³ a value that is in accordance with the heating time as estimated above.

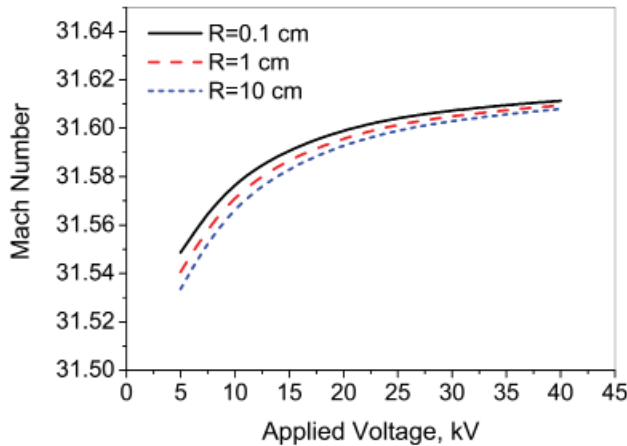


FIGURE 7. Variations of the Mach number of a streamer as a function of applied voltage and interelectrode distance.

III. STABILITY ANALYSIS

The breakdown process is usually characterized by two features, i.e., an initial development of thin discharge channels and a subsequent branching of these channels into complicated “bushlike” patterns. Apparently, the branching process is associated with the instability of the filament. In this section, the linear stability analysis of the axisymmetric perturbation of a filament surface with a certain electric charge density is presented. As long as the wavelength of the perturbation is much smaller than the length of the filament, the stability characteristics can be approximated by considering perturbations to a charged cylinder of constant radius as shown in Figure 8. The peak-to-peak amplitude and wave number of the disturbance are h and k , respectively. H is the depth of wave influence, and u is the velocity of liquid relative to the disturbance. Then, the surface of the perturbation can be represented by the following equation:

$$r = r_0 + \frac{h}{2} \exp(ikz + \omega t) \quad (26)$$

where ω is the oscillation frequency of the instability. To analyze the linear stability, the disturbance of the local electrostatic force, surface tension, and hydrodynamic pressure were considered following a geometrical perturbation. Generally, the surface tension tends to minimize the surface area and subsequently stabilize the disturbance, while the local enhancement of the electrostatic force tended to push the disturbance to grow. In the reference frame that moves together with the tip of the filament, the effects of these three forces were considered separately for the pressure balance between the crest and trough along the streamline (see Fig. 8).

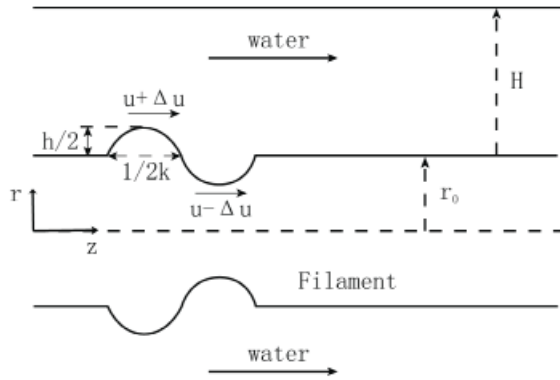


FIGURE 8. Schematic diagram of disturbance at the surface of a filament.

A. Electrostatic Pressure

According to Eqs. (6)–(9), the electrostatic pressure is proportional to the square of the local curvature of the interface, which is different at the crest and trough of the perturbation. Thus, the electrostatic pressures at the crest and trough, $P_{E,c}$ and $P_{E,t}$, become, respectively,

$$P_{E,c} = \epsilon_r \epsilon_0 \Phi_0^2 \frac{\chi_c^2}{4} \tag{27}$$

and

$$P_{E,t} = \epsilon_r \epsilon_0 \Phi_0^2 \frac{\chi_t^2}{4} \tag{28}$$

where ϵ_r is the relative permittivity of water, and χ_c and χ_t are the mean curvatures at the crest and trough, respectively. The expression for the mean curvature can be written as²⁹

$$\chi = \frac{1}{r\sqrt{1+(\partial_z r)^2}} - \frac{\partial_z(\partial_z r)}{(1+(\partial_z r)^2)^{3/2}} = \frac{1}{r} - \partial_z(\partial_z r) \tag{29}$$

Substituting Eq. (26) into Eq. (29), one can get expressions for M_c and M_t ,

$$\chi_c = \frac{1}{r_0 + h/2} + \frac{h}{2} k^2 \tag{30}$$

$$\chi_t = \frac{1}{r_0 + h/2} - \frac{h}{2} k^2 \tag{31}$$

Subsequently, $P_{E,c}$ and $P_{E,t}$ can be written as

$$P_{E,c} = \varepsilon_r \varepsilon_0 \Phi_0^2 \frac{\mathcal{X}_c^2}{4} = \varepsilon_r \varepsilon_0 \Phi_0^2 \left(\frac{1}{(2r_0 + h)^2} + \frac{hk^2}{2(2r_0 + h)} \right) \quad (32)$$

$$P_{E,t} = \varepsilon_r \varepsilon_0 \Phi_0^2 \frac{\mathcal{X}_t^2}{4} = \varepsilon_r \varepsilon_0 \Phi_0^2 \left(\frac{1}{(2r_0 - h)^2} - \frac{hk^2}{2(2r_0 - h)} \right) \quad (33)$$

Thus, the electrostatic pressure difference between the crest and trough becomes

$$\Delta P_E = P_{E,c} - P_{E,t} = -\frac{\varepsilon_r \varepsilon_0 \Phi_0^2 h}{2r_0^3} + \frac{\varepsilon_r \varepsilon_0 \Phi_0^2 hk^2}{2r_0} \quad (34)$$

B. Surface Tension

The pressures due to the surface tension across the interface at the crest and trough can be written as

$$P_{T,c} = \gamma \mathcal{X}_c = \gamma \left(\frac{1}{r_0 + h/2} + \frac{h}{2} k^2 \right) \quad (35)$$

and

$$P_{T,t} = \gamma \mathcal{X}_t = \gamma \left(\frac{1}{r_0 - h/2} - \frac{h}{2} k^2 \right) \quad (36)$$

Thus, the pressure difference due to surface tension between the crest and trough becomes

$$\Delta P_T = P_{T,c} - P_{T,t} = -\frac{\gamma h}{r_0^2 - h^2/4} + \gamma hk^2 \quad (37)$$

Since $r_0 \gg h$, the above equation can be simplified as

$$\Delta P_T = -\frac{\gamma h}{r_0^2} + \gamma hk^2 \quad (38)$$

C. Hydrodynamic Pressure

When there is a disturbance on the interface of the filament, the flow speed of liquid will be perturbed in the depth of wave influence, inducing a hydrodynamic pressure difference ΔP_H between the crest and trough,

$$\Delta P_{HD} = \frac{1}{2} \rho \left(u + \frac{\Delta u}{2} \right)^2 - \frac{1}{2} \rho \left(u - \frac{\Delta u}{2} \right)^2 = \rho u \Delta u \quad (39)$$

where $\Delta u/2$ is the perturbation in the flow speed caused by the shape of the wave. The dynamic pressure is related to the flow speed through Bernoulli's equation. The pressure difference from the electrostatic force and dynamic effect of the flow has the opposite sign due to the surface tension. For a balance between two kinds of oppositely directed pressure differences, one has

$$\rho u \Delta u + \frac{\gamma h}{r_0^2} - \gamma h k^2 - \frac{\epsilon_r \epsilon_0 \Phi_0^2 h}{2r_0^3} + \frac{\epsilon_r \epsilon_0 \Phi_0^2 h k^2}{2r_0} = 0 \tag{40}$$

In order to solve Eq. (40), the perturbed flow speed Δu must be expressed in terms of experimentally measurable quantities. The following derivation was inspired by Kenyon.³⁰

Assuming that the perturbed flow speed is constant over the depth of wave influence, the mass conservation equation through vertical cross sections between the crest and trough becomes

$$\left(u + \frac{\Delta u}{2}\right) \left(H - \frac{h}{2}\right) = \left(u - \frac{\Delta u}{2}\right) \left(H + \frac{h}{2}\right) \tag{41}$$

where H is the depth of wave influence. The above equation can be reduced to

$$u \cdot h = \Delta u \cdot H \tag{42}$$

The theoretical expression for H was given by Kenyon³¹ as

$$H = \frac{1}{2\pi k} \tag{43}$$

Using Eqs. (42) and (43) to eliminate H and Δu , Eq. (40) becomes

$$\rho \omega^2 = k \left(\gamma k^2 + \frac{\epsilon_r \epsilon_0 \Phi_0^2}{2r_0^3} - \frac{\gamma}{r_0^2} - \frac{\epsilon_r \epsilon_0 \Phi_0^2 k^2}{2r_0} \right) \tag{44}$$

Since this is a quadratic equation, there will be two different branches of the dispersion relation, and an instability occurs if $Re(\omega) > 0$. The first thing to note in Eq. (44) is that when the applied voltage Φ_0 is equal to zero and the surface is flat, in other words, when the radius of the filament r_0 goes to infinity, the above equation reduces to $\rho u^2 = \gamma k$, which is the equation for the classic 2D Rayleigh instability.

Figure 9 shows the instability growth rate ω at a low applied voltage, where the process is in Rayleigh mode. The dashed line represents the classic Rayleigh instability for $\Phi_0 = 0$ and $r_0 \rightarrow \infty$. For $\Phi_0 \neq 0$ and r_0 is finite, instability only happens at high wave numbers. When the voltage increases under this mode, the growth rate is decreased until fully suppressed at a certain critical value. The physical explanation for this can be as follows. The Rayleigh instability occurs due to surface tension, which always acts to break a cylindrical jet into a stream of droplets; on the other hand, the electrostatic force, which is proportional to the square of the applied voltage, always acts in the opposite direction of the surface tension. When the applied voltage increases, the Rayleigh instability would be suppressed when the two forces are balanced.

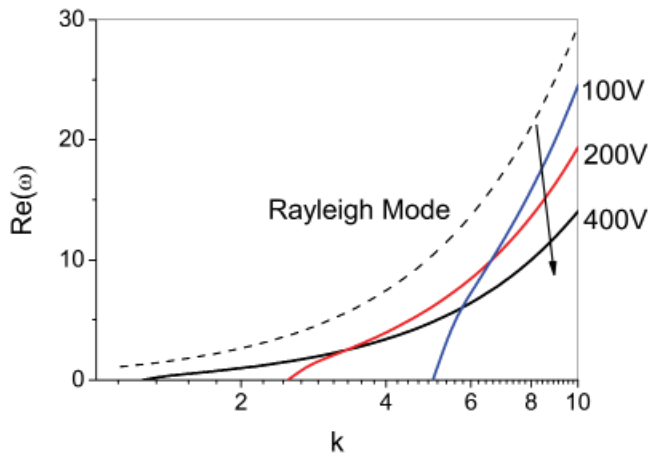


FIGURE 9. Instability growth rate ω at low applied voltages; k and ω are nondimensionalized using streamer radius r_0 and time scale $t = (\rho r_0^3 / \gamma)^{1/2}$.

As the voltage continues to increase, the instability enters the electrostatic mode, where the electrostatic force exceeds the force created by the surface tension and becomes the dominant force. Figure 10 shows the instability growth rate ω at a high voltage. Both the growth rate and the range of wave number increase as the voltage rises. The physics of this mode is a consequence of the interaction of the electric field with the surface charge on the interface; surface tension is a parameter of less importance for this mode. The mechanism for the instability is that a perturbation in the radius of the filament induces a perturbation in the surface charge density and therefore a perturbation in the electrostatic pressure. At a high voltage, the perturbation is amplified by the fact that the electrostatic pressure PE is proportional to Φ^2 , causing the instability. In contrast to the Rayleigh mode, the instability in the electrostatic mode is unavoidable at low wave numbers (long wavelength). This may explain why the filament always tends to branch into bushlike structures.

IV. CONCLUSIONS

The electric breakdown of water involves both the generation and propagation of low-density channels through the liquid. The different physical processes and interactions between different phases of the media should contribute to the complexity of the problem. In the present study, different modes of the streamer propagation were considered in simplified steps, with each step characterized by a driving force and the corresponding hydrodynamic drag. The effects of the electrostatic force and local heating on the streamer propagation were analyzed using simplified assumptions. It was shown that both of them were dominant for the streamer propagation, but at different time scales. Furthermore, a linear instability analysis was performed on a charged cylindrical streamer in an external electric field to understand the bushlike growth pattern of breakdown in

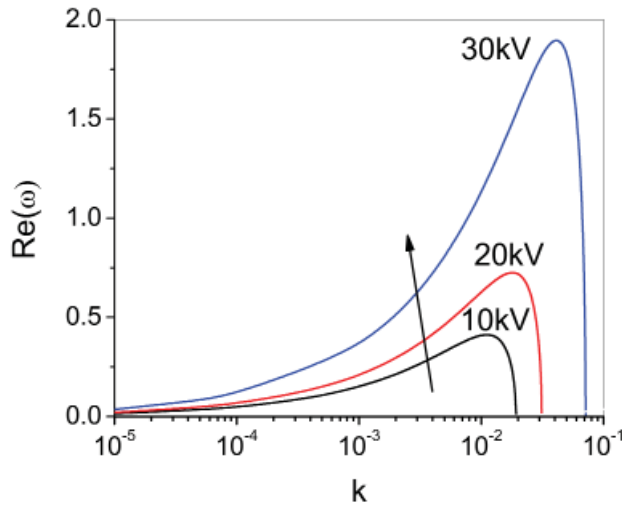


FIGURE 10. Instability growth rate ω at high applied voltages; k and ω are nondimensionalized as in Figure 9.

the liquid. It was shown that the stability may be caused by the competition between perturbations in the electrostatic pressure and surface tension caused by the disturbance of the streamer geometry. With increasing applied voltage, the electrostatic instability was found to grow, whereas the classic Rayleigh instability was found to be suppressed.

ACKNOWLEDGMENT

This work was supported by U.S. Department of Energy, National Energy Technology Laboratory, through Contract No. DE-NT0005308.

REFERENCES

1. Locke B, Sato M, Sunka P, Hoffman MR, Chang J-S. Electrohydraulic discharge and non-thermal plasma for water treatment. *Ind Eng Chem Res.* 2006;45:882–905.
2. Sunka, P. Pulse electrical discharges in water and their applications, *Phys Plasmas.* 2001;8:2587–94.
3. Akiyama H. Streamer discharges in liquids and their applications. *IEEE Trans Dielectr Electr Insul.* 2000;7:646–53.
4. Zahn M, Ohki Y, Fenneman DB, Gripshover RJ, Gehman VH. Dielectric properties of water and water/ethylene glycol mixtures for use in pulsed power system design. *Proc IEEE.* 1986;74:1182–221.
5. Aprile E, Ku WH-M, Park I. Delta electron production and the ultimate energy resolution of liquid argon ionization detectors. *IEEE Trans Nucl Sci.* 1988;35:37–41.
6. Laroussi M. Nonthermal decontamination of biological media by atmospheric-pressure plasmas: review, analysis, and prospects. *IEEE Trans Plasma Sci.* 2002;30:1409–15.

7. Beroual A. Electronic and gaseous processes in the prebreakdown phenomena of dielectric liquids. *J Appl Phys.* 1993;73:4528–33.
8. Jones HM, Kunhardt ES. Development of pulsed dielectric breakdown in liquids. *J Phys D.* 1995;28:178–88.
9. Lewis T. A new model for the primary process of electrical breakdown in liquids. *IEEE Trans Dielectr Electr Insul.* 1998;5:306–15.
10. Lewis T. Breakdown initiating mechanisms at electrode interfaces in liquids. *IEEE Trans Dielectr Electr Insul.* 2003;10:948–55.
11. Qian J, Joshi RP, Kolb J, Schoenbach KH, Dickens J, Neuber A, Krompholz H, Schamiloglu E, Gaudet J. Microbubble-based model analysis of liquid breakdown initiation by a sub-microsecond pulse. *J Appl Phys.* 2005;97:113304.
12. Qian J, Joshi RP, Schoenbach KH, Woodworth JR, Sarkisov G. Model analysis of self- and laser-triggered electrical breakdown of liquid water for pulsed-power applications. *IEEE Trans Plasma Sci.* 2006;34:1680–91.
13. An W, Baumung K, Bluhm H. Underwater streamer propagation analyzed from detailed measurements of pressure release. *J Appl Phys.* 2007;101:053302.
14. Watson P, Chadbank W. The role of electrostatic and hydrodynamic forces in the negative-point breakdown of liquid dielectrics. *IEEE Trans Electr Insul.* 1991;26:543–59.
15. Lisitsyn IV, Nomiya H, Katsuki S, Akiyama H. Thermal processes in a streamer discharge in water. *IEEE Trans Dielect Dielectr Electr Insul.* 1999;6:351–6.
16. Joshi RP, Qian J, Zhao G, Kolb J, Schoenbach KH, Gaudet J, Schamiloglu E. Are microbubbles necessary for the breakdown of liquid water subjected to a submicrosecond pulse? *J Appl Phys.* 2004;96:5129–39.
17. Kupershtokh AL, Medvedev DA. Anisotropic instability of dielectric liquids and decay to vapor-liquid system in strong electric fields. *Tech Phys Lett.* 32:634–7, 2006
18. Fridman A, Kennedy L. *Plasma physics and engineering.* New York: Taylor & Francis Group; 2006.
19. Morch KA. Reflections on cavitation nuclei in water. *Phys Fluids.* 2007;19:072104.
20. Gidalevich E, Boxman R. Sub- and supersonic expansion of an arc channel in liquid. *J Phys D.* 2006;39:652–9.
21. Sunka P, Babicky V, Clupek M. Generation of chemically active species by electrical discharges in water. *Plasma Sources Sci Technol.* 1999;8:258–265.
22. Lama W, Gallo C. Systematic study of the electrical characteristics of the trichel current pulses from negative needle-to-plane coronas. *J Appl Phys.* 1977;45:103–13.
23. Beroual A, Zahn M, Badent A, Kist K, Scwabe AJ, Yamashita H, Yamazawa K, Danikas M, Chadband WD, Torshin Y. Propagation and Structure of Streamers in liquid Dielectrics. *IEEE Electr. Insul. Mag.,* 14:6–14, 1998
24. Woodworth JR, Lehr J, Elizondo-Decanini J, Miller PA, Aragon B, Elizondo-Decanini J, Fowler W, Maenchen JE, Sarkisov GS, Corley J, Hodge K, Drennan S, Guthrie D, Mowrer D, Navarro M, Johnson DL. Optical and Pressure Diagnostics of 4-MV Water Switches in the Z-20 Test Facility. *IEEE Trans. Plasma Sci.,* 32:1778–89, 2004
25. White FM. *Viscous fluid flow,* 3rd ed.. Singapore: McGraw-Hill; 2006.
26. Itikawa Y. Electron-impact vibrational excitation of H₂O. *J Phys Soc Jpn.* 1974;36:1127–32.

27. Parry W, Bellows J, Gallagher J, Harvey A. ASME international steam tables for industrial use. New York: ASME; 2008.
28. Lange H, Huczko A. Carbon arc discharge: plasma emission spectroscopy and carbon nanostructure formation. *Trans Mater Res Soc Jpn.* 2004;29:3359–64.
29. Eggers J. Nonlinear dynamics and breakup of free-surface flows. *Rev Mod Phys.* 1997;69:865–930.
30. Kenyon KE. Capillary waves understood by an elementary method. *J Oceanogr.* 1998;54:343–6.
31. Kenyon KE. On the depth of wave influence. *J Phys Oceanogr.* 1983;13:1968–70.

Plasma-Controlled Cell Migration: Localization of Cold Plasma–Cell Interaction Region

O. Volotskova,¹ A. Shashurin,¹ M. A. Stepp,² S. Pal-Ghosh,² & M. Keidar^{1,*}

¹School of Engineering and Applied Sciences, Department of Mechanical and Aerospace Engineering, George Washington University, Washington, DC ²School of Medicine and Health Sciences, George Washington University, Washington, DC

*Address all correspondence to: M. Keidar, George Washington University, School of Engineering and Applied Sciences, Department of Mechanical and Aerospace Engineering, Phillips Hall, Suite 739, 801 22nd Street NW, Washington, DC 20052; keidar@gwu.edu

ABSTRACT: In order to characterize the optimal condition for cell treatment with a plasma jet, its UV-vis-NIR spectrum was evaluated. Furthermore, this study considers the ability of cold atmospheric plasmas to impact cell migration rates as a function of (i) the length of the plasma treatment time, (ii) the number of hours after treatment that cell migration is assessed, and (iii) localization of the treatment zone. Data show that the ability of plasma to reduce cell migration rates increases as a function of treatment time with a maximum of 30%, and that this affect persists for 33 hours after plasma treatment.

KEY WORDS: cold atmospheric plasma, fibroblast cells, migration rates, localization

I. INTRODUCTION

The unique chemical and physical properties of cold atmospheric plasmas enable their numerous recent applications in biomedicine.¹ A wide range of cold plasma applications have been investigated including sterilization, the preparation of polymer materials for medical procedures, wound healing, tissue or cellular removal, and dental drills.^{2–7} One of the recent research trends is the investigation of cold atmospheric plasmas' interaction with living tissue at the cellular level.^{6–9} Initial experiments on the direct interaction of cold plasmas with living cells demonstrated immediate detachment of treated cells from the extracellular matrix.² Later, it was demonstrated that cell detachment occurs for several different cell types including primary mouse fibroblast cells, PAM212 cancer cells, and BEL-7402 liver cancer cells.^{5–7} The effects of mild intensity and short duration cold plasma treatment below the threshold required for cell detachment have also been studied.^{6,7} It was observed that the migration rate of primary mouse fibroblast cells slowed significantly after mild intensity plasma treatment.⁶ Our more recent work⁷ was directed at understanding the mechanism by which the plasma jet alters cell migration and induced cell detachment. It was found that integrin expression at the cell surface reduced at plasma treatment. Integrins (transmembrane proteins) are cell adhesion receptors having a dual function, namely, intracellular (integrin occupancy coordinates the assembly of cytoskeletal filaments and signaling complexes) and extracellular (engaging either extracellular

matrix macromolecules or counter receptors on adjacent cell surfaces). Integrins function in maintaining cell adhesion, tissue integrity, cell migration, and differentiation.^{10–12}

Although several recent studies have begun to sort out the cellular and subcellular events altered when cold plasmas interact with living cells, these studies have yet to address the dose response (the relationship between duration of plasma jet interaction with living tissue and a change in the migration rates) and permanency of the migration effects induced in cells by cold plasmas. These types of studies are crucial to allow us to develop safe and practical applications for cold plasmas. Thus, the UV-vis-NIR spectrum of cold plasma jets¹³ used in current studies is evaluated. In this paper, we use tertiary-passaged mouse dermal fibroblast cells to show the ability of plasma to reduce cell migration rates, demonstrate the effect of the treatment time, and show the localization of the treatment zone in a single well. Further experiments assess the impact of cold plasma on the pH of the cell culture media immediately after plasma treatment.

II. METHODOLOGY

A. Materials

Wild-type tertiary mouse fibroblast cells were cultured in Dulbecco's modified eagle medium (DMEM) (Invitrogen Corp.) enriched with 5% serum, 1% NEAA, 1% L-glutamine, and 1% Pen-Strep. Diluted cells (30% confluence) were plated in multiwell plates (having a well diameter of about 32 mm) and treated with plasma on the third day in culture. During the experiments, plates with cells were kept on the slide moat (heating plate) (Boekel scientific, model 240000) to maintain the media temperature at 37°C. Trypan blue stain 0.4% (Invitrogen Corp.) was used in "alive-vs-dead" testing.

B. Plasma Jet

The plasma jet operated at 4.5–5 kV, 26–28 KHz, and helium flow rate of about 17 L/min.^{6,13} The average discharge power $[(1/T) \int_0^T U I dt]$, where U is the output voltage applied to discharge electrodes, I is the discharge current, and T is the period] was ~4.3 W. The plasma jet was targeted to the well center and had a diameter of about 4–5 mm at contact with the well. Cells were kept in the media during the treatment; 2 mL of media per well was used, and the depth of the media was around 2 mm. This amount of media (2 mL per well) was chosen to prevent cell desiccation⁶). The distance between the jet outlet and well surface was around 2 cm. Plasma treatment was conducted with durations from 100 to 500 s (i.e., 430, 860, 1290, 1720, and 2150 J of discharge energy corresponding to 100, 200, 300, 400, and 500 s, respectively). For controlling purposes, cells treated with pure helium for 100 and 300 s (no plasma) and untreated cells were used. The spectrum of the cold atmospheric plasma jet in the air was monitored by means of fibro-optical portable spectrometer (EPP2000 HR Model, StellarNet-Inc) in the UV-vis-NIR range of wavelengths (200–900 nm) with a fibro-optical probe (diameter 1 mm) oriented along and perpendicular to the jet as shown in Figure 1.

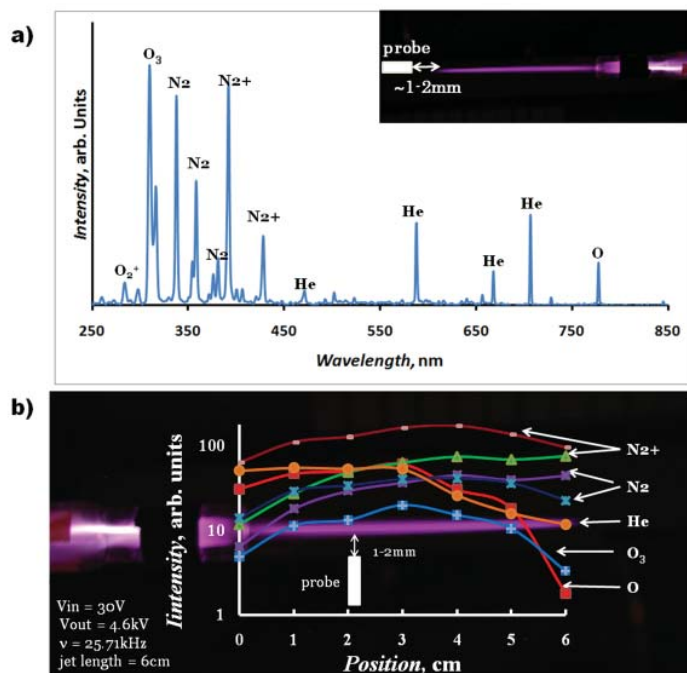


FIGURE 1. (A) UV-vis-NIR spectrum of the jet with assigned elements; schematic of the measurements at the end of jet is shown in the inserted picture. (B) Schematic of the spectroscopic measurements along the jet, and given plasma jet parameters are shown—intensities of O₃, N₂, N₂⁺, He, and O are plotted in logarithmic scale.

C. Time-Lapse Studies

Further time-lapse studies were performed on an Olympus IX81 research microscope (Olympus America, Center Valley, Pennsylvania) equipped with a Proscan motorized stage (Prior Scientific Instruments Ltd., Rockland, Massachusetts) and placed in a temperature- and CO₂-controlled chamber (LiveCell Incubation System, Neue Biosciences, Camp Hill, Pennsylvania). Using relief-contrast optics, images (schematic of the axial point distribution is shown in Fig. 2) were taken per well every 10 min for 16 h and 40 min (100 images) and the next 16 h and 40 min to see the dynamics in ~33 h. Images were transferred to a workstation equipped with Metamorph image analysis software (Molecular Devices Corporations, Chicago, Illinois) where velocities of 10 cells were calculated using the track cell module in each tracked location. A more detailed description can be found elsewhere.¹⁴

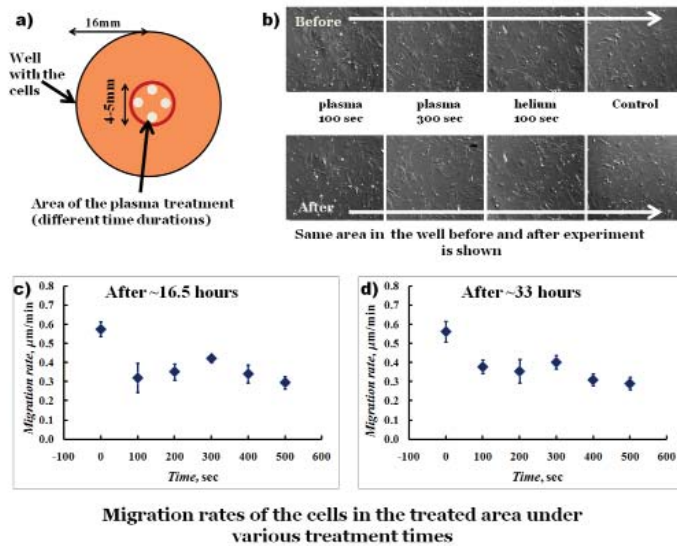


FIGURE 2. (A) Schematic representation of the experiment is shown: reduction in migration rates' dependence on the length of the plasma treatment. Four points were taken inside the treated area and 40 cells analyzed. (B) "Alive-vs-dead" testing of the treated cells with trypan blue stain with the same area in the well analyzed before and after treatment. Cell migration rates for ~0–16.5 h (C) and ~16.5–33 h (D) after treatment as functions of treatment duration. Error bars indicate the standard deviations of data points.

III. RESULTS AND DISCUSSION

Figure 1 shows spectroscopic measurements of the cold atmospheric plasma jet along the plasma jet with given parameters (output voltage ~4.6 kV, frequency ~26 kHz, and helium flow rate ~17 L/min). The assigned spectrum measured at the jet's end is shown in Figure 1A (this spectrum characterizes radiation from the whole length of the plasma column including the discharge inside the Pyrex tube). The presence of atomic helium (He) and oxygen (O) was found in the range 450–900 nm; neutral nitrogen N_2 (second positive system) and N_2^+ (first negative system) degraded to shorter wavelengths; O_2^+ (first negative system, degraded to longer wavelengths) and O_3 (however, its values might be also attributed as a combination of O_2^+ and O^+ species) were identified in the range 200–450 nm.¹⁵ Thus, ionized nitrogen and highly reactive oxygen radicals are presented during the cell treatment. There is no change in the subset of the identified species was found with the increasing of the distance from the nozzle, although there was some variability in the intensities of spectral lines along the jet. The dependences of the intensities of O_3 , N_2 , N_2^+ , He, and O along the plasma jet are shown in Figure 1B

(logarithmic scale). It was observed that the intensity of nitrogen lines increase with distance from the nozzle, while the intensity of He and O₃ decrease. The atomic O does not show significant changes up to 6 cm. Based on these measurements, we can conclude that the optimal condition for maximization of radiation intensity would be 2–3 cm from the nozzle.

Next, we treated cells with cold plasma for times ranging from 100 to 500 s. A schematic diagram indicating how these treatments were made is shown in Figure 2A. Controls included cells treated with helium alone for the same times. Cells were treated with plasma immediately after plasma treatment with trypan blue. We have shown previously that plasma treatments can cause cell death as assessed using trypan blue.¹⁰ Trypan blue is a vital dye that is excluded from entering live cells; dead cells fill with the blue dye. Data shown in Figure 2B for cells treated with plasma or helium alone for the times tested indicate that trypan blue is excluded from cells and, therefore, these treatment times do not cause cell death.

When cell migration is assessed as a function of the duration of plasma treatment, we found in Figure 2C that 100 s significantly reduced cell migration rates when assessed from 0 to 16.5 h after plasma treatment. Treatment times up to 500 s did not further reduce cell migration significantly when assessed between 0 and 16.5 h; however, when migration rates were assessed between 16.5 and 33 h, we again found that 100 s significantly reduced cell migration rates—but also, 500 s of treatment reduced the migration rate even further compared to 100 s. Thus, the general trend becomes: as treatment time increases, the cells migrate slower.

In order to address the effect of plasma treatment on the pH level of DMEM media, we conducted treatments of media at standard experimental conditions described above. One of the components of cell culture media is the acid-base indicator phenol red. At acidic pH, the color of phenol red is yellow; at basic pH, phenol red is pink; and at neutral pH, phenol red is red/orange. These features of phenol red, along with its lack of toxicity, make it an excellent indicator of pH in cell culture media. No change of media color was observed after the 60, 120, and 200 s treatments of media (data not shown), indicating that the pH level of the media remained unchanged at plasma treatment.

In the current study, experiments were performed using tertiary dermal fibroblast cells whereas previously we used primary dermal fibroblasts.⁸ This change reduced variability in the cells within each culture and enhanced our ability to obtain statistically significant data. The cell density was carefully controlled by the volume of cells plated and maintaining the cells in culture for three days. It is known that fibronectin fibrils begin to accumulate around cells after three days increasing cell confluence. These fibrils can reduce cell migration rates.

The ability of cold atmospheric plasma treatment to impact cell migration was further considered by evaluating cell migration rates as a function of the distance from the plasma treated zone. A schematic of the experiment is shown in Figure 3A. Three locations of interest were considered, namely, inside the plasma treated area (red circle indicates the treated area, diameter of around 5 mm) and further equidistant at the second and

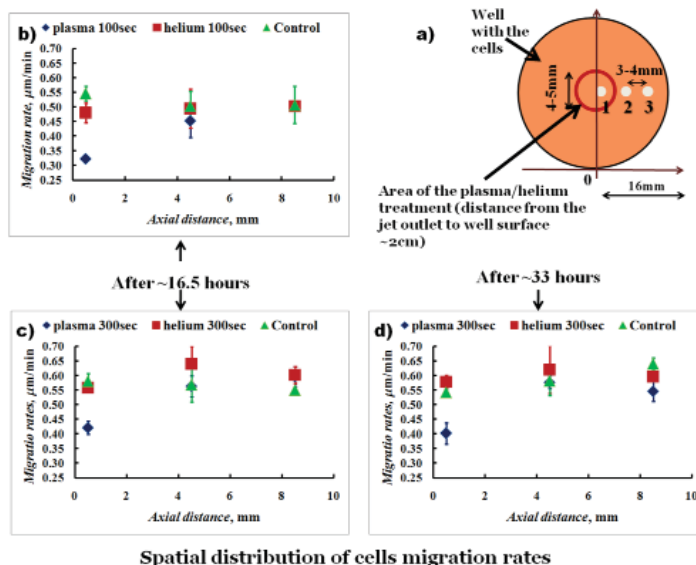


FIGURE 3. (A) The experimental setup for spatial distribution of the cell migration rates for a single well is shown. (B–D) The dependence of cell migration rates versus distance from the center of the treated zone for cells tracked during 0–16.5 h after 100 and 300 s plasma treatment, respectively (B, C), for cells tracked during 16.5–33 h after 300 s plasma treatment (D). Cells treated with plasma, with helium only, and untreated cells are shown. Data is given with standard deviations. The reduction in migration rate is around 30% in the treated area after ~16.5 h (B, C). This trend remains after ~33 h (D) of cell tracking.

third locations outside—each location between two neighbor points was ~3–4mm apart. The average velocity of 10 cells per each tracked location was calculated after 16.5 h. To increase the statistical significance of the results, data were taken symmetrically in six different locations, thus giving 20 cells per point of interest. Experiments were repeated several times with various treatment times of 100 and 300 s. Thus, overall, ~60 cells per each location were analyzed. Figure 3B shows the spatial distribution of migration rates after 100 s of plasma treatment (data shown for 20 cells at each point after 16.5 h of tracking). Neither the only helium or control velocity distributions show any significant changes. However, plasma treated cells showed a localized reduction in their migration rates of around 30–40%. The standard deviation is indicated with vertical bars at the data points; it does not exceed 5%.

Spatial characteristics of the effect on cell migration induced by the plasma treatments are shown in Figures 3B and 3C for cells tracked between 0 and 16.5 h after treatment (cells treated during 100 and 300 s) and in Figure 3D for cells tracked between 16.5 and 33 h after treatment (time duration of treatment 300 s). Again, for controlling

purposes, only helium treated cells and untreated cells are shown. Figures 3B and 3C show that cells treated with plasma (100 s and 300 s) have the slowest migration rates in the treated area (~1 mm from the center of the plate), while cells outside the treated area (5 and 8 mm from the center) migrate at the same rates as untreated cells. Also, no reduction of cell migration was observed in the cells treated with the only helium. It was observed that reduction (around 30%) in cell migration is persistent for 33 h (see Figure 3D).

The reduction of the rates of cell migration can be related to the changes in the integrin expression reported previously by Shashurin et al.⁹ It was found that plasma treated cells have a reduction in α_v and α_1 integrins expression, whose functions are related to cell motility and cell adhesions.^{8,14} A media bicarbonate buffering system was able to maintain the pH level unchanged,¹⁶ thus, we can conclude that this amount of plasma treatment was not enough to affect it.

IV. CONCLUSIONS

It was shown that the reduction in cell migration under cold plasma treatment is confined to within 5 mm of the treatment zone, which is comparable with the diameter of the plasma jet (4–5 mm). The reduction in cell migration after plasma treatment is shown to be around 30%, which is in the agreement with previous data.⁶ This change in cell migration has not only spatial effects, but also temporal, i.e., localization in the migration rate persists at least for 33 h after treatment. The tertiary fibroblast cells used in these experiments provided more statistically reliable data.

REFERENCES

1. Fridman A. Plasma chemistry. New York: Cambridge University Press; 2008.
2. Fridman G, Friedman G, Gutsol A, Shekhter AB, Vasilets VN, Fridman A. Plasma Process Polym. 2008;5:503-533.
3. Stoffels E, Sakiyama Y, Graves DB. IEEE Trans Plasma Sci. 2008;36(4):1441
4. Laroussi M. IEEE Trans Plasma Sci. 2008;36:1612-1614.
5. Lu X, Cao Y, Yang P, Xiong Q, Xiong Z, Xian Y, Pan Y. IEEE Trans Plasma Sci. 2009;37:668.
6. Stoffels E, Kieft IE, Sladek REJ, Van den Bedem LJM, Van der Laan EP, Steinbuch M. Plasma Sources Sci Technol. 2006;15:S169.
7. Zhang X, Li M, Zhou R, Feng K, Yang S. Appl Phys. Lett. 2008;92:021502.
8. Shashurin A, Keidar M, Bronnikov S, Jurjus RA, Stepp MA. Appl Phys Lett. 2008;93:181501.
9. Shashurin A, Stepp MA, Hawley TS, Pal-Ghosh S, Brieda L, Bronnikov S, Jurjus RA, Keidar M. Plasma Process Polym. 2010;7:294–300.
10. Hynes RO. Integrins: a family of cell surface receptors. Cell. 1987;48:549-554.
11. Bokel C, Brown Integrins in development: moving on, responding to, and sticking to the extracellular matrix. NH. Dev Cell. 2002;3:311–321.

12. Humphries JD, Byron A, Humphries MJ. Integrin ligands at a glance. *J Cell Sci.* 2006;119(19):3901-3903.
13. Shashurin A, Shneider MN, Dogariu A, Miles RB, Keidar M. Temporary-resolved measurement of electron density in small atmospheric plasmas. *Appl Phys Lett.* 2010;96 :171502.
14. Jurjus RA, Liu Y, Pal-Ghosh S, Tadvalkar G, Stepp MA. Primary dermal fibroblasts derived from *sdc-1* deficient mice migrate faster and have altered αv integrin function. *Wound Rep Reg.* 2008;16:649–60.
15. Pearse WB, Gaydon AG. *The identification of molecular spectra*, Hoboken, NJ: Wiley; 1976.
16. Eagle H. Amino acid metabolism in mammalian cell cultures. *Science.* 1971;174(4008):500–503.

Live Pig Skin Tissue and Wound Toxicity of Cold Plasma Treatment

Danil Dobrynin¹, Andrew Wu², Sameer Kalghatgi¹, Sin Park³, Natalie Shainsky¹, Kimberly Wasko², Essel Dumani⁴, Robert Ownbey⁴, Suresh Joshi², Rachel Sensenig², Ari D Brooks²

¹Electrical and Computer Engineering Department, Drexel University, Philadelphia, PA ²Department of Surgery, Drexel University College of Medicine, Philadelphia, PA ³School of Biomedical Engineering, Drexel University, Philadelphia, PA ⁴Department of Pathology, Drexel University College of Medicine, Philadelphia, PA

ABSTRACT: Cold atmospheric pressure plasmas have emerged as a promising new tool for medical applications. Compared to conventional thermal plasma, such as arc coagulators and desiccators, cold plasma can be more selective in its application and may be used for effective sterilization of skin and wound tissue, wound healing and tissue regeneration, cancer treatment and blood coagulation. One of the key questions that has to be answered before these plasma technologies are introduced in medical practice is the safety of plasma treatment of living tissues, i.e. toxic dose levels of plasma exposure should be determined. It is well established that porcine (pig) skin closely resembles human skin; hence we evaluated the potential toxic effects of plasma treatment on intact and wounded skin in a Yorkshire pig model. Varying doses of Floating Electrode Dielectric Barrier Discharge (FE-DBD) and microsecond Pin-to-Hole Spark Discharge (PHD) plasmas were applied to determine a dosage regime where tissue damage occurs.

KEY WORDS: Non-equilibrium plasma, cold plasma, dielectric barrier discharge, spark discharge, skin toxicity, animal model, plasma medicine

I. INTRODUCTION

It is evident from the large number of recent reviews in the literature that there are many potential applications of non-equilibrium plasma discharges in biology and in medicine.¹⁻¹⁰ This is, in part, driven by the continued development of novel plasma sources and modification of existing ones^{1,4,11-21} and by advances in modeling, simulation, and characterization of these sources, including characterization and quantification of biological effects^{1,11,22-34}. The major focus in applications of plasma in medicine has been its antimicrobial effect, although some reports of wound healing applications have been presented^{3,6,11,15,29,35,36}. In studying antimicrobial effects of plasma it is essential to evaluate the potential damage plasma can inflict on living tissues.

This manuscript investigates toxicity in the direct application of two different types of plasma to living tissue: (a) Floating Electrode Dielectric Barrier Discharge which is an inherently non-thermal discharge that generates a multitude of reactive oxygen species (ROS) and (b) Pin-to-Hole spark Discharge which is a thermal discharge that generates ROS together with reactive nitrogen species (RNS). Both discharges have been considered before for antimicrobial treatment of living tissues. However, little work has

been reported on the possible damage these discharges could inflict in the process. We show that low doses of plasma (previously reported to be quite sufficient for sterilization, see^{10,37} for example) do not cause any visible or microscopic damage to live pig skin and wound tissue. Higher doses do, in fact, cause damage and the damage appears to be related to the surface temperature of the tissue. Thus, if the plasma temperature is reduced (through shorter pulses, for example) this heating and thus the damage may potentially be avoided.

II. MATERIALS AND METHODS

A. Floating Electrode Dielectric Barrier Discharge (FE-DBD)

Non-thermal atmospheric pressure dielectric barrier discharge plasma was generated using an experimental setup similar to the one previously described by the authors³⁸⁻⁴². In short, the discharge was generated by applying alternating polarity pulsed (500 Hz – 1.5 kHz) voltage of ~20 kV magnitude (peak to peak), 1.65 μ s pulse width and a rise time of 5 V/ns between the insulated high voltage electrode and the sample undergoing treatment. One mm thick, polished clear fused quartz was used as an insulating dielectric barrier covering the 2.54 cm diameter copper electrode. The discharge gap between the bottom of the quartz and the treated skin or wound surface was fixed at 1.5 mm using a special electrode holder (Figure 1, a) or a modified planar electrode (Figure 1, b). Discharge power density was measured to be 0.13 W/cm² (at 500 Hz), 0.15 W/cm² (at 800 Hz), 0.17 W/cm² (at 1 kHz), and 0.31 W/cm² (at 1.5 kHz). Rotational and vibrational temperatures were measured to be 313.5 ± 7.5 K and 3360 ± 50 K respectively⁴³.

B. Microsecond Pin-to-Hole Spark Discharge (PHD)

Atmospheric pressure spark discharge was generated in a pin-to-hole electrode configuration similarly as in^{44,45}. A needle anode (1.5 mm diameter) was coaxially fixed in an insulator with gas inlet openings (room air at ~0.5 L/min), which is surrounded by an outer cylindrical cathode (7 mm diameter) with an axial opening (2 mm diameter) for plasma outlet (Figure 2). Both electrodes were made of stainless steel. For all experiments, the plasma discharge was ignited by applying a 4 kV positive potential to the central electrode. To provide high discharge energy while keeping average gas temperature low the electrode system was powered through a 0.33 μ F capacitor. This formed a 35 μ s dense energetic discharge with average energy of ~1.8 J/pulse. The average gas temperature was measured using a K-type thermocouple as a function of distance from the cathode (Figure 3). The plasma temperature was calculated as 9030 ± 320 K by the Boltzmann method, which was adequate to produce nitric oxide, although the average gas temperature was near room temperature^{46,47}. The PHD plasma discharge radiates intensively in the UV range: the measured total plasma UV irradiation with and without gas feeding was 90 and 140 μ W/cm² respectively⁴⁷. DNA damage by UV-C and UV-B radiation occurs after about 0.4 mJ/cm² and 10 mJ/cm² respectively^{48,49}. The discharge

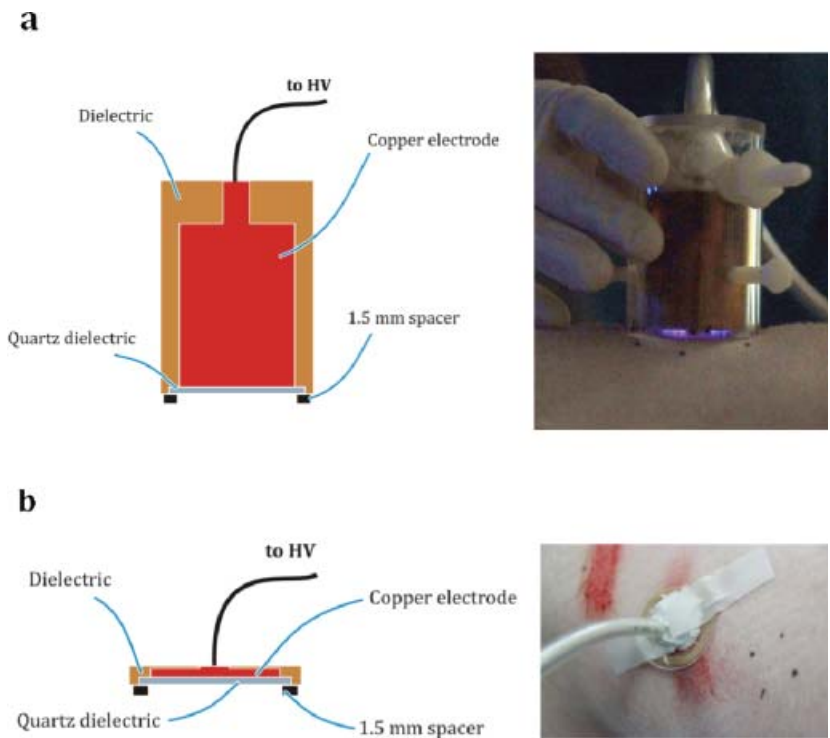


FIGURE 1. General schematics and photographs of the FE-DBD electrodes: conventional (a), and modified planar (b).

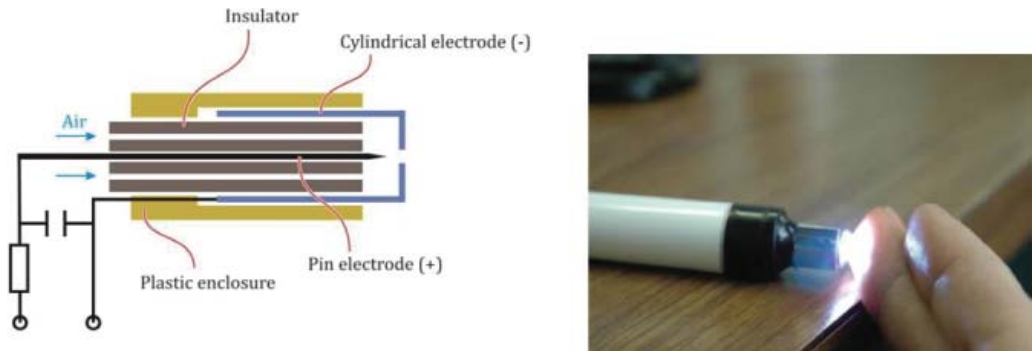


FIGURE 2. General schematic of the PHD electrode (left), and a photograph of the discharge in operation (right).

produces hydrogen peroxide in liquid (PBS) with concentration up to 60 μM in about 30 seconds of treatment (210 pulses)⁴⁷. Plasma-produced nitric oxide in gas reached 2000 ppm and rapidly diffused into liquid and cells: 1400 - 1600 nM NO was detected in PBS and 1000 nM NO was detected in endothelial cells immediately following 240

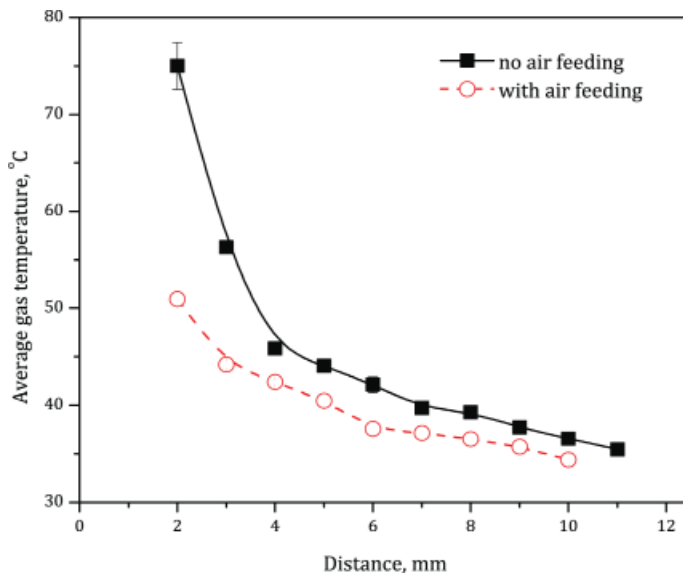


FIGURE 3. PHD afterglow gas temperature measured with thermocouple as a function of distance from the cathode.

plasma pulses⁴⁶. These data suggest that this plasma may provide a novel method for delivering NO locally and directly for enhanced wound healing.

C. Animal Model

We evaluated the potential toxic effects of the FE-DBD and PHD plasmas on both intact and wounded porcine skin in 12 Yorkshire pigs. Standard operative procedure included the following: the pig was anesthetized and the dorsum of the pig was marked and divided for treatment areas (Figure 4, a). When intact skin toxicity was studied, the FE-DBD electrode was placed 1.5 mm above the skin, and plasma was applied for different doses by varying the power and time of treatment. Spark discharge was applied at fixed power at a 5 mm distance from the skin for various amounts of time. When wounded skin was studied, a dermatome knife was used to create a skin abrasion (Figure 4, b), removing about 2×3 cm of the epidermis and dermis (approximately 3 mm ± 1 mm deep), followed by plasma treatment. Pigs were then sacrificed immediately or 24 hours after the treatment. Tissue specimens from each treatment area were harvested and sent for histopathologic analysis.

For the intact skin model (3 pigs) of treatment with FE-DBD, we had a total of 85 treatment areas on the three pigs that were harvested 24 hours after surgery. One area of intact skin (n=3) was treated with a high frequency desiccator (positive control, Bovie[®], Figure 4, c), and one area of intact skin (n=3) was left untreated (negative control). The remaining 80 areas were treated with 4 discharge frequency (power) settings for different time points: from 30 seconds, and up to 15 minutes (Table 1).



FIGURE 4. Marked treatment areas of the pig skin (a), creation of skin abrasion with dermatome (b), and skin treatment with a high frequency desiccator Bovie®, positive control (c).

TABLE 1. Number of areas for intact skin FE-DBD plasma treatment and corresponding exposure dose (in J/cm²)

| Treatment time, min | FE-DBD frequency, kHz (corresponding power density, W/cm ²) | | | |
|---------------------|---|----------------------------|-----------------------------|-----------------------------|
| | 0.5 (0.13) | 0.8 (0.15) | 1.0 (0.17) | 1.5 (0.31) |
| 0.5 | - | - | 3 (5.1 J/cm ²) | 3 (9.3 J/cm ²) |
| 1 | - | 4 (9 J/cm ²) | 7 (10.2 J/cm ²) | 9 (18.6 J/cm ²) |
| 2 | 2 (15.6 J/cm ²) | 4 (18 J/cm ²) | 5 (20.4 J/cm ²) | 7 (37.2 J/cm ²) |
| 3 | - | 8 (27 J/cm ²) | 4 (30.6 J/cm ²) | 5 (55.8 J/cm ²) |
| 5 | - | 5 (45 J/cm ²) | 2 (51 J/cm ²) | 5 (93 J/cm ²) |
| 15 | 2 (117 J/cm ²) | 2 (135 J/cm ²) | - | - |

For the wounded skin model (4 pigs) treated with FE-DBD, we had a total of 56 treatment areas on 2 pigs harvested immediately after treatment, and 38 treatment areas on 2 pigs harvested 24 hours after procedure. Animals were treated with two discharge power settings for various amounts of time (see Table 2) using planar DBD electrode, with a high frequency desiccator (n=8), or left untreated as control (n=7).

TABLE 2. Number of areas for intact skin FE-DBD plasma treatment and corresponding exposure dose (in J/cm²)

| Treatment time, min | FE-DBD frequency, kHz (corresponding power density, W/cm ²) | |
|---------------------|---|-----------------------------|
| | 0.5 (0.13) | 1.5 (0.31) |
| 0.5 | 6 (3.9 J/cm ²) | 6 (9.3 J/cm ²) |
| 1 | 8 (7.8 J/cm ²) | 8 (18.6 J/cm ²) |
| 3 | 9 (23.4 J/cm ²) | 9 (55.8 J/cm ²) |
| 5 | 9 (39 J/cm ²) | 9 (93 J/cm ²) |
| 15 | 6 (117 J/cm ²) | 7 (279 J/cm ²) |

For the intact and wounded skin model (5 pigs) treated with PHD, we had a total

of 39 (intact skin) and 36 (wounded skin) treatment areas on 4 pigs that were harvested immediately after the procedure, and 48 (intact skin) and 36 (wounds) treatment areas on 4 animals that were harvested 24 hours after plasma exposure. Skin was treated with spark plasma at 5 mm for 5 to 300 seconds (see Table 3).

TABLE 3. Number of areas for intact and wounded skin PHD plasma treatment

| Treatment time, s | 5 mm, intact skin | 5 mm, wounds |
|-------------------|----------------------------------|----------------------------------|
| 5 | 2 (non-survival) 4 (survival) | 2 (non-survival) 2 (survival) |
| 15 | 2 (non-survival) 4 (survival) | 4 (non-survival) 4 (survival) |
| 30 | 2 (non-survival) 4 (survival) | 4 (non-survival) 4 (survival) |
| 60 | 2 (non-survival) 4 (survival) | 4 (non-survival) 4 (survival) |
| 90 | 2 (survival) | - |
| 120 | 6 (non-survival) 4 (survival) | - |
| 180 | 5 (non-survival) 4 (survival) | 4 (non-survival) 4 (survival) |
| 240 | 2 (survival) | - |
| 300 | 4 (non-survival) | - |

D. Histological Analysis

All specimens were analyzed with microscopic histological analysis. Specimens were longitudinally sectioned and fixed for 24 hours in formalin. Sections for histology were processed in a standard fashion and stained with hematoxylin-eosin. The pathologists were blinded to all specimens and categorized each specimen into a burn grading system for the intact and wounded skin data analysis. For intact skin, the specimens were either classified as normal, minimal change, epidermal damage, or full burn through the dermis. For wounded skin, the specimens were either classified as normal, presence of a clot or scab, and full burn through the dermis.

E. pH and Temperature Analysis

In order to check the change of skin temperature and pH of the skin sample after plasma treatment, fresh pig skin samples with average thickness of about 1 cm were placed on aluminum foil and kept at constant initial temperature of about 37°C. Skin samples were exposed to both discharges for the same amount of time as in in-vivo study. These changes were monitored using infrared thermometer (OS53x-CR, Omega) and skin pH/temperature meter (HI 99181, Hanna).

All procedures were performed in compliance with the animal welfare and protection act following the Drexel University's Institutional Animal Care and Use Committee (IACUC) approval, Protocols #17030 (intact skin) and #17335 (wounded skin).

III. RESULTS AND DISCUSSION

Endpoints for toxicity analysis consisted of recording both gross and histological examination of the intact skin and wounded skin specimens. Gross observation was correlated with the histological grading system as mentioned previously.

A. Treatment of Intact Skin

FE-DBD plasma treatment was evaluated on 3 pigs with intact skin at 4 different frequency (power) settings, all harvested 24 hours after the procedure. The results for 3 discharge frequencies are shown on Figure 5 in terms of normalized number of observation of no or minimal changes in skin, epidermal damage, or burn after certain treatment dose. Untreated skin appeared normal on gross histological observation. With minimal change, there was a small area of erythema on the skin. With epidermal damage, there was mild erythema that resolved itself usually within 20 minutes. With full burn through the dermis, there was diffuse erythema that remained until time of harvest (Table 4). Positive controls, i. e. samples treated with HF desiccator, all showed full thickness burn. Representative photographs and histological images are shown in Table 4. One can notice that resulting toxic effects (epidermal damage, burn) depends not only on the exposure dose, but dose rate (frequency dependent): the higher the frequency, the lower dose required for skin damage to occur.

The results of intact skin treatment with spark discharge plasma at 5 mm distance from the skin are shown in Figure 6 and in Table 4. In this case a burn was observed after 3 minutes of treatment, while, for example, inactivation of bacteria in liquid requires an exposure time of several seconds^{44,45}.

Overall results of the skin toxicity trials on pigs are similar to those on human cadaver skin and on SKH1 mice^{39,42} – only rather high doses of plasma, those far greater than needed for sterilization or blood coagulation, are able to damage skin; while doses required to achieve desired medically relevant therapeutic effect are significantly below the damage threshold.

B. Ex-vivo Treatment of Porcine Skin Samples

In order to estimate the effect of global increase of temperature and pH of skin after the plasma treatment on induction of tissue damage, we have measured these parameters on skin samples ex vivo. The results of temperature measurements (Figure 7, a) indicate, that after about 3 minutes of treatment by both plasmas, skin temperature increases by 11-14 degrees, which is the critical temperature for skin burn^{50,51}, and is in good agreement with our experimental observations (see Figure 5 and Figure 6). The effect of the decrease of pH due to plasma treatment is probably negligible for both discharges (Figure 7, b).

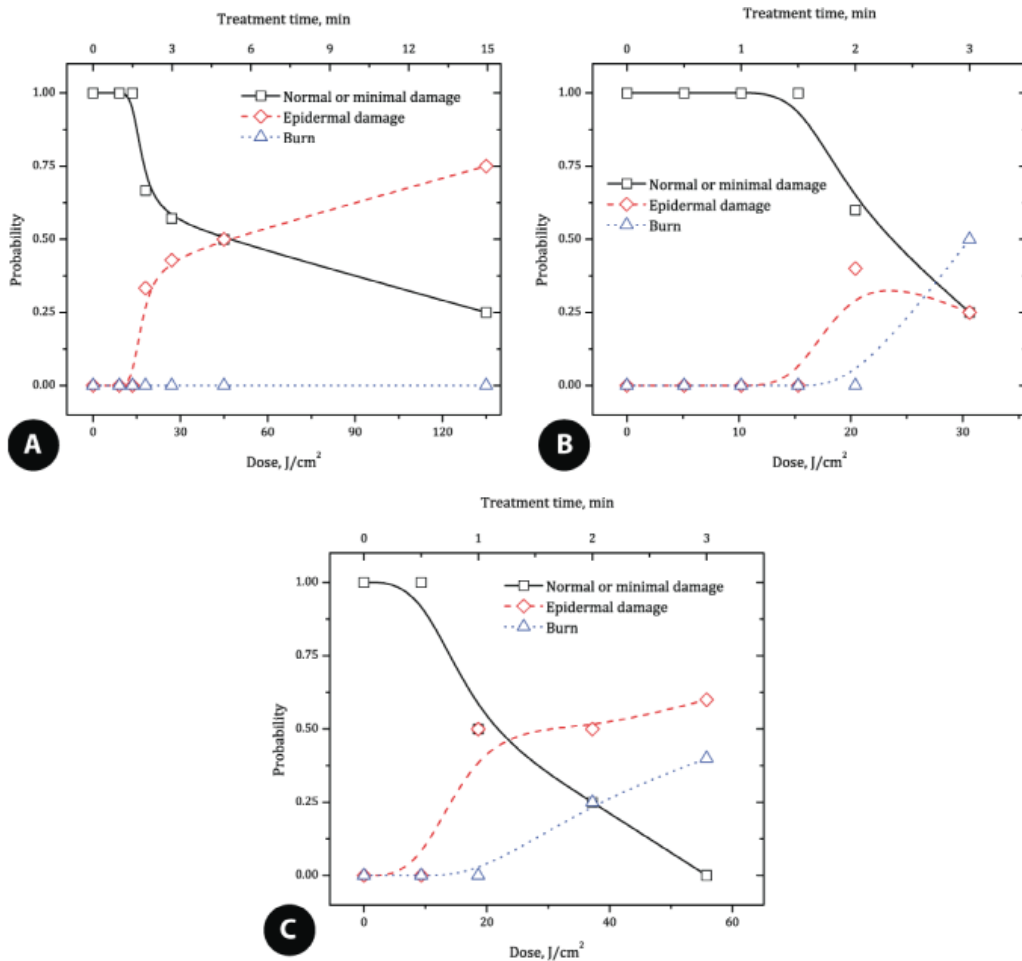


FIGURE 5. Results of the intact porcine skin treatment with FE-DBD plasma operated at 800 (a), 1000 (b) and 1500 (c) Hz frequency.

C. Toxicity of Wound Treatment

One of the potential applications of FE-DBD and spark plasma treatment is sterilization and healing of wounds and/or coagulation of bleeding capillaries (see end of section II.B above). We were able to test the efficacy and toxicity of such treatment on a superficial partial thickness skin wound similar to that of scraping one's knee. Once the animal was anaesthetized the wound was made with a small hand-held dermatome knife (Zimmer, Franklin County, OH, USA) originally designed to remove precise-thickness skin grafts from a donor surface. These are partial thickness wounds with the blade set to cut no deeper than a millimeter into the skin. This exposes the top layer of skin and breaks

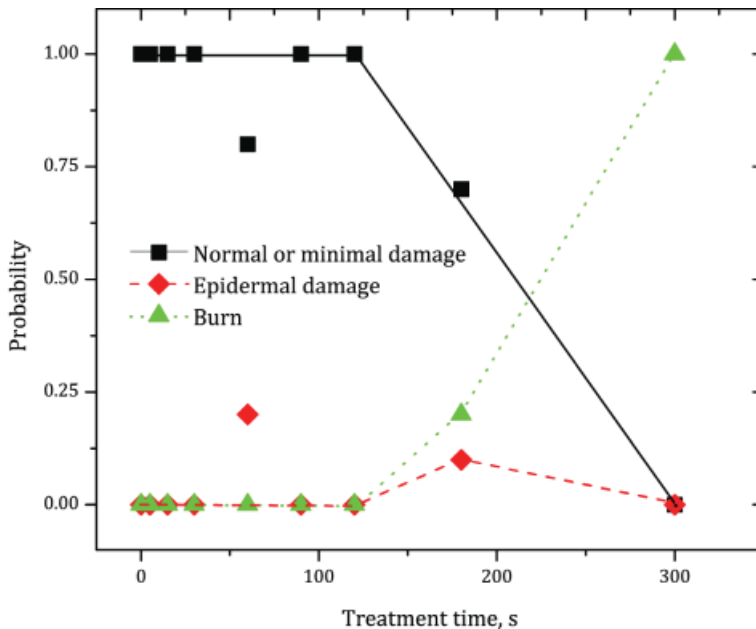
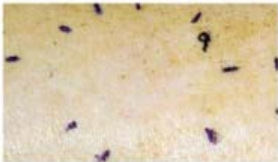
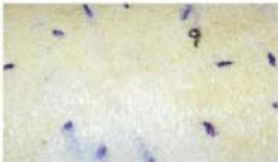
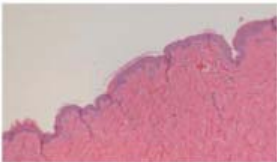

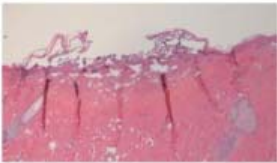

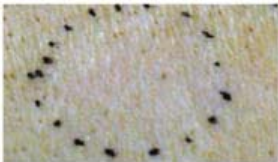
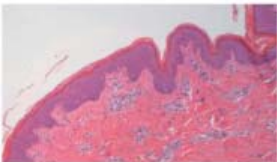


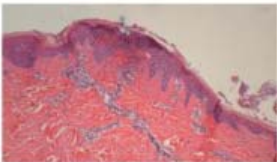


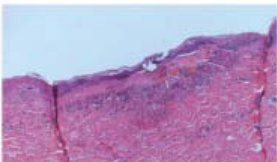


FIGURE 6. Results of the intact porcine skin treatment with PHD plasma operated at 5 mm distance from the skin surface.

capillaries located in the skin, but not the bigger vessels. Thus, the bleeding is slow and manageable. This is not a severe wound and the bleeding would normally self-terminate quickly. Immediately after the wound is made we proceed with the selected treatment.

Results of the various FE-DBD and PHD plasma treatments of wound surface and histological images of these skin samples are detailed in Table 5. Similar to the intact skin, treatment with Bovie[®] knife quickly coagulates blood and desiccates the tissue but causes quite significant damage (see Table 5). Although the wound may be closed, there is a significant level of tissue damage which may prolong the wound healing process over that if the wound was simply left with no treatment in this case. While the Bovie[®] electrosurgery knife causes significant tissue damage, both plasma treatments can be applied to the tissue for up to 15 minutes with no or minimal damage to this tissue (Table 5). One other observation is that even after a short treatment, the blood appears to be coagulated and (although this is not visible on the photograph below) the wound looks to be covered with a thin layer of clear coagulum. We have seen such a thin transparent cork formation before with treatment of blood and blood plasma samples^{39,42}. This film was claimed to be a thin layer of coagulated blood plasma – both FE-DBD and PHD seem to quickly form a layer of coagulated blood on the surface of the wound which protects the wound from further external disturbances.



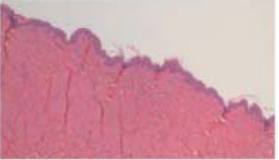
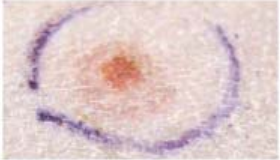
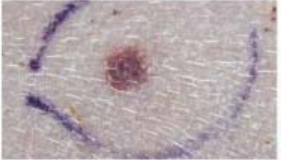
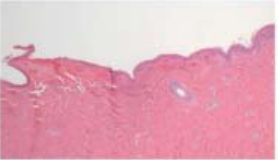
TABLE 4. Representative photographs and histological images of the intact skin after treatment with FE-DBD and PHD plasmas.

| Treatment | Gross observation: | | Histology |
|--|---|---|--|
| | right after treatment | 24 hours after treatment | |
| No treatment |  |  |  |
| | <p>Appearance: Normal skin Histology: Normal skin</p> | | |
| Positive control Bovie® |  | |  |
| | <p>Appearance: Burn: Immediate burning and charring of tissue Histology: Disruption of epidermis and papillary dermis, areas of dermis coagulated, no dermal nuclei, hair follicles still intact</p> | | |
| FE-DBD 45 J/cm ² 5 min @ 0.8 kHz |  |  |  |
| | <p>Appearance: Normal skin Histology: Normal skin</p> | | |
| FE-DBD 135 J/cm ² 15 min @ 0.8 kHz |  |  |  |
| | <p>Appearance: Epidermal damage; Diffuse redness with a distinct area of mild erythema Histology: Small area of burn in epidermis</p> | | |
| FE-DBD 37.2 J/cm ² 2 min @ 1.5 kHz |  |  |  |
| | <p>Appearance: Burn Small Central area of increasing redness surrounded by erythema after 1 min treatment. Area of necrosis forming centrally surrounded by area of erythema Histology: Similar to Bovie®, burn through to dermis</p> | | |

IV. CONCLUSION

The purpose of this work was to determine the toxic doses of cold plasma treatment of living tissue for both intact and wounded skin. In this study we have used a well-

TABLE 4. Representative photographs and histological images of the intact skin after treatment with FE-DBD and PHD plasmas. (Continued)

| Treatment | Gross observation: | | Histology |
|---------------------|---|---|--|
| | right after treatment | 24 hours after treatment | |
| PHD 60 s @ 5 mm |  |  |  |
| | Appearance: Normal skin Histology: Normal skin | | |
| PHD 180 s @ 5 mm |  |  |  |
| | Appearance: Burn Histology: Similar to Bovie®, burn through to dermis | | |

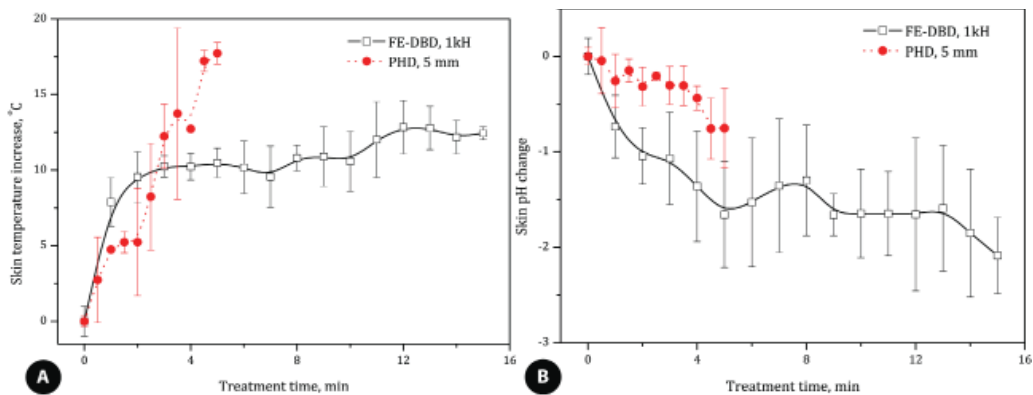


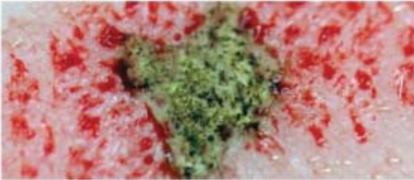

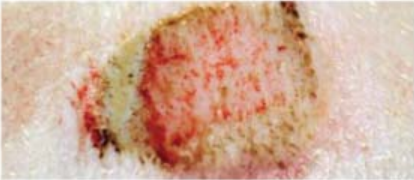
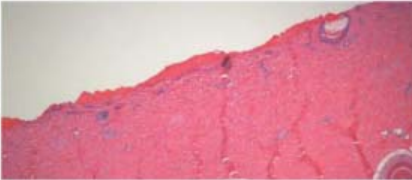
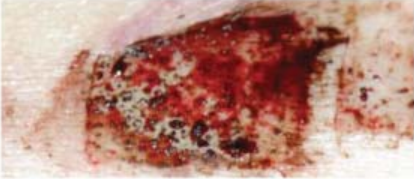
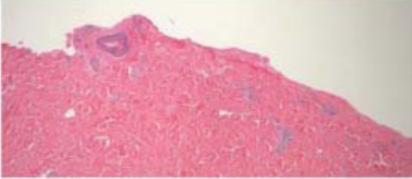
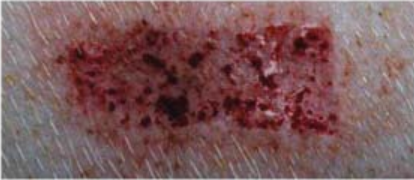
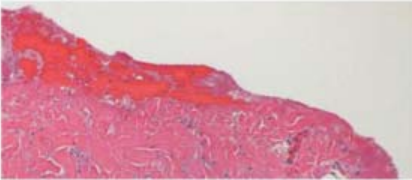


FIGURE 7. The results of temperature (a) and pH (b) measurements of the porcine skin ex-vivo treatment with FE-DBD and PHD plasmas.

established method for evaluation of tissue toxicity, where a Yorkshire pig intact or wounded skin was exposed to a plasma source and macroscopic toxic effects were studied histologically. In order to evaluate the possible source of plasma toxicity, we have used two plasma sources in which discharges are ignited and applied in completely different ways – direct non-thermal dielectric barrier discharge, and indirect thermal spark discharge. The results of our study show that, despite the fundamental differences of these two discharges, toxic effects (epidermal damage and tissue burn) are related to global increase of temperature of the treated skin, and are highly dependant not only on the dose of plasma exposure, but also on the dose rate – the lower the frequency of a discharge, the higher plasma dose may be applied to skin without damaging it. Plasma

TABLE 5. Representative photographs and histological images of the wounded skin after treatment with FE-DBD and PHD plasmas.

| Treatment | Gross observation | Histology |
|--|---|--|
| No treatment |  |  |
| | Appearance: Normal wound Histology: Normal wound | |
| Positive control Bovie® |  |  |
| | Appearance: Eschar formation, burn formation immediately after treatment Instant blood coagulation Necrotic tissue Histology: Necrosis deep in the dermis. Disruption of the dermis. No dermal nuclei. Hair follicles still intact | |
| FE-DBD 117 J/cm ² 15 min @ 0.5 kHz |  |  |
| | Appearance: No burn. Blood clot formation Histology: Clot on surface. No damage to wound tissue. Intact hair follicles | |
| FE-DBD 93 J/cm ² 5 min @ 1.5 kHz |  |  |
| | Appearance: No burn. Coagulation. Histology: Clot on the surface of the wound. No damage to wound tissue. | |
| PHD 180 s @ 5 mm |  |  |
| | Appearance: No burn. Coagulation Histology: Clot visible. No damage to dermis. Intact hair follicles. | |

treatment of wounded tissue, on the other hand, did not result in any toxic effects to the tissue itself, but in effective and fast blood coagulation. This blood clot, apparently, protected underlying wound tissue from plasma damage. Overall, we have shown that plasma treatment is safe for living intact and wounded skin when applied for doses several times higher than required for effective inactivation of bacteria on surface of agar or in liquid. In the future studies we plan to expand on these findings, analyzing the dose and dose rate dependence; we also plan to reduce surface temperature by creating more uniform shorter pulse plasmas.

REFERENCES

1. Weltman KD, Dieter K, Kindel E, von Woedtke T, Hähnel M, Stieber M, Brandenburg R. Atmospheric-pressure plasma sources: Prospective tools for plasma medicine. *Pure and Applied Chemistry*, 2010;82(6):1223-1237.
2. Cheruthazhekatt S, Cernak M, Slavicek P, Havel J. Gas plasmas and plasma modified materials in medicine. *Journal of Applied Biomedicine*, 2010;8(2):55-66.
3. Lloyd G, Friedman G, Jafri S, Schultz G, Fridman A, Harding K. Gas Plasma: Medical Uses and Developments in Wound Care. *Plasma Processes and Polymers*, 2010;7(3-4):194-211:115011.
4. Morfill GE, Kong MG, Zimmermann JL. Focus on Plasma Medicine. *New Journal of Physics*, 2009;11.
5. Kong MG, Kroesen G, Morfill G, Nosenko T, Shimizu T, van Dijk J, Zimmerman JL. Plasma medicine: an introductory review. *New Journal of Physics*, 2009;11:115012.
6. Dobrynin D, Fridman G, Friedman G, Fridman A. Physical and biological mechanisms of direct plasma interaction with living tissue. *New Journal of Physics*, 2009;11:115020.
7. Massines F, Gherardi N, Naudé N, Ségur P. Recent advances in the understanding of homogeneous dielectric barrier discharges. *European Physical Journal-Applied Physics*, 2009;47(2):21-24.
8. Laroussi M. Low-Temperature Plasmas for Medicine? *Ieee Transactions on Plasma Science*, 2009;37(6):714-725.
9. Vasilets VN, Gutsol A, Shekhter AB, Fridman A. Plasma medicine. *High Energy Chemistry*, 2009;43(3):229-233.
10. Fridman G, Friedman G, Gutsol A, Shekhter AB, Vasilets VN, Fridman A. Applied Plasma Medicine. *Plasma Processes and Polymers*, 2008;5(6):503-533.
11. Babaeva NY, Kushner MJ. Intracellular electric fields produced by dielectric barrier discharge treatment of skin. *Journal of Physics D-Applied Physics*, 2010;43(18):185206.
12. Cao Z, Nie Q, Bayliss DL, Walsh JL, Ren CS, Wang DZ, Kong MG. Spatially extended atmospheric plasma arrays. *Plasma Sources Science & Technology*, 2010;19(2) :025003.
13. Walsh JL, Iza F, Janson NB, Law VJ, Kong MG. Three distinct modes in a cold atmospheric pressure plasma jet. *Journal of Physics D-Applied Physics*, 2010;43(7) :075201.

14. Sarrette JP, Cousty S, Merbani N, Nègre-Salvayre A, Clément F. Observation of antibacterial effects obtained at atmospheric and reduced pressures in afterglow conditions. *European Physical Journal-Applied Physics*, 2010;49(1):13108.
15. Nosenko T, Shimizu T, Morfill GE. Designing plasmas for chronic wound disinfection. *New Journal of Physics*, 2009;11:115011.
16. Martines E, Zuin M, Cavazzana R, Gazza E, Serianni G, Spagnolo S, Spolare M, Leonardi A, Deligianni V, Brun P, Aragona M, Castagliuolo I. A novel plasma source for sterilization of living tissues. *New Journal of Physics*, 2009;11:115014.
17. Nie QY, Cao Z, Ren CS, Wang DZ, Kong MG. A two-dimensional cold atmospheric plasma jet array for uniform treatment of large-area surfaces for plasma medicine. *New Journal of Physics*, 2009;11:115015.
18. Morfill GE, Shimizu T, Steffes B, Schmidt -U. Nosocomial infections-a new approach towards preventive medicine using plasmas. *New Journal of Physics*, 2009;11:115019.
19. Lu X, Xiong X, Zhao F, Xian Y, Xiong Q, Gong W, Zou C, Jiang Z, Pan Y. A simple atmospheric pressure room-temperature air plasma needle device for biomedical applications. *Applied Physics Letters*, 2009;95(18):181501.
20. Choi J, Matsuo K, Yoshida H, Namihira T, Katsuki S, Akiyama H. Double-Layered Atmospheric Pressure Plasma Jet. *Japanese Journal of Applied Physics*, 2009;48(8):086003.
21. Staack D, Farouk B, Gutsol A, Fridman A. Stabilization of the ionization overheating thermal instability in atmospheric pressure microplasmas. *Journal of Applied Physics*, 2009;106(1):013303.
22. Bekstein A, Yousif M, Bentienni M, Ducasse O, Eichwald O. Drift and reactions of positive tetratomic ions in dry, atmospheric air: Their effects on the dynamics of primary and secondary streamers. *Journal of Applied Physics*, 2010;107(10):103308.
23. Rauscher H, Kylián O, Benedikt J, von Keudell A, Rossi F. Elimination of Biological Contaminations from Surfaces by Plasma Discharges: Chemical Sputtering. *Chemphyschem*, 2010;11(7):1382-1389.
24. Yousfi M, Bekstein A, Merbani N, Eichwald O, Ducasse O, Benhenni M, Gardou JP. Basic data for atmospheric pressure non-thermal plasma investigations in environmental and biomedical applications. *Plasma Sources Science & Technology*, 2010;19(3):034004.
25. Malovic G, Puač N, Lazovic S, Petrovic Z. Mass analysis of an atmospheric pressure plasma needle discharge. *Plasma Sources Science & Technology*, 2010;19(3):034014.
26. Jiang N, Cao ZX. Experimental studies on an atmospheric pressure He plasma jet. *Acta Physica Sinica*, 2010;59(5):3324-3330.
27. Xiong Q, Lu XP, Ostrikov K, Xian Y, Zou C, Ziong Z, Pay Y. Pulsed dc- and sine-wave-excited cold atmospheric plasma plumes: A comparative analysis. *Physics of Plasmas*, 2010;17(4):043506.
28. Shashurin A, Shneider MN, Dogariu A, Miles RB, Keidar M. Temporary-resolved measurement of electron density in small atmospheric plasmas. *Applied Physics Letters*, 2010;96(17):171502.
29. Xiong Q, Lu X, Xian Y, Liu J, Zou C, Xiong Z, Gong W, Chen K, Pei X, Zou F, Hu J, Jiang Z, Pan Y. Experimental investigations on the propagation of the plasma jet in the open air. *Journal of Applied Physics*, 2010;107(7):073302.
30. Park GY, Hong YJ, Lee HW, Sim JY, Lee JK. A Global Model for the Identification of the Dominant Reactions for Atomic Oxygen in He/O-2 Atmospheric-Pressure Plasmas. *Plasma*

- Processes and Polymers, 2010;7(3-4):281-287.
31. Xian Y, Lu X, Tang Z, Xiong Q, Gong W, Liu D, Jiang Z, Pan Y. Optical and electrical diagnostics of an atmospheric pressure room-temperature plasma plume. *Journal of Applied Physics*, 2010;107(6):063308.
 32. Sato T, Ochiai S, Urayama T. Generation and transport mechanisms of chemical species by a post-discharge flow for inactivation of bacteria. *New Journal of Physics*, 2009;11, 11:115018.
 33. Helmke A, Hoffmeister D, Mertens N, Emmert S, Schuette J, Vioel W. The acidification of lipid film surfaces by non-thermal DBD at atmospheric pressure in air. *New Journal of Physics*, 2009;11,11:115025.
 34. van Dijk J, Kroesen GMW, Bogaerts A. Plasma modelling and numerical simulation. *Journal of Physics D-Applied Physics*, 2009;42(19):190301.
 35. Isbary G, Morfill G, Schmidt HU, Georgi M, Ramrath K, Heinlin J, Karrer S, Landthaler M, Shimizu B, Steffes B, Bunk W, Monetti R, Zimmerman JL, Pompl R, Stolz W. A first prospective randomized controlled trial to decrease bacterial load using cold atmospheric argon plasma on chronic wounds in patients. *British Journal of Dermatology*, 2010;163(1):78-82.
 36. Weltmann KD, Kindel R, Brandenburg R, Meyer C, Bussiahn R, Wilke C, von Woedtke T. Atmospheric Pressure Plasma Jet for Medical Therapy: Plasma Parameters and Risk Estimation. *Contributions to Plasma Physics*, 2009;49(9):631-640.
 37. Fridman G, Peddinghaus M, Balasubramanian H, Ayan H, Fridman A, Gutsol A, Brooks A. Blood coagulation and living tissue sterilization by floating-electrode dielectric barrier discharge in air. *Plasma Chemistry and Plasma Processing*, 2006. 26(4): p. 425-442.
 38. Dobrynin D, Friedman G, Fridman A. Physical and biological mechanisms of direct plasma interaction with living tissue *New J. Phys.*, 2009;11:115020.
 39. Fridman G, Peddinghaus M, Balasubramanian H, Ayan H, Fridman A, Gutsol A, Brooks A. Blood coagulation and living tissue sterilization by floating-electrode dielectric barrier discharge in air. *Plasma Chemistry and Plasma Processing*, 2006;26(4):425-442.
 40. Fridman G, Brooks AD, Balasubramanian M, Fridman A, Gutsol A, Vasilets VN, Ayan H, Friedman G. Comparison of Direct and Indirect Effects of Non-Thermal Atmospheric Pressure Plasma on Bacteria. *Plasma Processes and Polymers*, 2007;4:370-375.
 41. Fridman G, Shereshevsky A, Jost M, Brooks A, Fridman A, Gutsol A, Vasilets V, Friedman G. Floating Electrode Dielectric Barrier Discharge Plasma in Air Promoting Apoptotic Behavior in Melanoma Skin Cancer Cell Lines. *Plasma Chemistry and Plasma Processing*, 2007;27(2):163-176.
 42. Fridman G, Shekhter AB, Vasilets VN, Friedman G, Gutsol A, Fridman A. Applied Plasma Medicine. *Plasma Processes and Polymers*, 2008;5(6):503-533.
 43. Ayan H, Staack D, Fridman G, Gutsol A, Mukhin Y, Starikovskii A, Friedman A. Application of nanosecond-pulsed dielectric barrier discharge for biomedical treatment of topographically non-uniform surfaces. *J. Phys. D: Appl. Phys.*, 2009;42:125202.
 44. Gostev V. Cold Plasma in Biological Investigations. in NATO Advanced Study Institute (ASI): Plasma Assisted Decontamination of Biological and Chemical Agents. 2007, Cesme, Turkey.
 45. Gostev VaD. D. Medical microplasmatron in 3rd International Workshop on Microplasmas 2006, Greifswald, Germany.
 46. Dobrynin D, Barbee KA, Fridman A, Friedman G, Morss-Clyne A. Direct and controllable

- nitric oxide delivery into biological media and living cells by a pin-to-hole spark discharge (PHD) plasma. submitted to Journal of Physics D: Applied Physics, 2010.
47. Dobrynin D, Fridman G, Friedman G. Pin-to-Hole Spark Discharge (PHD) Plasma for Biological and Medical Applications, in to appear in Proceedings of the 37th International Conference on Plasma Science. June 20-24, 2010: Norfolk, VA, USA.
 48. Landsberg K. Cold atmospheric plasma generated UV light - friend or foe?, in Second International Conference on Plasma Medicine. March 16-20, 2009: San Antonio, Texas, USA.
 49. GUIDELINES ON LIMITS OF EXPOSURE TO ULTRAVIOLET RADIATION OF WAVELENGTHS BETWEEN 180 NM AND 400 NM (INCOHERENT OPTICAL RADIATION), T.I.C.o.N.-I.R. Protection, Editor. 2004: Oberschleissheim, Germany.
 50. Leach EH. Experimental Thermal Burns, Especially the Moderate Temperature Burn. *Exp Physiol*, 1943;32(1):67-86.
 51. Suzuki T, Hirayama T, Aihara K, Hirohata Y. Experimental studies of moderate temperature burns. *Burns*, 1991;17(6):443-451